SUPPORTED Ru BASED AMMONIA SYNTHESIS CATALYSTS

A THESIS SUBMITTED TO
THE GRADUATE SCHOOL OF NATURAL AND APPLIED SCIENCES
OF
MIDDLE EAST TECHNICAL UNIVERSITY

BY
MUSTAFA YASİN ASLAN

IN PARTIAL FULFILLMENT OF THE REQUIREMENTS
FOR
THE DEGREE OF MASTER OF SCIENCE
IN
CHEMICAL ENGINEERING

OCTOBER 2012

Approval of the thesis:

SUPPORTED Ru BASED AMMONIA SYNTHESIS CATALYSTS

submitted by **MUSTAFA YASİN ASLAN** in partial fulfillment of the requirements for the degree of **Master of Science in Chemical Engineering Department, Middle East Technical University** by,

Prof. Dr. Canan Özgen _____
Dean, Graduate School of **Natural and Applied Sciences**

Prof. Dr. Deniz Üner _____
Head of Department, **Chemical Engineering**

Prof. Dr. Deniz Üner _____
Supervisor, **Chemical Engineering Dept., METU**

Examining Committee Members:

Prof. Dr. Timur Doğu _____
Chemical Engineering Dept., METU

Prof. Dr. Deniz Üner _____
Chemical Engineering Dept., METU

Prof. Dr. Güngör Gündüz _____
Chemical Engineering Dept., METU

Prof. Dr. Serpil Takaç _____
Chemical Engineering Dept., Ankara University

Assoc. Prof. Dr. Naime Aslı Sezgi _____
Chemical Engineering Dept., METU

Date: 01.10.2012

I hereby declare that all information in this document has been obtained and presented in accordance with academic rules and ethical conduct. I also declare that, as required by these rules and conduct, I have fully cited and referenced all material and results that are not original to this work.

Name, Last name: Mustafa Yasin ASLAN

Signature:

ABSTRACT

SUPPORTED Ru BASED AMMONIA SYNTHESIS CATALYSTS

Aslan, Mustafa Yasin

M.Sc. Department of Chemical Engineering

Supervisor: Prof. Dr. Deniz Üner

October 2012, 131 pages

Ru/C type ammonia synthesis catalysts are known to be poisoned by hydrogen. In order to elucidate a mechanism for hydrogen poisoning, H_2 adsorption and spillover on Ru based ammonia synthesis catalysts were investigated.

Supported Ru catalysts and Na promoted Ru catalyst were prepared by incipient wetness impregnation of $Ru(NO)(NO_3)_3$ on SiO_2, SBA-15, CNT and Vulcan supports. Dispersion value of the catalysts was determined via H_2 chemisorption and Transmission Electron Microscopy (TEM) characterization techniques. Over SBA-15 support, the dispersion of the catalyst determined by two different characterization techniques were in agreement. On the other hand, over CNT and SiO_2 supports dispersion measured by TEM characterization method was higher than H_2 chemisorption method.

H_2 chemisorption measurements performed over extended periods of time were used to determine the spilled over hydrogen amounts over Ru/Vulcan and Na-Ru/Vulcan catalysts at 375 torr and 10 torr H_2 pressure at room temperature. By using H_2 uptake data measured for extended periods of 6 – 24 hours, diffusion coefficient of hydrogen species over Vulcan support was calculated assuming a point source diffusion mechanism. Coefficient of diffusion for Ru/Vulcan and Na-

Ru/Vulcan was found as 1.39 x 10^{-14} cm^2/sec and 1.23 x 10^{-14} cm^2/sec, respectively at 375 torr. Similarly, at 10 torr, diffusion coefficients of Ru/Vulcan and Na-Ru/Vulcan catalysts were determined as 1.51 x 10^{-15} cm^2/sec and 1.81 x 10^{-15} cm^2/sec, respectively.

Keywords: Ammonia synthesis, Ru catalysts, Microkinetic modeling, H_2 Spillover

ÖZ

DESTEKLİ Ru ESASLI AMONYAK SENTEZ KATALİZÖRLERİ

Aslan, Mustafa Yasin

Yüksek Lisans, Kimya Mühendisliği Bölümü

Tez Yöneticisi: Prof. Dr. Deniz Üner

Ekim 2012, 131 sayfa

Ru/C tipi amonyak sentez katalizörlerinin hidrojen tarafından zehirlendiği bilinmektedir. Hidrojen zehirlenmesine bir mekanizma açıklamak için, Ru esaslı amonyak sentez katalizörleri üzerinde H_2 adsorpsiyonu ve taşması araştırılmıştır.

Destekli Ru katalizörleri ve Sodyum (Na) ile güçlendirilmiş Ru katalizörü $Ru(NO)(NO_3)_3$ tuzu kullanılarak SiO_2, SBA-15, CNT ve Vulcan destekleri üzerine ıslaklık başlangıcı emdirme metodu ile hazırlanmıştır. Katalizörlerin metal dağılımları H_2 kimyasal adsorpsiyon ve TEM (Geçirimli Elektron Mikroskobu) teknikleri ile belirlenmiştir. SBA-15 desteği üzerinde iki farklı teknik ile hesaplanan metal dağılım değerleri birbirleri ile uyumludur. Diğer tarafta, CNT ve SiO_2 destekleri üzerinde TEM tekniği ile ölçülen metal dağılım değerleri H_2 kimyasal adsorpsiyonu ile ölçülen metal dağılım değerlerinden daha büyük çıkmıştır. Deney sonuçlarındaki tutarsızlık hidrojen yayılmasına bağlanmıştır.

Uzun zaman aralıklarında, yayılmış H_2 miktarını belirlemek için 375 ve 10 torr H_2 basıncında H_2 kimyasal adsorpsiyon ölçümleri oda sıcaklığında gerçekleştirilmiştir. 6 – 24 saat gibi uzun zaman aralıklarında ölçülmüş H_2 adsorplanma verileri kullanılarak, Vulcan destek üzerinde nokta kaynak difüzyon

mekanizması varsayılarak hidrojen türlerinin difüzyon katsayısı hesaplanmıştır. Ru/Vulcan ve Na-Ru/Vulcan katalizörlerinin 375 torr H_2 basıncındaki difüzyon katsayıları sırasıyla 1.39 x 10^{-14} cm^2/s ve 1.23 x 10^{-14} cm^2/s olarak hesaplanmıştır. 10 torr basınç altında yapılan deneylerde ise Ru/Vulcan ve Na-Ru/Vulcan katalizörlerinin difüzyon katsayıları 1.51 x 10^{-15} cm^2/s ve 1.81 x 10^{-15} cm^2/s olarak belirlenmiştir.

Anahtar Kelimeler: Amonyak sentezi, Ru katalizörler, Mikrokinetik modelleme, Hidrojen Taşması

To My Family

ACKNOWLEDGEMENTS

The author wishes to express her deepest gratitude to his supervisor Prof. Dr. Deniz Üner for her guidance, advice, insight and encouragements throughout the research and life.

The author would like to thank former and present CACTUS research group members for their companionship and help. Particularly, Necip Berker Üner is acknowledged for writing the FORTRAN code for microkinetic analysis.

Special gratitude is due to Merve Başdemir, Okan Özkök, Güvenç Oğulgönen, and Burcu Gökbudak for their friendship.

Prof. Dr. J. Joerg Schneider and Dipl. Ing. Hermann Tempel provided the carbon nanotubes through the collaborative project supported by the Scientific and Technological Research Council of Turkey (TUBITAK) with research grant number: INTEN-C 107M447.

TEM measurements were performed at METU Central Laboratory facilities.

The author would like to thank the financial support during the initial stages of his research from TUBITAK INTEN-C 107M447 project and TUBITAK BIDEB 2228 for M.S. studies. Last but not the least METU-Uşak University YOK-OYP program was acknowledged for support through his graduate studies.

.

TABLE OF CONTENTS

LIST OF TABLES

TABLES

LIST OF FIGURES

FIGURES

NOMENCLATURE

UHV	: Ultra High Vacuum
LHHW	: Langmuir-Hinshelwood-Hougen-Watson
T_{Huttig}	: Huttig Temperature, K
T_{Tamman}	: Tamman Temperature, K
$T_{Melting}$	: Melting Temperature, K
P_i	: Partial pressure of species i
k_i	: Forward (or reverse) rate constant
a_i	: Activity of species i
X	: Fractional conversion
K	: Equilibrium constant
UPS	: Ultraviolet photoelectron spectroscopy
LEED	: Low energy electron diffraction
q	: Reactant feed ratio
TPD	: Temperature programmed desorption
DFT	: Density functional theory
HRTEM	: High resolution transmission electron microscopy
XPS	: X-ray photoelectron spectroscopy
XRD	: X-ray diffraction
NMR	: Nuclear magnetic resonance
D	: Diffusion coefficient of H_2, cm^2/sec
IEA	: International energy agency
EJ	: Ega-Joule (1 EJ = 10^{18} J)

CHAPTER 1

INTRODUCTION

Global food demand has been increasing with the sharp increase of the world population since the beginning of 20th century. To supply such quantities, the use of synthetic fertilizers has an important role. The steady increase of fertilizer consumption and world population over the years are shown in Figure 1 where a direct correlation between the two is apparent. Fundamentally, synthetic fertilizers consist of three main ametals, N, P and S. Among these, the addition of atomic nitrogen content to the composition of synthetic fertilizers is the necessary and the most difficult step. The manufacturing of synthetic ammonia from N_2 requires both catalyst and high production cost related to high temperatures and pressures needed.

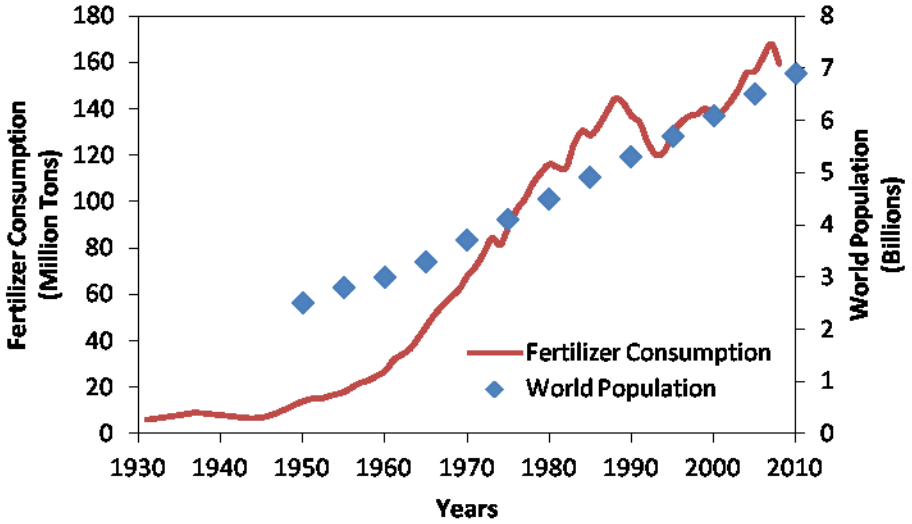

Figure 1. World fertilizer consumption and population in the past century [1-3]

1.1 Synthetic Ammonia Production Catalysts

After the discovery of osmium as ammonia synthesis catalyst by Fritz Haber, first systematic research for ammonia synthesis reaction catalysts was done by Alois Mittash. In Haber's laboratories, Mittash tried 2500 different catalysts for ammonia synthesis reaction and found that in addition to osmium, ruthenium and iron have high activity for ammonia synthesis reaction. Ozaki and Aika published the volcano plot for ammonia synthesis catalysts (Figure 2) in 1981 [4]. In this figure, volcano plot is designed in such a way that ammonia synthesis activity was plotted against the number of electrons in d orbital. It is interesting that the most active three metals have the same number of electrons in their d orbital which is seven. Among these three transition metals, the most commonly used catalyst is still magnetite because of its cost and availability issues in comparison to ruthenium and osmium.

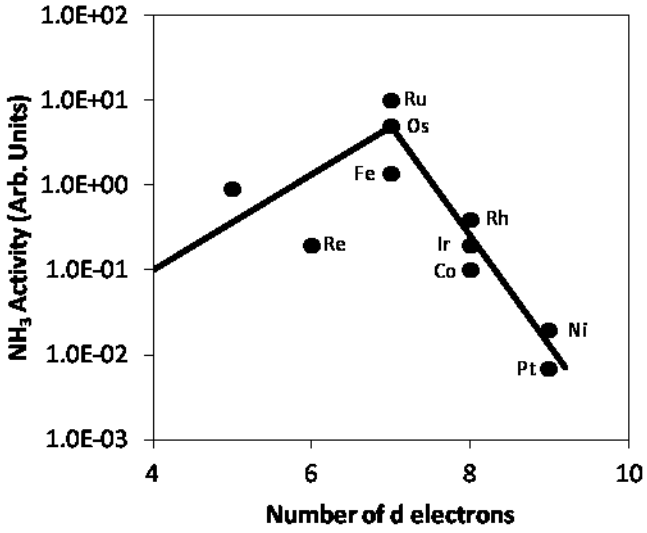

Figure 2. Volcano plot of ammonia synthesis catalysts [4]

1.1.1 Traditional Magnetite Catalyst

The detailed composition of traditional magnetite catalyst is doubly promoted with K_2O and Al_2O_3 iron oxide catalyst. Chemical analysis of promoted iron oxide catalyst is given in Table 1. Iron has a body centered cubic crystal structure. The crystal structure of magnetite is shown in Figure 3.

Over 100 years, several characterization techniques were applied to learn the surface characteristics of catalyst and mechanism of the reaction over the magnetite catalyst. Surface reaction mechanism is important to know the reaction pathways for a catalytic reaction to improve the production process and identify an improved reactor design.

Table 1. Approximate chemical analysis of promoted iron oxide catalyst [5]

Material	**Weight Percent, % wt.**
Fe_3O_4	94.3
K_2O	0.8
Al_2O_3	2.3
CaO	1.7
MgO	0.5
SiO_2	0.4

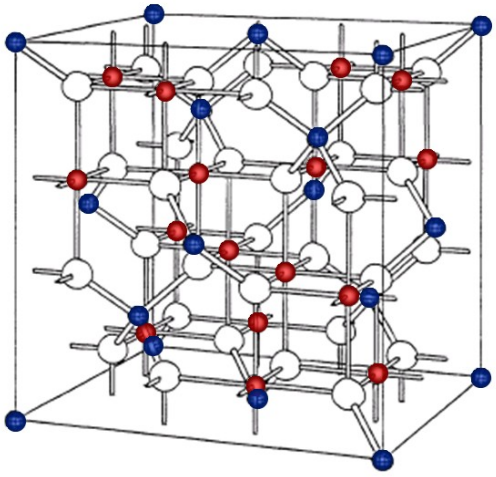

Figure 3. Crystal structure of Fe_3O_4 [6]

In 1980s, Gerhard Ertl and his group published an article that describes the ammonia synthesis reaction mechanism over promoted magnetite catalyst (Figure 4) [7]. The mechanism of the reaction revealed the activation barrier for the N_2

dissociation was the rate limiting and inhibiting step. They performed their experiments under ultra high vacuum (UHV) conditions.

After Ertl published his mechanism, Stoltze and Norskov published all forward and backward reaction rate constants [8]. The experiments were done at UHV conditions, where the kinetic parameters were optimized to fit the model with the overall kinetics.

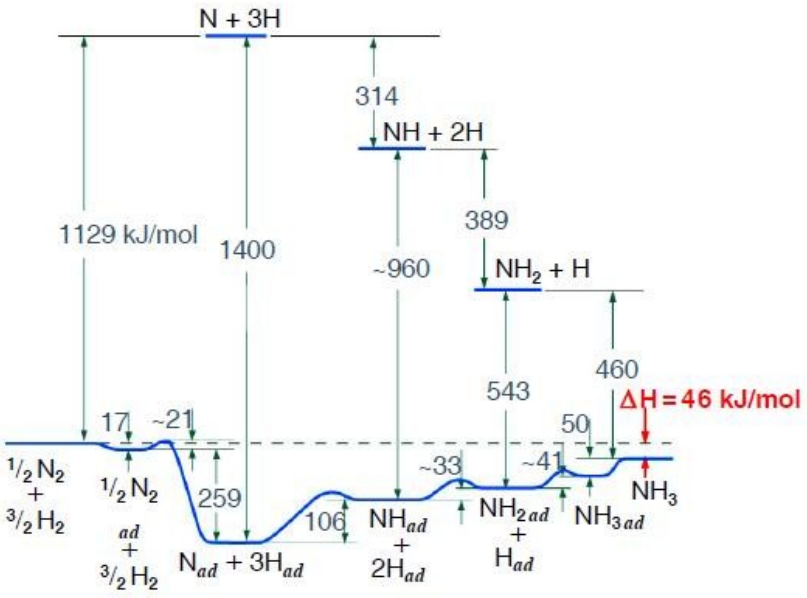

Figure 4. Ammonia synthesis reaction mechanism over magnetite catalyst [7]

1.1.2 2nd Generation Ruthenium Catalysts

In 1960s, K.Aika used supported ruthenium catalysts instead of bulk iron oxide catalyst [9,10]. Dispersing a noble metal on a high surface area support is a common practice instead of using the expensive metal as a bulk. The results of laboratory scale experiments were found promising. Following Aika's experimental studies, Tennison expressed in 1991 that ruthenium would be the 2nd generation catalyst for ammonia synthesis reaction in 1991[5].

The reason why Ru catalyst is the best transition metal for ammonia synthesis reaction was proposed by Jacobsen et al. as B_5 type active sites [12]. B_5 type active

sites consist of two atoms at above and three atoms at below [12]. In addition to Jacobsen et al.'s explanation, Honkala et al. also proposed that B_5 type active sites are located at the edge and corner sites of the Ru metal [13]. B_5 type active sites are shown to be responsible for dissociation of N_2 molecules. The problem arises at this point. H_2 molecules can adsorb at each active site of Ru catalyst including B_5 sites. At high H_2 partial pressures, all of the B_5 type active sites are covered (or poisoned) by hydrogen species. In such a case, N_2 molecules cannot be adsorbed on these specialized active sites to dissociate.

In order to suppress the inhibition effect of hydrogen species over Ru catalysts, many studies were conducted over years. Finally, two most common solutions among the others were found. The first one is addition of alkali promoter to Ru catalyst [9,14,15] and the second one is the change of reactant feed ratio (H_2/N_2) [16,17].

1.1.3 Comparison of Catalysts Considering Process Cost and Reaction Activity

The selection of the best catalyst for ammonia synthesis reaction is an important parameter. It directly influences the production rate and the cost of production process. Besides, stability, durability and regeneration characteristics of the catalyst should be considered. Both magnetite and Ru catalysts are stable at operating conditions. Melting point of magnetite and ruthenium are 1597 ^{o}C and 2334 ^{o}C, respectively. One of the main concerns about the stability of magnetite and ruthenium catalysts is the change of the particle size at operating conditions. Sintering effect directly changes the particle size of metals. The sintering effect can be monitored via Huttig and Tamman temperatures. In the literature Tamman and Huttig temperatures are defined as;

$$T_{Huttig} = 0.3*T_{Melting}$$

$$T_{Tamman} = 0.5*T_{Melting}$$

At Huttig temperature, metal particles begin to be mobile. Particle sizes of the metal particles start to grow larger diameters. At Tamman temperature, metal

particles are highly mobile than Huttig temperature. Huttig temperatures of magnetite and ruthenium are 530 ^{o}C and 700 ^{o}C, respectively. Operating temperature of the ammonia production process has the same range. So, stability of both magnetite and Ru catalysts isnot a concern at this step.

Durability of catalysts is another important point. Both magnetite and ruthenium catalysts are deactivated in the presence of sulfur [18]. For magnetite catalyst, ammonia has poisoning effect but this does not deactivate the catalyst. Similarly for ruthenium catalyst, hydrogen has poisoning effect by blocking special sites for nitrogen dissociation.

Other important parameter for the choice of catalyst for a process is activity. Recent studies have shown that conversion of reactants in the presence of ruthenium catalyst is two times higher than magnetite catalyst. In addition to activity advantage of ruthenium, ruthenium catalyst show high activity with lower hydrogen amounts with respect to stoichiometric (H_2:N_2 = 3) ratio [17]. On the other hand, supported ruthenium catalyst is 10^4 times more expensive than magnetite catalyst. Taking disadvantageous and advantageous of Ru catalyst into account, Kellogg Brown Company released a new ammonia synthesis reactor in 1990 which consist of 4 catalytic beds. 1st, 2nd and 4th beds contain promoted magnetite catalyst and the 3rd bed contains supported-promoted ruthenium catalyst [19].

1.2 History of Synthetic Ammonia Process

1.2.1 Discovery Process of Synthetic Ammonia Production

Ammonia was first isolated by J.B. Priestley in 1774 [20]. Chemical formula of ammonia was first determined by W. Henry in 1809 [21]. In parallel to these discoveries, scientists discovered the nitrogen cycle in nature and showed that nature cannot use free nitrogen. In order to add free nitrogen into nitrogen cycle, free nitrogen should be fixed chemically. Thus, production of synthetic ammonia story had begun with these requirements.

In 19th century, world population began to increase drastically. This reality has brought many problems with it. The main problem was the food supply for the growing population. Between the years 1800 and 1900, world population increased two times from 1 billion to 2 billion [22]. The growth of population led to increase in synthetic fertilizer demand. In order to produce an increasing amount of fertilizer, the production of synthetic ammonia became an obligation.

1.2.2 History of Synthetic Ammonia Production & First Attempts

After the scientists discovered that in order to add free nitrogen into nitrogen cycle for providing the needs of agriculture and defense industries, the scientists began working on the fixation of nitrogen in a synthetic way. Some of the fixation processes proposed were;

1. Norwegian-Arc Process
2. Cyanamide Process
3. Haber Process

Norwegian-Arc process was first developed by J.P. Priestly and based on the reaction of dinitrogen and dioxygen at 2000 ^{o}C [23]. It needed continuous electric spark to forward the reaction and this was the main limitation of the process. Second industrial attempt for the nitrogen fixation and also for ammonia production was the cyanamide process. Cyanamide process was based on the calcium cyanamide which can be produced by the reaction between calcium carbide and nitrogen at high temperatures around 1100 ^{o}C [24]. The main disadvantages of these processes were high temperature requirement of production and further technology need for bulk production. In 1918, Fritz Haber received the Nobel Prize on discovering how to produce synthetic ammonia by using its elements. This process also demanded high temperatures (500-700 ^{o}C), high pressures (50 – 100 bar) and a catalyst for high volume production. Although production of ammonia had some limitations, Fritz Haber said in his Nobel lecture in 1920 that when compared to other suggested

processes, the most efficient way of of produce synthetic ammonia was his process [25].

1.2.3 Importance of Synthetic Ammonia Production (from 1900s to now)

Ammonia is one of the most produced and consumed chemical in the world. The main reason of the wide use of ammonia is the fact that it is the raw materials of defense and fertilizer industries. All of the explosives such as nitroglycerin and nitrotoluene contain nitrogen in their chemical formulas. Glycerin, toluene and similar aromatic organics do not contain nitrogen in their formula. Nitrogen oxides in their structures give them the explosive property.

Ammonia has a crucial role in the fertilizer industry. The salts of ammonia are widely use in farming. Because compounds of phosphorus and nitrate in soil decrease in time. These compounds are important for soil if the soil is used for farming. Besides, ammonium salts are easily dissolved in water and can be supplied via any irrigation technique in farming.

The complex relationship between the world population, the synthetic fertilizer consumption, and the fertilizer input to the meat production is presented in Figure 5. In the same figure, the world population fed by the Haber-Bosch nitrogen is also shown.

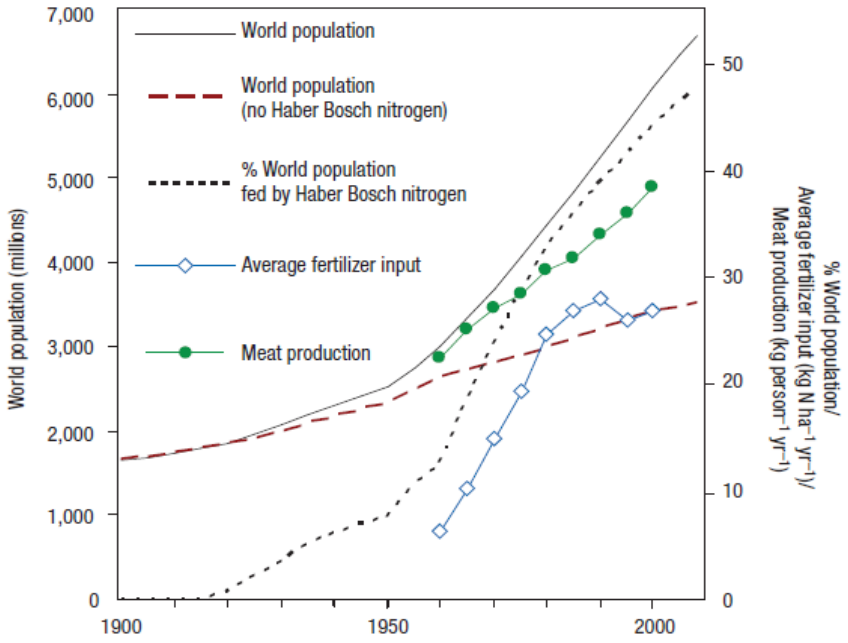

Figure 5.Trends in human population and nitrogen use throughout the 20th century[26]

1.2.4 Fritz Haber, Carl Bosch, Alois Mittash and Others

Fritz Haber was the inventor of the synthetic ammonia process over magnetite catalyst. He used dihydrogen and dinitrogen, the former is obtained from coal and the latter is obtained from air. When he proposed such a process, there were many limitations for bulk production. First of all, hydrogen can be explosive at high temperatures and pressures. Therefore it had never been used as a reactant in such a high temperature and high pressure system. Second limitation was the production of hydrogen. For example, the first ammonia production plant had a capacity of 30000 tones ammonia/year [27]. In order to reach such production rates, 5300 tones hydrogen was needed at least. The third limitation was about the reactor. Such a catalytic reactor had never been used so far in the world. In order to achieve reaction at 500-700 ^{o}C and 50-100 bar, reactants should have been passed through a catalyst bed. As a result, the ammonia synthesis process has opened a new perspective for chemical technology.

After BASF Company began to be interested in Haber's process instead of Norwegian Arc Process, Carl Bosch and his colleagues from BASF Company started working on Haber's synthetic ammonia production process. The process was commercialized by BASF and it is still called as Haber-Bosch process.

As mentioned previously, catalytic ammonia production process via its elements pioneered lots of different areas in chemical technology. Ken-ichi Aika started investigating Ru catalysts for ammonia synthesis in 1960 [9,10]. He showed that at same operating conditions ruthenium has higher activity than magnetite catalyst. In addition to Aika's studies, Gerhard Ertl is also one of the scientists that contributed to the understanding of ammonia synthesis reaction. He won the Nobel Prize for his discovery of the mechanism of ammonia synthesis over magnetite catalysts in 2007 [28]. But, in industry, the cost of ruthenium catalyst is still a problem.

1.3 Industrial Reactors for Synthetic Ammonia Production

First industrial ammonia synthesis reactor was built by BASF Company in 1910. This reactor has an intercooling system for a better temperature distribution and a catalyst bed. The length of the reactor was 4 m. Modern ammonia converters are not so much different from the old ones. Over years, catalytic beds in reactors were increased from 1 to 3 or 4 and an effective heat exchange design was built. The heat exchange area between cold gas, pre-heated gas and inlet gas are increased for a more efficient heat transfer. In Figure 6, ammonia converters from two different industrial companies were given.

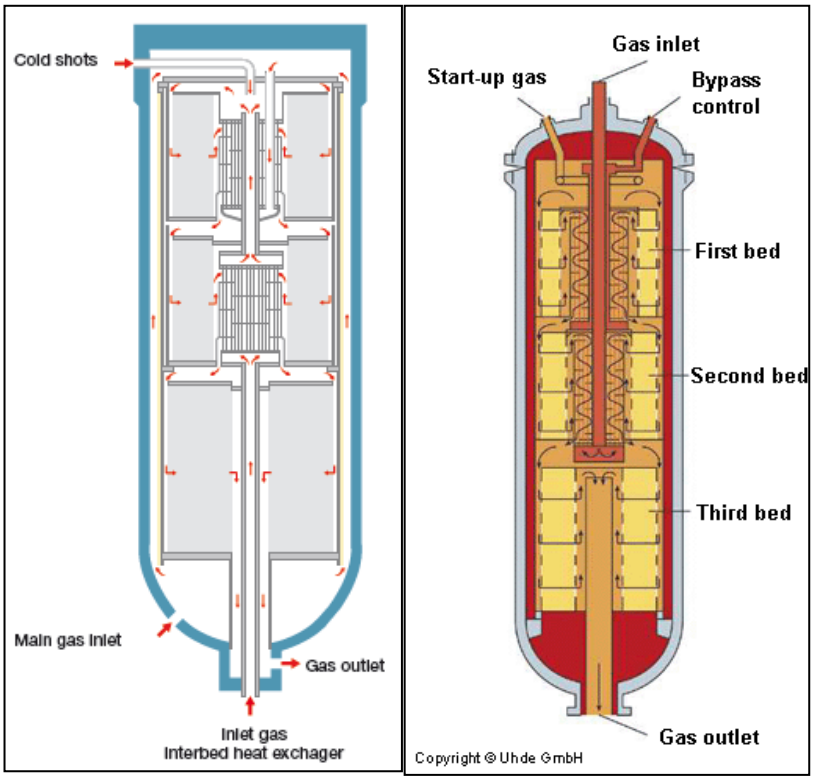

(a) (b)

Figure 6. a) Haldor Topsoe S-300 [29] three bed, intercooling ammonia converter, b) Uhde three bed ammonia converter [30]

Flow dynamics of Haldor Topsoe S-300 and Uhde three bed ammonia converter have an important characteristic in common. In these reactors, gases flow in radial direction. This design makes the reactor more efficient in terms of conversion, intercooling and volume by eliminating high pressure drops in axial directions.

1.4 Alternative Methods of Ammonia Synthesis

In this section, the alternative methods of ammonia synthesis is reviewed. The focus is the methods of electrochemical route for ammonia synthesis, photocatalytic ammonia synthesis and enzymatic ammonia synthesis.

1.4.1 Electrocatalytic Ammonia Synthesis

Electrocatalytic ammonia synthesis is one of the alternative ways for ammonia synthesis. This method is based on the reduction of the NO_3^- to NO_2^- or electrolysis of water in a special cell system including a cathode and anode.

Hasnat et al. in 2010, studied ammonia synthesis with supported bimetallic Pd catalysts by reduction of NO_3^- to NO_2^- [31]. They tried Pt-Pd, Ni-Pd, Ag-Pd, Cu-Pd and Rh-Pd bimetallic catalysts for electrocatalytic ammonia synthesis reaction in the cathode side of the special cell. In the anode side of the cell, they used Pt catalyst for electrolysis of the water. They obtained the highest activity in the presence of Rh-Pd catalyst.

Skodra and Stoukides studied electrocatalytic ammonia synthesis in 450 – 700 ^oC in the presence of Ru catalysts [32]. They used a similar solid electrolyte cell with Hasnat et al. Skodra and Stoukides electrolyzed the steam in the cell and H+ ions went through the cathode side of the cell. In the same time, they fed cathode side with N_2. The rate of the reaction was found as 1.6 x 10^{-9} mol/g_{cat}-sec at 450 ^oC.

1.4.2 Photocatalytic Ammonia Synthesis

The history of photocatalytic synthesis of ammonia started with Guth and Schrauzer's studies in 1970s [33]. They synthesized ammonia using desert sand with the following reaction;

$$N_2 + 3H_2O + h\nu \rightleftharpoons 2NH_3 + \frac{3}{2} O_2 \qquad 1$$

Desert sand is mainly composed of TiO_2. When desert sand are combined with Ru (so Ru/TiO_2 catalyst is obtained), photocatalytic activity appeared. TiO_2 in the presence of Ru metal splits the water into H_2 and O_2 and then H_2 reacted with N_2 (air) in the presence of Ru metal to obtain NH_3. Several studies for ammonia synthesis via photocatalytic route have been reported till now [34 – 36].

In nature, ammonia can easily be produced via bacteria at room temperature and atmospheric pressure. But synthetic ammonia can only be produced at high

temperatures and high pressures. The mechanism of natural ammonia synthesis is intriguing.

1.4.3 Enzymatic Ammonia Synthesis

In 1964, Vol'pin and Shur published an article for ammonia synthesis using transition metal complexes similar to enzyme that is responsible for ammonia synthesis [37]. In 1987, Shilov published detailed study about the chemical structure of the ammonia synthesis enzyme [38]. The enzyme which is called as nitrogenase (FeMoco) composed of 2 molybdenum, 34 iron and 26-28 sulfur elements (Figure 7). Shilov synthesized transition metal complexes with structure for ammonia synthesis catalysts. They are promising for ammonia synthesis but have never been used up to now. In 1990s and 2000s, Norskov et al. calculated the activation energy vs. reaction coordinate graph of FeMoco enzyme for ammonia synthesis and compared the steps with ruthenium catalyst. Norskov et al. observed that both FeMoco and Ru catalysts gave rise to nearly the same energy diagram [39]. Norskov et al. concluded that in the presence of FeMoco enzyme all of the steps are achieved electrochemically, but in the presence of ruthenium catalyst, hydrogen addition to the system is different from the biological route. If hydrogen can be injected to the system somewhat electrochemically, ammonia synthesis at room temperature and pressure can be achieved over Ru catalysts.

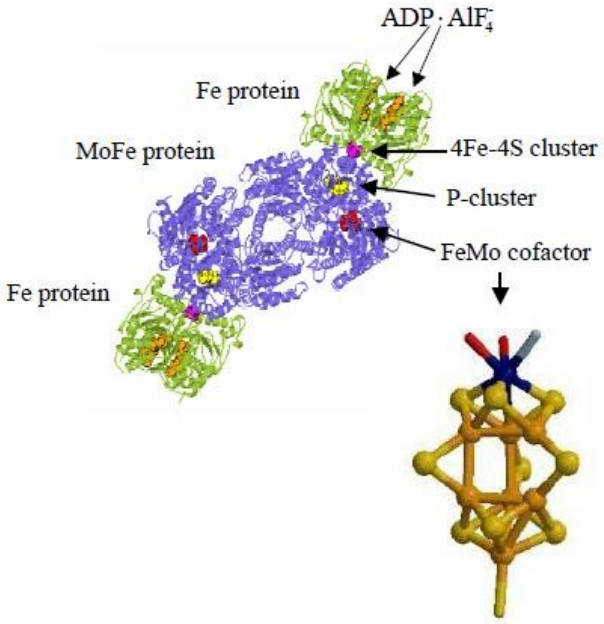

Figure 7. Nitrogenase enzyme and FeMo cofactor [40,41]

Under the light of all historical findings, experimental studies and industrial experiences, the aim of this study is thus to investigate the adsorption characteristics of hydrogen on ammonia synthesis reaction in the presence of supported-promoted Ru-based catalysts. Decreasing the hydrogen amount would bring lots of advantages such as decreasing hydrogen production cost and compression cost and suppressing the poisoning effect of hydrogen on the Ru catalyst.

CHAPTER 2

LITERATURE SURVEY

2.1. Reaction Mechanism of Ammonia Synthesis Reaction over Ruthenium Based Catalysts

Reaction mechanism and kinetics of ammonia synthesis over magnetite and/or ruthenium have been studied over the years. Temkin was one of the first known scientists who has attempted to discover the kinetics of ammonia synthesis in 1940s. Temkin and Phyzev published a general reaction rate expression for ammonia synthesis over magnetite catalyst [42]. Temkin reaction rate expression is given below;

$$r = k_1^{'} P_{N_2} \left(\frac{P_{H_2}^3}{P_{NH_3}^2} \right)^{\alpha} - k_2^{'} \left(\frac{P_{NH_3}^2}{P_{H_2}^3} \right)^{1-\alpha} \qquad (2.1)$$

Temkin reaction mechanism is modified over the years in order to adapt to the performance of different catalysts. Temkin kinetics is based on the dissociative adsorption of N_2 and H_2. In addition to this, Temkin reaction rate assumes that all surface is dominated by N* species.

Temkin kinetics for ammonia synthesis over magnetite catalyst fits well with experimental data. But it could not elucidate the steps of ammonia synthesis over a catalytic surface.

In 1980, Gerhard Ertl proposed a pathway for ammonia synthesis over Fe-based catalysts [7]. Furthermore, Ertl published the related activation energy vs. reaction coordinate diagram for ammonia synthesis. Reaction mechanism studies were carried out at UHV conditions. All of spectroscopic measurements such as

Ultraviolet Photoelectron Spectroscopy (UPS), Low Energy Electron Diffraction (LEED) were taken at UHV conditions.

The results of microkinetic model showed that LHHW (Langmuir – Hinshelwood/Hougen – Watson) kinetics can be used for ammonia synthesis reaction over Fe based catalysts. Stoltze and Norskov studied on the same mechanism via first principles calculations [43]. They achieved the similar results with Ertl's findings. Stoltze and Norskov were aware of that reaction mechanisms of ammonia synthesis studies are determined at UHV conditions. But, ammonia synthesis reaction is performed at high temperature and high pressure conditions. Therefore, Stoltze and Norskov set up a microkinetic model for ammonia synthesis reaction based on LHHW kinetics [44]. They calculated the ammonia synthesis reaction rate values using proposed mechanism at operating conditions and compared with real experimental data. The experimental data and microkinetic model output fitted accordingly. As a result, a reasonable connection between UHV condition studies and real operating conditions was made. They also revealed that using a specific catalytic surface for determination of the all reaction parameters are enough for the whole reaction mechanism at real operating conditions. In 1989, Dumesic and Trevino repeated the Stoltze and Norskov's calculations and reanalyzed each elementary step [45].

In 2006, Rossetti et al. published the modified Temkin reaction rate expression [16]. They both investigated the LHHW approach and the approach of Ferraris et al. [46] for defining a rate expression which can describe the kinetics of ammonia synthesis at all operating conditions. Rossetti et al. [18] reported a modified Temkin rate expression in order to obtain values close to the experimental results over Ru-based catalysts. The modified reaction rate expression is given below,

$$\frac{dX}{d\tau} = k_f \lambda(q) \frac{(a_{N_2})^{0.5}\left[\frac{(a_{H_2})^{0.375}}{(a_{NH_3})^{0.25}}\right] - \frac{1}{Ka}\left[\frac{(a_{NH_3})^{0.75}}{(a_{H_2})^{1.125}}\right]}{1 + K_{H_2}(a_{H_2})^{0.3} + K_{NH_3}(a_{NH_3})^{0.2}} \qquad (2.2)$$

where (X) is fractional conversion, (τ) is time factor,(λ) is stoichiometric coefficient, (q) is reactant feed ratio, and (a_i) indicates the activity of species. As shown in

equation (2.2), in the denominator, activity of hydrogen and ammonia are existent. It means that, as partial pressures of hydrogen and ammonia increase the overall reaction rate decreases over the Ru catalyst. In other words, hydrogen and ammonia poison the Ru catalyst.

2.1.1 Microkinetic Analysis of Ammonia Synthesis Reaction proposed by G.Ertl

In 1979, British Petroleum Company took a patent for Ru/Carbon catalyst [17]. In 1990, Kellogg Brown Company announced a new ammonia synthesis process and ammonia synthesis reactor that uses Ru catalyst in one of the catalytic beds.

In 1996, Hinrichsen et al. published the mechanism in the presence of Cs-Ru/MgO [47]. Hinrichsen et al. assumed the same reaction mechanism with Ertl's approach. This microkinetic reaction model was run by modeling the microreactor as a series of mixed flow reactors.

The results of microkinetic model and experimental study were consistent with each other. In addition to agreement in the theoretical and experimental results, in the beginning of the model establishment, nitrogen dissociation was assumed as the slowest step of the mechanism. As a result of microkinetic model and N_2 Temperature Programmed Desorption (TPD) experiments, sticking coefficient for N_2 was found as about 10^{-10} at 300 K which is a very low value. Therefore surface coverage of the dissociated nitrogen species are determined as expected very low number with respect to surface coverage of hydrogen species.

In the beginning of the mechanism studies of ammonia reaction over Ru catalyst, scientist agreed with the same elementary steps with magnetite catalyst. Although Hinrichsen's microkinetic model was verified with real experimental data, there was a gap between the microkinetic model and theoretical results. Logadottir and Norskov reported the energy diagram for ammonia synthesis reaction using first principles calculations method and proved that N_2 dissociation step is the only energy required therefore rate limiting step of the ammonia synthesis [48]. This publication was a breakthrough for ammonia synthesis reaction over Ru-based

catalyst due to apparently prove the rate limiting step as N_2 dissociation. There was no contradictory idea about the elementary steps of ammonia synthesis.

Rod et al., Logadottir and Norskov, and Dahl et al.'s [39,48,49] studies were based on Density Functional Theory. As nature of DFT calculations, Rod et al., Logadottir and Norskov, and Dahl et al. showed the possible places of the reactant over catalytic surfaces and they gave the binding energies of these reactants at these specified places. As a result of DFT studies, binding energy of N_2 molecule at step sites is determined as lower than the terrace sites of the Ru surface. In the other step of the reaction, binding energies for both steps sites and terrace sites are found to be similar to each other. Hereby, Norskov et al. also showed that the rate limiting step for ammonia synthesis is dissociation of nitrogen over Ru catalyst [13,48].

For Fe based catalysts, one of the main assumptions of the mechanism was determined as dissociation of nitrogen step of the reaction. But this assumption could not been proven with surface coverage data. For Ru based catalyst, surface coverages of the nitrogen is below the detection limits of the measurement techniques. In 2009, Hellman et al. published surface coverages of the dissociated nitrogen, dissociated hydrogen, empty sites and some intermediates such as NH_2 [50]. Results showed that surface coverage of nitrogen cannot exceed 0.5% of the whole active sites.

McClaine et al. published the intrinsic reaction rate of ammonia synthesis over Ba promoted Ru/zeolite X catalysts [51]. They showed that the reaction orders for N_2, H_2 and NH_3 are 1, -1 and weakly inhibition, respectively. When they analyzed the surface coverages via using LHHW kinetics, they realized that dissociated hydrogen covers nearly all of the sites. They reported H_2 and N_2 coverages at stoichiometric reaction conditions as 0.99 and 0.01 respectively.

2.2. Role of H_2 and N_2 over Ruthenium Catalyst

In 2007, Larichev et al. investigated the distinct reaction rate difference in the presence of alkali promoted Cs-Ru/MgO catalyst in comparison to Ru/MgO catalyst [52]. They revealed via High Resolution Transmission Electron Microscopy

(HRTEM) images that, Cs promoter is creating an amorphous surface. Authors indicated that covering of an amorphous surface containing cesium caused decreasing binding energy of Ru at $3d_{5/2}$ band in Cs-Ru/MgO with respect to Ru/MgO which are obtained by X-Ray Photoelectron Spectroscopy (XPS) measurements with respect to Ru/MgO catalyst. Larichev also published another article that investigating directly the valance state of the ruthenium [53]. They observed a X-ray amorphous state for Ru/MgO catalysts prepared with different Ru salt. They showed that different Ru salts determine the ratio of X-ray amorphous state in whole catalyst and also the particle size of the catalyst

Szmigiel et al. examined Ba-Ru/BN as a ammonia synthesis catalyst in 2005 [54]. By using in-situ measurements via XRD and TPR-MS techniques, they explained that the reactivity of Ba-Ru/BN catalyst depended on the precursor of BN (boron nitride) support. BN support was prepared using B_2O_3 material. Szmigiel et al. [54] suggested that decreasing the oxygen amount in the precursor of the BN increased the reaction rate. Because, oxygen species on the BN support reacts with ammonia and this reaction deactivate the catalyst. Besides, Truszkiewicz et al. is interested in Ba-Ru/C catalyst [55]. In-situ XRD, TPR-MS characterization techniques were applied in order to determine the state of Ba. Ba was found as BaO over Ru catalyst. Finally, Rarog-Pilecka et al. studied a Cs-Ru/C catalyst. They similarly determined the state of the Cs promoter via using characterization techniques [56] as in-situ XRD, TPR-MS. They found that Cs salt started decomposing after 100 – 120 ^oC and directly react with oxygen and water vapor. As a result, $CsOH.H_2O$ intermediate is detected. Further investigation showed that Cs promoter partially located as Cs_xO_y structure.

Support material for Ru based catalysts can also play a role to increase the reaction rate. Yang et al. used $BaCeO_3$ as support material and prepared $Ru/BaCeO_3$ catalyst for NH_3 synthesis [57]. They achieved superior performance for ammonia synthesis at low temperatures such as 623 K compared to conventional supports such as Al_2O_3, MgO, and CeO_2. They concluded in the light of their spectroscopic

measurements that, there is a strong relationship between Ru metal and Ce metal. They attributed the electronic promotion for the increased the activity.

Xu et al. synthesized microwave assisted MgO-CNT support for ammonia synthesis [58]. They took the TEM images of Ru/MgO, Ru/CNT, Ru/MgO-CNT which was synthesized by conventional method of wet impregnation and microwave assisted Ru/MgO-CNT catalysts. They saw that in microwave assisted Ru/MgO-CNT catalysts; Ru particles are well dispersed with respect to other catalysts. Besides, there is an evident Ru crystal peak in the XRD measurement of the microwave assisted Ru/MgO-CNT catalysts at $2\theta = 44.3^{\circ}$. The activity measurements of all catalyst are observed and the most active catalyst is determined as microwave assisted Ru/MgO-CNT catalyst.

Luo et al. studied with Ru/CeO_2-La_2O_3 catalyst with different La_2O_3 loadings [59]. It is seen that when La_2O_3 loading increases in the Ru/CeO_2-La_2O_3 catalyst, reaction rate increases. Authors explained this situation related to increasing the amount of La loading on the catalyst as; La_2O_3 promotes the oxygen reduction over CeO_2 surface and Ce metal reduce from Ce^{+4} state to Ce^{+3} state. This facilitates to obtain more active sites over Ru metal and enhance the change for activating the N_2 bond for dissociation.

As seen from the literature that the main focus in ammonia synthesis reaction is to increase the reaction rate or operating the system at milder conditions. Increasing N_2 dissociation rate is a way for achieving the goal. But, eliminating the poisoning effect of hydrogen is another important aspect. In the next topic of the thesis, literature is given directly related with H_2 poisoning effect over Ru catalyst and solutions to this problem.

2.2.1. N_2 Dissociation over Ru metal

As mentioned earlier, the slowest step for ammonia synthesis is dissociation of nitrogen molecule to atomic nitrogen. Hinrichsen et al. [47], Logadottir and Norskov [48], and Dumesic and Trevino [45] revealed that increasing the N_2 dissociation rate causes increasing the rate of total reaction mechanism. On the other

hand, Ru catalyst has more activity than Fe catalyst at the same operating conditions for ammonia synthesis reaction. Therefore, a valid question to ask is how Ru metal dissociates N_2 molecules easier than Fe metal.

The answer of this question was proposed by Hansen et al. in 2001 [60]. Hansen et al. investigated Ba-Ru/BN catalyst while ammonia synthesis reaction was carrying on via in-situ TEM characterization technique. They explained that Ru metal has a hexagonal cubic crystal structure. In the edge and corners of the Ru metal, there are special active sites which are responsible for N_2 dissociation. These special active sites are named as B_5 type active sites. B_5 type active sites composed of 5 Ru atoms which mainly two of them are in the bridge at above, and the other three of them are in three-hold hollow at below [12]. In addition to this, TEM images of Hansen et al. study showed that earth alkaline promoter barium is located over Ru metal in the catalyst. Earlier studies, it is evidently concluded that, in the presence of alkali or earth alkali promoter, activity of Ru metal increases.

Jacobsen et al. showed that the highest activity for ammonia synthesis reaction in the presence of Ru catalyst was obtained when the particle size of the Ru metals are approximately 2 nm [11]. Jacobsen et al. revealed that there is a relationship between particle size of Ru metal and number of active sites with respect to particle size of Ru atoms. When, the particle size of the Ru metal atoms increase, fraction of the edge atoms decrease. In the same manner, if the particle size of Ru metals increase, number of total active sites for Ru metal decreases. Therefore, Jacobsen et al. concluded that B_5 type active sites are present and they are at the edge and corners of the Ru metal. Veisz et al. published a paper concerning about the determination of total number of metal atoms in a perfect crystal via TEM images of the metal particle [61]. The related equations are given step by step:

In a perfect crystal, total number of atoms equal to bulk atoms and surface atoms

$$N_T = N_B + N_S \tag{2.3}$$

Total number of surface atoms equal to numbers of edge, corner and face atoms, therefore,

$$N_S = N_E + N_C + N_F \quad (2.4)$$

For face centered cubic (fcc) crystals such as Pd, the relation between the diameter of metal particle size and total number of atoms can be given as

$$d_{sphere} = 1.105 d_{atom} {N_T}^{1/3} \quad (2.5)$$

Using these equations, the number of metal atom in the surface and number of atoms in the bulk can be calculated.

After breakthrough about the special active sites over Ru metal, Aika et al. published an article in 2007 with using Ru/BHA (barium hexaluminate) catalyst [62]. BHA was prepared via microemulsion-mediated synthesis technique and Ru catalyst was prepared via impregnation method. Activity of Ru/BHA catalyst was higher than Ba-Ru/MgO catalysts. K. Aika et al. proposed that BHA support increase the epitaxial growth of truncated hexagonal pyramid shape of Ru metal which is directly related with the number of B_5 active sites.

Similar epitaxial growth of Ru particles over h-BN by Yang et al. [63] was observed. Yang et al. reported particle size of Ru metal as 0.21 nm with the help of TEM images. Ru particles growth epitaxially on h-BN support which is the main effect of such a particle size of Ru particle.

CHAPTER 3

MATHEMATICAL MODELS FOR HYDROGEN ADSORPTION AND DIFFUSION OVER SUPPORT

3.1 Adsorption and Diffusion of H_2 on Solid Surfaces

Spillover phenomenon was proposed by Boudart in 1960s [65] over Pt/Carbon catalyst[66,67]. Sinfelt et al. observed the hydrogenation of ethylene with spilled over H_2 over Pt/SiO_2 to Al_2O_3 [66]. Similarly, Khoobiar prepared a physical mixture of Pt/Al_2O_3 and WO_3 [76]. In room temperature when mixture was exposed to H_2, WO_3 bronze was obtained. Falconer and Conner published a review on spillover in heterogeneous catalysis [68]. In this review publication, they examined many different aspects about the spillover.

Robell et al. [65] investigated the H_2 uptake over Pt/Carbon catalysts. They exposed hydrogen to %0.2 and %1 wt. Pt/Carbon catalysts at high temperatures to show the relationship of H_2 uptake with time. They obtained the H_2 uptake values of different Pt catalysts with respect to time. Robell et al. concluded that, slow uptake of the molecular H_2 can be explained as diffusion of hydrogen from one active site to other active sites. Additionally, they calculated the number of Pt particles used as a source for H_2 spillover as 3.16×10^{17}, coefficient of diffusion as 3.4×10^{-19} and 5.8×10^{-17} $cm^2/sec.$ at 300 and 390 ^oC, respectively, and H_2 uptake at 300 ^oC and 60 cm Hg H_2 pressure as 10^{15} H atoms/cm^2.

Kramer and Andre studied the adsorption of hydrogen over alumina support by spillover [69]. They obtained the normalized H_2 uptake data over 1 wt.% Pt/Alumina catalyst at 400 ^oC with respect to time. When the H_2 uptake of Kramer

and Andre's data are compared with the Robell et al.'s data [74], they are similar. Besides, H_2 uptake over 1 wt.% Pt/Alumina reached equilibrium after 20 hours. They calculated the amount of spiltover hydrogen from Pt metal to alumina surface via point source diffusion approach. In this approach, diffusion of hydrogen from metal particle (point source) to alumina is in the core of the phenomenon. The process should obey the Fick's 2nd law which is

$$\frac{\partial^2 C}{\partial x^2} + \frac{\partial^2 C}{\partial y^2} + \frac{\partial^2 C}{\partial z^2} = \frac{1}{D}\frac{\partial C}{\partial t} \qquad (3.1)$$

The general solution of this differential equation was given by H.S. Carslaw and J.C. Jeager in their book entitled "Conduction of Heat in Solids" as

$$C = \frac{C_o}{8(\pi D t)^{3/2}} e^{\{(x-\Delta x)^2+(y-\Delta y)^2+(z-\Delta z)^2\}/4Dt} \qquad (3.2)$$

This solution is applicable for both instantaneous and continuous point source. In this study, we are interested in continuous point source due to nature of chemisorption experiment.

For continuous point sources, the amount of total mass transfer at a rate of $\phi(t')$ per unit time from t=0 to t=t at the point (x', y',z'), the concentration at (x,y,z) at time t is, by integrating general solution for differential equation ,

$$\frac{1}{8(\pi D)^{3/2}} \int_0^t \phi(t') e^{-r^2/4Dt} \frac{dt}{t^{3/2}} \qquad (3.3)$$

where r^2 can be defined as,

$$r^2 = (x-\Delta x)^2 + (y-\Delta y)^2 + (z-\Delta z)^2 \qquad (3.4)$$

This distribution of concentration is said to be due to a continuous point source of strength $\phi(t')$ from t=0 onwards.

If $\phi(t')$ is constant and equal to M, we have

$$C = \frac{M}{4(\pi D)^{3/2}} \int_{1/\sqrt{t}}^{\infty} e^{-r^2\tau^2/4D} d\tau \qquad (3.5)$$

On putting,

$$\tau = t^{-1/2} \qquad (3.6)$$

Finally,

$$C = \frac{M}{4\pi Dr} erfc \frac{r}{\sqrt{4Dt}} \qquad (3.7)$$

And the value of concentration at a distance r from the point source on an infinite plane surface is thus given by J. Crank in his book entitled "The Mathematics of Diffusion"

$$C = \frac{M}{4\pi Dt} e^{(-\frac{r^2}{4Dt})} \qquad (3.8)$$

Kramer and Andre used the equation below in order to fit their H_2 uptake data with time.

$$C = C_e \left[1 - \frac{8}{\pi^2} \exp\left(-\frac{\pi^2 Dt}{b^2}\right)\right] \qquad (3.9)$$

where, b is the mean distance between the metal particles. Measuring by the amount of spilled over hydrogen (diffused out hydrogen from metal particle), diffusion of coefficient was calculated for several cases using equation (3.9).

Kramer and Andre calculated the coefficient of diffusion for 1 wt.% Pt/Alumina catalyst at 400 ^oC in the presence of 0.8 and 710 torr H_2 as 1.05 x 10^{-15} and 0.9 x 10^{-15} cm^2/sec., respectively. Besides, they assumed that the rate limiting step of the H_2 adsorption process as spillover of H_2 to alumina support. They observed that H_2 spillover rate increases with temperature increase. Therefore, they calculated the activation energy of diffusion process as 117 kJ/mol for Pt/Alumina catalyst with a BET surface area of 105 m^2/g.

The effect of alkali promoters on Ru catalysts on the mechanism and kinetics of adsorption of H_2 were investigated by Uner et al. via solid state ^1H NMR and H_2 chemisorption techniques [70]. Solid state NMR spectroscopy allowed them to identify two different adsorbed states of hydrogen, α and β over Ru/SiO_2 surface. α

state was revealed to hydrogen in close proximity to the surface, with a chemical shift equal to the chemisorbed hydrogen. β state, on the other hand, was weakly bound adsorbed hydrogen that is in fast exchange with the gas phase. ^{1}H NMR measurements revealed that in the presence of Na promoter, β state peak could not be observed.

Uner [71] later demonstrated through a reaction model study that weakly bound hydrogen has an important role for Fischer-Tropsch reaction in terms of products distribution. In the presence of weakly bound hydrogen, products of Fischer-Tropsch reaction shifted to paraffinic materials. In the absence of the β state hydrogen, products shifted to olefin based products which are desired due to their high reactivity compared to paraffinic products.

In addition, Uner et al. [72] further demonstrated that alkali promoter interacts with silanol groups, the hydroxyl groups over SiO_2 support, decreasing the number of protons on the support surface. They demonstrated that alkali promoters on the support surface inhibited hydrogen spillover. This study was further used in the literature to design highly selective catalyst for selective CO oxidation reaction. Pedrero et al. [73] have demonstrated that by the elimination of spilled over hydrogen, using alkali promoters, it was possible to increase the selectivity of CO oxidation reaction.

A mathematical model for hydrogen adsorption over Ag promoted Ru was reported by Kumar et al. [74] and Savargoankar et al. [75]. They made H_2 adsorption over Ru/SiO_2 and Ag promoted Ru/SiO_2 catalysts. They observed that when Ag promoter was added to the Ru catalyst, the amount of adsorbed hydrogen decreased. Kumar et al. proposed and published the portal model for hydrogen adsorption over $Ru\text{-}Ag/SiO_2$. In the model, they proposed that Ag is located the H_2 adsorption gateways on Ru catalyst (Figure 8). So, H_2 molecules cannot go through Ru surface for dissociating. The equations of mathematical model and the related parameters are given below;

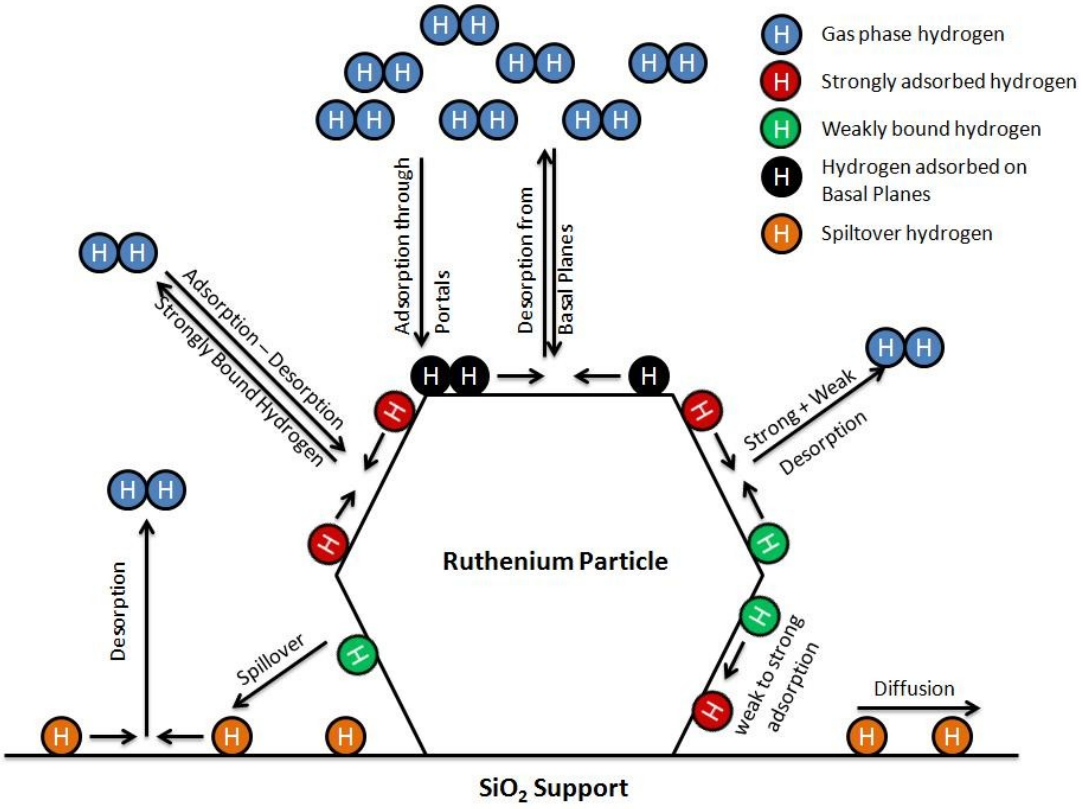

Figure 8. Schematic of portal mediated site adsorption proposed by Kumar et al.

For determining the strongly bound hydrogen coverage equation (3.10) was used;

$$R\frac{d\theta}{d\tau} = 2P\alpha_p f_p - 2\beta_1 R\theta^2 - \lambda\theta\phi - \theta(1-\phi) - \eta\theta \qquad (3.10)$$

The corresponding reactions related to symbolic values of equation (3.10) were given below,

$2P\alpha_p f_p$: $H_2 + 2S_{B.P.} \rightarrow 2HS_{B.P.}$

$2\beta_1 R\theta^2$: $2HS_W \rightleftharpoons H_2 + 2S_W$

$\lambda\theta\phi$: $HS_W + HS_S \rightarrow H_2 + S_W + S_S$

$\theta(1-\phi)$: $HS_W + S_S \rightleftharpoons HS_S + S_W$

$\eta\theta$: $HS_W + S_{S.P.} \rightarrow HS_{S.P.} + S_W$

For determining the weakly bound hydrogen coverage equation (3.11) was used;

$$\frac{d\phi}{d\tau} = 2P\frac{\alpha_b}{R}(1-\phi)^2 - 2\frac{\beta_2}{R}\phi^2 - \lambda\theta\phi + \theta(1-\phi) \qquad (3.11)$$

Similarly, the reactions related with corresponding to equation (3.11) were given below;

$2P\frac{\alpha_b}{R}(1-\phi)^2$: $HS_{B.P.} + S_S \rightarrow HS_S + S_{B.P.}$

$2\frac{\beta_2}{R}\phi^2$: $2HS_S \rightleftharpoons H_2 + 2S_S$

$\lambda\theta\phi$: $HS_W + HS_S \rightarrow H_2 + S_W + S_S$

$\theta(1-\phi)$: $HS_W + S_S \rightleftharpoons HS_S + S_W$

where, θ and ϕ represent the fractional coverages of strongly and weakly bound hydrogen respectively. S_S, S_W, $S_{S.P.}$and $S_{B.P.}$ correspond to the strong, weak, spillover and basal plane adsorption sites. R is the ratio between the total weak and strong binding sites. f_p is the fraction of all edge and corner sites act as a portal sites. All the other parameters are rate constants. Rate constant of all possible mechanisms such as adsorption, desorption and spillover are normalized by the rate constant for movement of weakly bound hydrogen to strong binding sites. The rate constants are given in Table 2.

Table 2. Model parameters and their values of mathematical model of Kumar et al.

Normalized rate constant	Values
$\alpha_p = k_{ap}\frac{N}{k_m S_o W_o}$	1.0×10^{-6}
$\alpha_b = \frac{k_{abs}}{k_m}$	1.0×10^{-7}
$\beta_1 = \frac{k_{db}}{k_m}$	3.0×10^{-2}
$\beta_2 = \frac{k_{dbs}}{k_m}$	1.4×10^{-5}
$\lambda = \frac{k_{d2}}{k_m}$	1.0×10^{-4}
$\eta = \frac{k_{sp}}{k_m S_o}$	1.0×10^{-8}
$R = \frac{W_o}{S_o}$	1

Further, in order to define the spillover rate from Ru metal to SiO_2 support, Kumar et al. assumed that spillover rate from Ru metal to support surface is a first order process. The related equations and boundary conditions are given below;

$$\frac{\partial \psi}{\partial \tau^*} = \frac{\mu}{\varkappa}\frac{\partial}{\partial \varkappa}\left(\varkappa \frac{\partial \psi}{\partial \varkappa}\right) - \psi^2 \qquad (3.12)$$

$$-\frac{\partial \psi}{\partial \varkappa}\Big|_{\varkappa=1} = k_{sp}\theta\frac{W_o}{2\pi\rho D} \qquad (3.13)$$

$$\frac{\partial \psi}{\partial \varkappa}\Big|_{\varkappa=\varkappa_{mid}} = 0 \qquad (3.14)$$

where, $\varkappa$ represents the radial distance from the center of Ru metal particle to a location on SiO_2 support in polar coordinates, ψ is coverage of spillover hydrogen on the SiO_2 support and μ is the ratio between the diffusion constant on support to desorption rate constant which is shown in Eqn 3.14;

$$\mu = \frac{D}{k_{ds}{R_p}^2} \cong 0.05 \quad (3.15)$$

In simple terms, over a surface where adsorption taking place by Langmuir method, the coverage can be expressed as

$$\theta = \frac{KP}{1+KP} \quad (3.16)$$

It is clear from the above equation that the coverage of the hydrogen decreases either by a decrease in the pressure of the gas or by a decrease in the equilibrium constant of the species. As demonstrated by Uner [71] very explicitly for Fischer Tropsch synthesis, the net effect of the addition of alkali promoters was to decrease the equilibrium constant of hydrogen adsorption. Since the surface coverage of the spilled over hydrogen is directly proportional to the surface coverage of chemisorbed hydrogen over Ru, decreasing the surface coverage over Ru immediately inhibits the spillover process.

A similar effect can be obtained by simply decline of the hydrogen pressure. Another solution proposed for increasing ammonia synthesis reaction rate was to change the reactant feed ratio (H_2/N_2) from the stoichiometric value of 3 to 1.5. In 1979, British Petroleum Company took the patent of Ru on graphite support for M.W. Kellogg Brown Company for the purpose of declining of feed ratio [76]. After doing test studies for Ru catalysts, Kellogg Brown Company announced KAAP process in 1990 [77]. Decreasing the amount of H_2 in the feed decreases compression cost of the ammonia production process. So, activity and cost of the production process relationship in the presence of Ru and Magnetite catalysts gain a different perspective. Therefore, possibility of using Ru catalysts increased due to improvement on activity and production cost relation instead of Magnetite catalysts.

Siporin and Davis studied on intrinsic reaction rate of ammonia synthesis reaction over Ru and alkali promoted Ru catalysts [78]. It is observed that in the presence of alkali promoted Ru catalyst the reaction order for hydrogen was - 0.37, but for unpromoted Ru catalyst, it is - 1.

In 2000, Satoh et al. published the characteristic of hydrogen adsorption on sulfated zirconia supported Pt catalyst [79]. They prepared 0.5% wt. $Pt/SO4^{-2}$-ZrO_2 and Pt/ZrO_2 catalysts. Similar to the past H_2 adsorption and spillover studies, they reduced the catalysts and sent H_2 at 50 torr. They observed the change in the H_2 uptake on catalysts with time. Their results showed that the H_2 uptake amount of Pt/SO_4^{-2}-ZrO_2 catalyst is approximately two times higher than Pt/ZrO_2 catalyst. H_2 uptake amount for Pt/SO_4^{-2}-ZrO_2 and Pt/ZrO_2 catalysts were measured after 2 hours as 6.5 x 10^{19} and 3.7 x 10^{19}atoms/$g_{catalyst}$, respectively at 523 K. Then, they decided that the rate limiting step of the H_2 adsorption process over catalyst as spillover process. They calculated the activation energy for spillover process as 84 kJ/mol for Pt/SO_4^{-2}-ZrO_2 catalyst with a BET surface area of 121 m^2/g.

Hydrogen spillover can be a measurable phenomenon but cannot be detected by any measurement technique or observed directly. In 2003, Mitchell et al. proposed a technique called inelastic neutron scattering to quantify and detect spilled over hydrogen [80]. They claimed that two types of hydrogen species detected on Pt/C or Ru/C catalysts. First hydrogen species is on at the edge sites of the carbon support and the second hydrogen species is on the weakly bound layer of the carbon support.

Ralph T. Yang and his group focused on H_2 storage on support materials such as high surface area carbon materials. A big portion of H_2 storage into the support materials were achieved via spillover process [81]. In order to obtain dissociated or adsorbed hydrogen over support material precious metals were used. The highest amount of H_2 storage was achieved in the presence of Ru/AC.

Wang et al. investigated the role of oxygen groups for H_2 spillover over AX-21 doped with Pd nanoparticles [82]. They prepared two different AX-21 supports. One of them is oxygen modified, the other one is unmodified. When results of H_2 storage experiments are examined, the H_2 amount in the oxygen modified AX-21 material is higher than unmodified AX-21 material. In the light of experimental work, they commented that in the presence of oxygen groups, H_2 storage is more favorable. Similar results were obtained by Li and Lueking. Li and Lueking

investigated the effect of surface oxygen groups and water on H_2 spillover [83]. They enriched the Pt/AC surface via KOH treatment. XPS and FTIR results showed that oxygen density is higher than the untreated one. H_2 adsorption experiments showed that KOH treated sample has higher H_2 uptake amount, because after samples are treated with KOH, the amount of surface oxygens on the catalyst increased. These findings showed that spillover process carries on fast when the density of oxygen on the surface is higher.

Bhowmick et al. investigated the behavior of Pt doped and undoped single walled carbon nanotube on the exposure of hydrogen molecules [84]. They exposed the Pt doped and undoped SWCNTs to H_2 and at the same time measured the electrical conductivity of the samples. They observed that the electrical conductivity of the Pt-SWCNT is reduced rapidly than undoped SWCNT. Authors explained this observation as; in the presence of Pt metal, H_2 dissociated on the Pt-SWCNT and dissociated hydrogen species started migrating on the SWCNT. Electrical conductivity characteristics of the SWCNT materials mainly come from unsaturated bonds. In other words, SWCNT contains lots of double and/or triple C-C bond in its structure. This causes higher electrical conductivity via free electrons. These unsaturated bonds are saturated by spiltover hydrogen and electrical conductivity decreases.

In 2012, Roel Prins published a review about the spillover [85]. He argued that spillover in the presence of reducible oxide supported precious metal is a real phenomenon. But for non-reducible supports such as SiO_2, Al_2O_3 is not suitable for spillover. He supported his idea via DFT calculations and bonding energies of the hydrogen species over surfaces. He claimed that required bonding energy for a hydrogen species to bound non-reducible support is higher than available energy level.

In summary, H_2 and N_2 adsorption over Ru surfaces is competitive. There is an activation energy barrier for N_2 dissociative adsorption, but there is none for H_2. So, H_2 molecules can easily adsorb rather than N_2 molecules. This causes the H_2

poisoning effect in the presence of unpromoted Ru catalyst. In the presence of alkali promoted Ru catalysts, alkali promoter locates at the main gateways of H_2 adsorption and blocks the excess amount of hydrogen adsorption. As a result, amount of adsorbed hydrogen species are minor on surface in comparison to the unpromoted catalyst.

CHAPTER 4

AMMONIA SYNTHESIS PROCESS PERSPECTIVE

4.1 Ammonia Market & Economics

Ammonia has the second place in terms of production of inorganic chemicals around the world [86]. Annual ammonia production over the world was about 157 million tonnes in 2009 [86,87]. The produced ammonia was consumed mainly by three industries. The first one is fertilizer industry with approximately 80%. The second ammonia consumer is the fiber industry consuming about 10% of world ammonia production, and third explosive industry with 5% consumption (Figure 9).

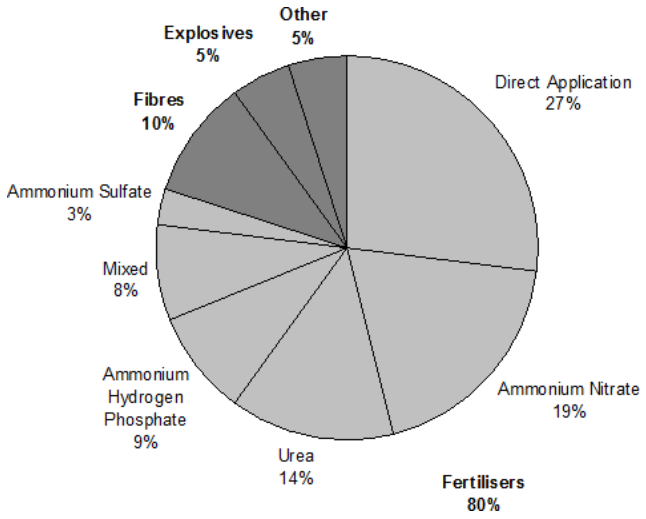

Figure 9. Uses of ammonia in market, by percentage [88]

According to IEA's (International Energy Agency) report, ammonia production is one of the most energy intensive processes in chemical technology. Ammonia plants having a production capacity of 1.5 million tons per year consume

approximately 2.25 EJ ($2.25x10^{18}$ Joule) energy [89]. The top energy consuming processes are given in Figure 10.

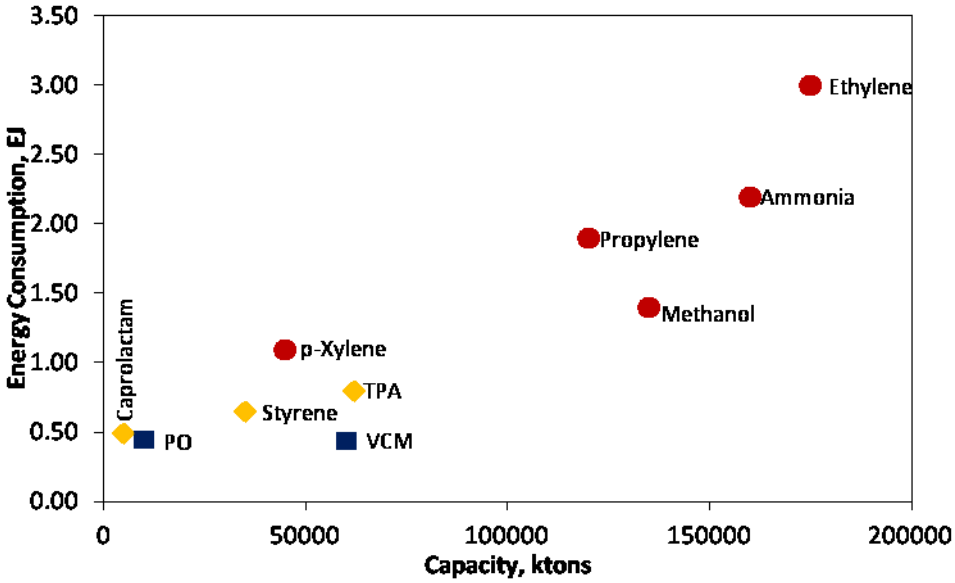

Figure 10. Top energy consuming processes over the world [89]

The main cost items of ammonia synthesis process come from compression cost required by the high pressure process and hydrogen production and purification steps. In order to decrease the cost of the process, hydrogen should be produced with less energy requirement and overall process should be operated at lower temperature and pressures. Although, over 100 years (the most important milestones for improvement of ammonia production process over years was given in (Figure 11), scientists and industry developed lots of technology to decrease the cost of ammonia synthesis, it is still in the first place in terms of the energy requirements. Decreasing the energy requirement can be possible with various system changes such as introducing a new catalyst or catalyst system which is active at lower temperatures and pressures or developing a kind of intensification on the process.

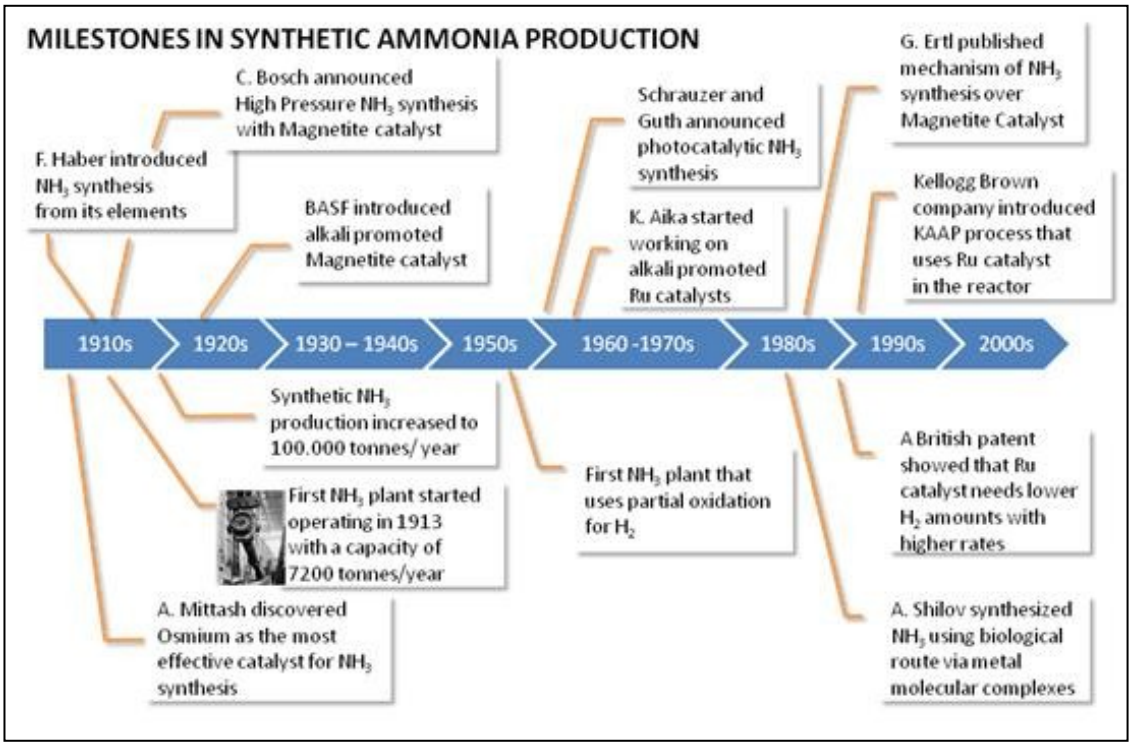

Figure 11. Milestones of synthetic ammonia production over 100 years

4.2 Process Details and Thermodynamics of Synthetic Ammonia Production

Today, there are three common ways of producing hydrogen for synthetic ammonia via Haber - Bosch process. These ways are;

- Steam reforming of light hydrocarbons
- Partial oxidation of heavy hydrocarbons
- Coal gasification

All of the three processes depend on the production of synthesis gas at first step. Conceptually the other steps are similar which mainly consists of conversion of by-products to hydrogen, purification of reactants and ammonia synthesis.

The main flow diagrams of steam reforming and partial oxidation route for ammonia synthesis are given below:

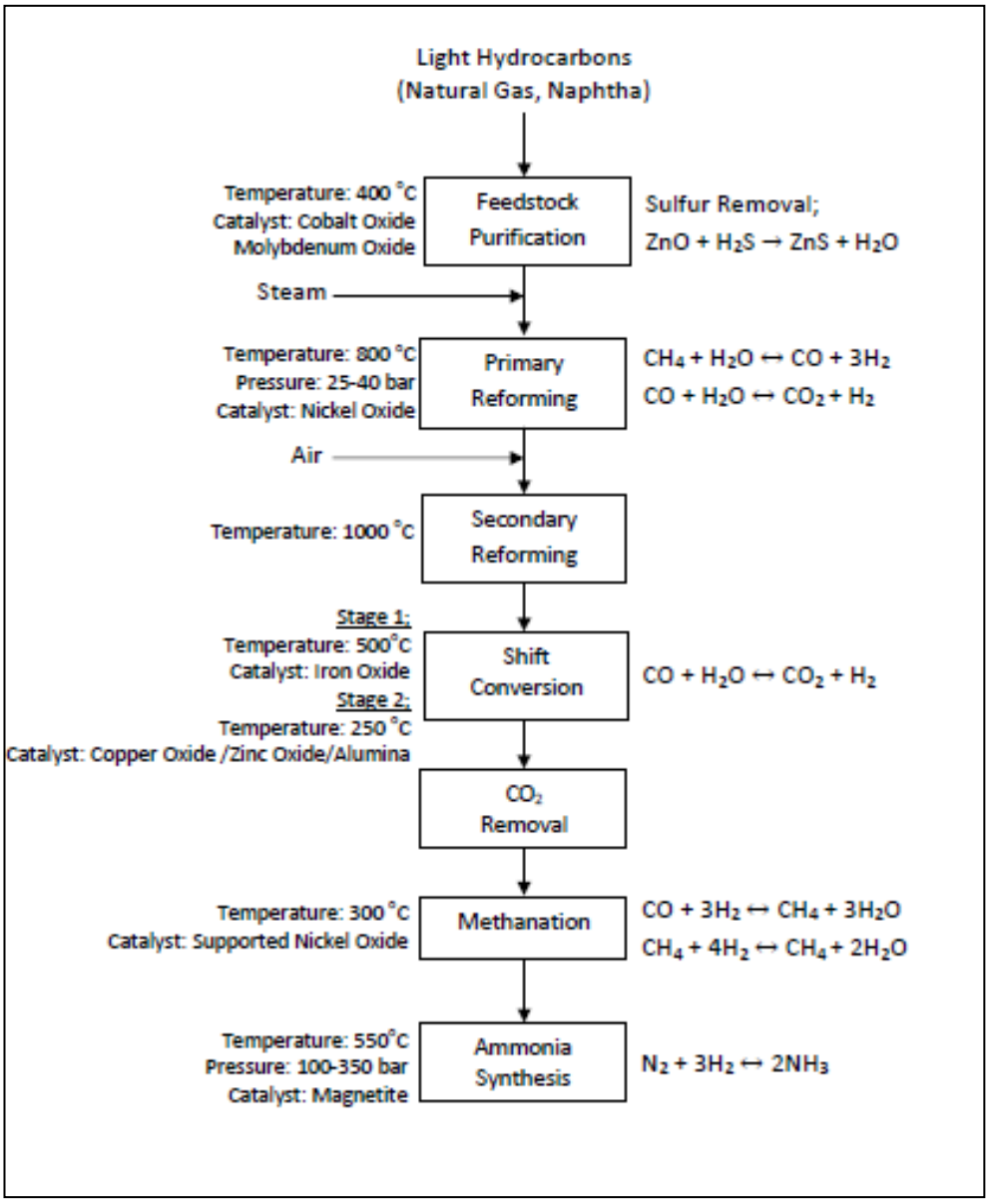

Figure 12. Flow diagram of steam reforming of light hydrocarbons route for ammonia synthesis [90]

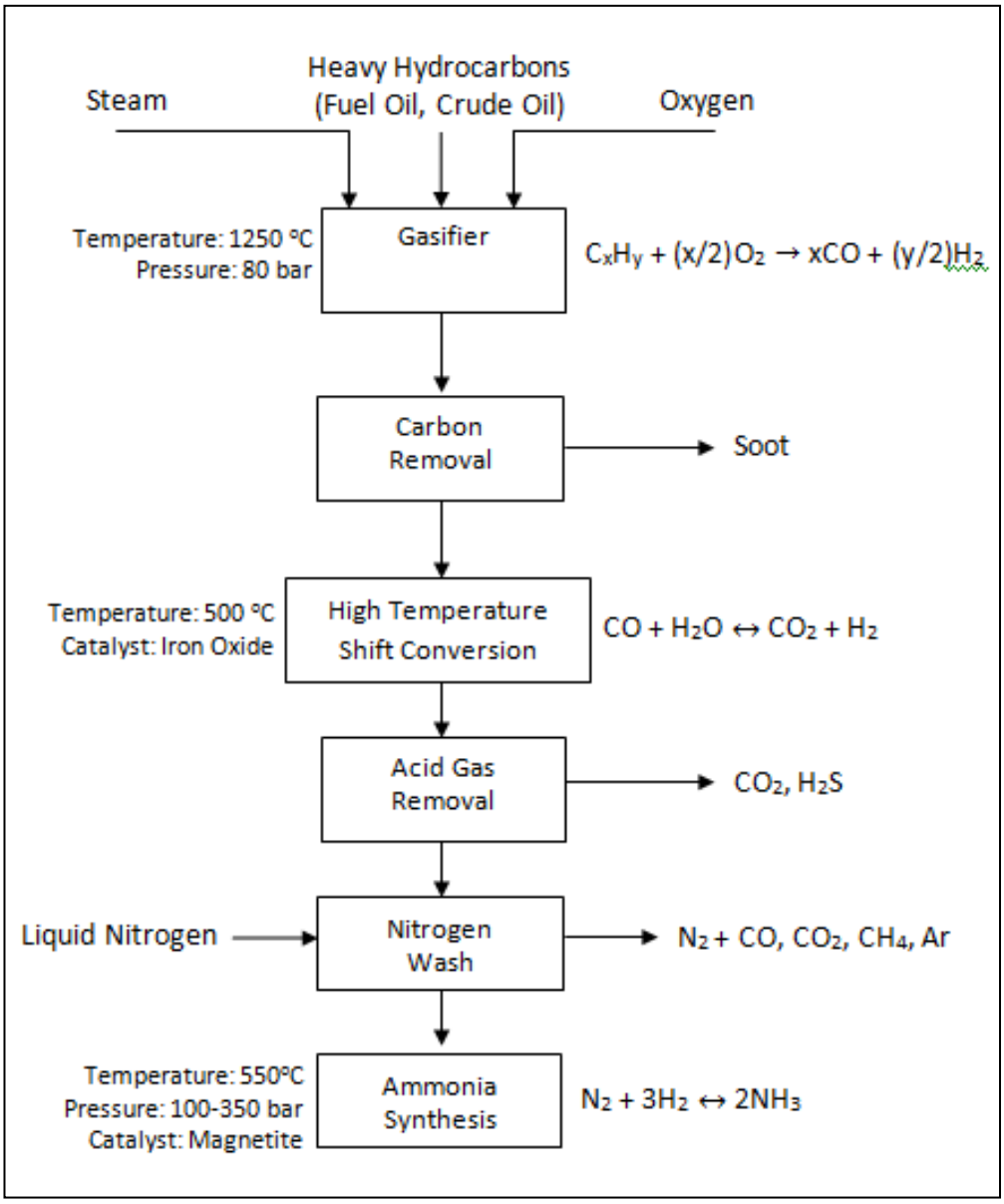

Figure 13. Flow diagram of partial oxidation of heavy hydrocarbons route for ammonia synthesis [90]

Figure 12 and Figure 13 show detailed process steps for ammonia synthesis via light hydrocarbons such as natural gas, naphtha and heavy hydrocarbons such as crude oil, and fuel oil, respectively. If these two diagrams are examined carefully, it is easily observed that ammonia production is done at the last step of the process. The main aim of other steps is the hydrogen production from hydrocarbon and its

purification. Any improvement in these steps via process intensification decreases the energy requirement of the process.

4.2.1 Why Do We Need High Pressures?

The net reaction ammonia synthesis from its elements is shown below;

$$N_{2_{(g)}} + 3H_{2_{(g)}} \rightleftharpoons 2NH_{3_{(g)}} \qquad 2$$

If the reaction stoichiometry is examined carefully, four volumes of reactants enter the reaction and only 2 volumes of products can be obtained. We can make the same statement for pressure, number of molecules. According the Le-Chatalier's principle, "*If a chemical system at equilibrium experiences a change in concentration, temperature, volume, or partial pressure, then the equilibrium shifts to counteract the imposed change and a new equilibrium is established*"[91]. Equilibrium constant of the system defined in terms of activities are

$$K = \frac{(a_{NH_3})^2}{(a_{N_2})(a_{H_2})^3} \qquad (4.1)$$

where

$$a_i = \frac{\bar{f}_i(T,P,y)}{\bar{f}_i{}^o(T,P=1\ bar,y_i{}^o)} \qquad (4.2)$$

If we choose the standard state as the pure gas at 1 bar then this equation reduces to

$$a_i = \frac{\bar{f}_i(T,P,y)}{1\ bar} \qquad (4.3)$$

At high pressures, the activity takes the following form

$$a_i = \frac{P_i\varphi_i(T,P,y_i)}{1\ bar} \qquad (4.4)$$

At lower and moderate pressures, the activity simplifies to

$$a_i = \frac{P_i}{1\ bar} \qquad (4.5)$$

In terms of fugacities and mole fractions, equilibrium constant for ammonia synthesis reaction

$$K = \frac{(y_{NH_3})^2(\varphi_{NH_3})^2}{[(y_{H_2})^3(\varphi_{H_2})^3][(y_{N_2})(\varphi_{N_2})]}\frac{1}{P_T^2} \qquad (4.6)$$

where y_i is the mol fraction, P_T is total pressure and φ is fugacity coefficient of components. At high temperatures, fugacities of all components are approximately 1, so it can be negligible. It means that equilibrium shifts to the products. In Figure 14, equilibrium conversion values for ammonia synthesis reaction are given. Because of ammonia synthesis reaction from its elements has an exothermic character, at low temperatures, conversion values go to 1. This characteristic also indicates decreasing the energy requirements at low temperatures. But, at low temperatures the reaction rates are very low, even in the presence of catalysts. Designing a new catalyst working at low temperatures and pressures will be the next breakthrough in ammonia synthesis.

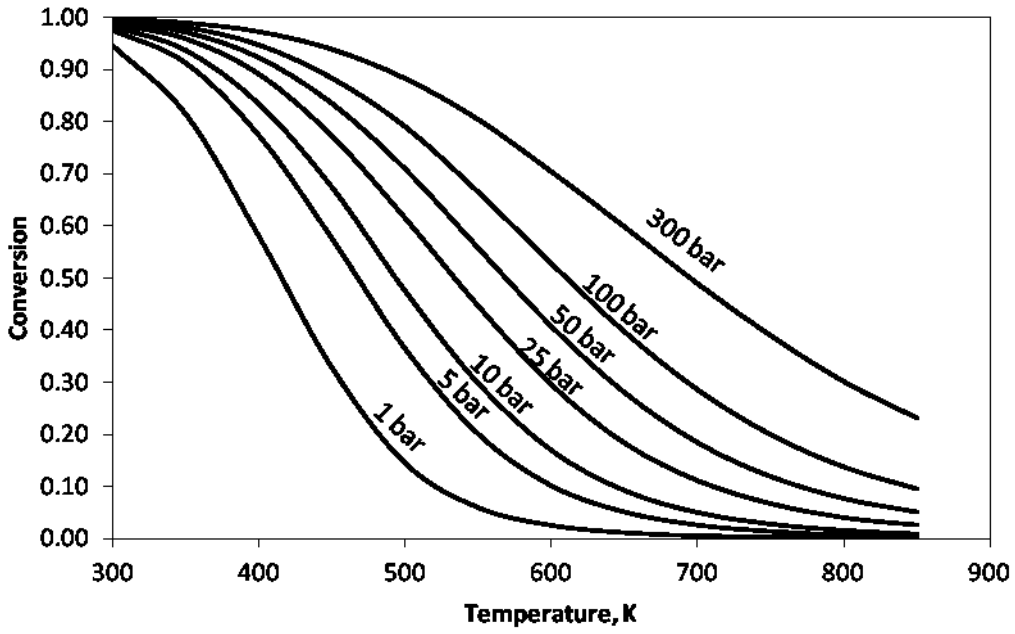

Figure 14. Equilibrium conversion curves at different operating pressures

4.2.2 Why Do We Need High Temperatures?

Another important parameter for ammonia synthesis is the temperature. Ammonia synthesis process is carried out at high temperatures such as 500 – 700 ^{o}C. Deciding operating temperature for ammonia synthesis depends on some parameters. First of all, at lower temperatures, conversion of nitrogen and hydrogen to ammonia is favorable. But at these temperatures reaction rate is too slow. At very high temperatures, equilibrium conversion is not favorable but the reaction rate is higher than that at lower temperatures. When these two distinct properties are taken into consideration, operating the process at higher reaction rates is preferred. The reason of that is directly related with the cost of the production. Cost of production for energy intensive processes are defined as the energy requirement per unit of desired product.

4.3 Existing Problems of Synthetic Ammonia Production at Industrial Scale

Over 100 years, there are lots of improvements in ammonia synthesis process such as radial flow ammonia synthesis reactor, innovations in H_2 production, heat recovery systems etc. Although lots of improvements are conducted up to now, ammonia production process has some bottlenecks which directly influence the efficiency and the cost of the process. These can be listed as:

1. Ammonia synthesis is a thermodynamically equilibrium reaction
2. Ammonia synthesis catalysts have a maximum conversion of 30% per pass in reactor.
3. Ammonia synthesis process should be operated at high pressure
4. Ammonia synthesis process requires excess H_2

Ammonia synthesis reaction from its elements is a thermodynamically equilibrium reaction. Changing of equilibrium constant with respect to temperature is given in Figure 15. As seen in Figure 15, equilibrium conversion of ammonia synthesis reaction at operating temperatures (673 – 773 K) is too small. At a defined

operating temperature and pressure, achievable conversion is fixed by the equilibrium limitations.

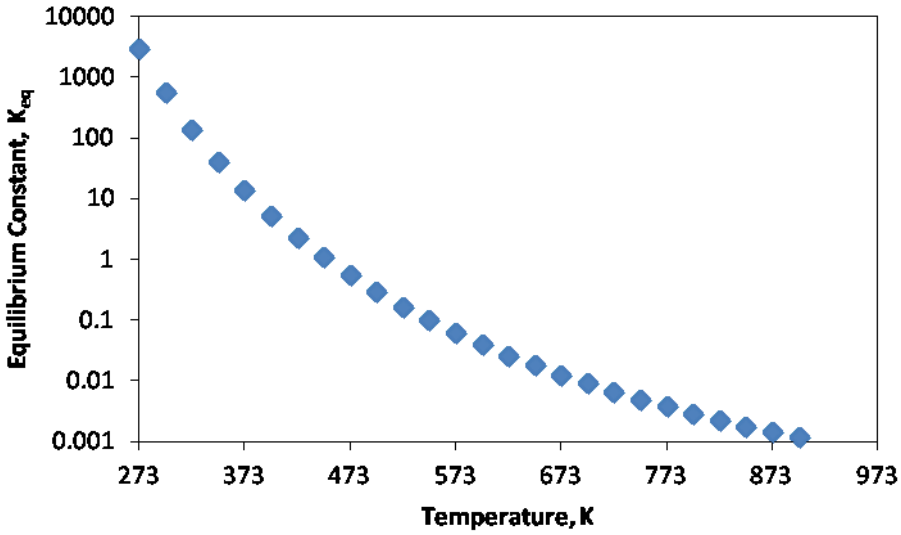

Figure 15. Change of equilibrium constant of ammonia synthesis reaction with temperature

Ammonia synthesis catalysts can be active at high temperature and pressure conditions. H_2 can easily adsorb either Fe based or Ru based catalysts at room temperature. However, N_2 generally behaves as an inert gas at room temperature. Dissociation of N_2 over ammonia synthesis catalyst can be achieved at high temperatures. Therefore, in order to achieve higher reaction rates, ammonia synthesis reaction should be carried out at higher temperatures.

One of the main cost items for ammonia production is compressor duty. There are several ammonia synthesis loops for ammonia production. Different characteristics of the loops cause different compressor duties. The main effect of variations of compressor duty from one loop to another come from the amount of added fresh reactant to the loop and the amount of recycled reactant inside the loop.

Reactant feed ratio directly influence the process cost per unit of produced ammonia. Due to the low conversions dictated by thermodynamic equilibrium, the presence of unconverted reactants is inevitable in the reactor. Hence, decreasing the

amount of hydrogen in the feed stream should not create reactant limitation problems in the reactor. By limiting the hydrogen amounts, the poisoning effect can be reduced as well as the compression cost due to the recycling. The amount of hydrogen in the reactant stream is an optimization problem which should be based on the detailed mechanism on the surface.

4.4 Analysis of the Main Problems of Ammonia Production at Industrial Scale

4.4.1 Modeling of Adiabatic Ammonia Synthesis Reactor using Temkin Reaction Rate

Temkin and Phyzev published a general reaction rate based on experimental data over magnetite catalysts [42]. Rossetti et al. published modified Temkin reaction rate expression over Ru/C catalyst [16]. This rate expression was verified by authors of the publication with experimental data. Modified Temkin rate expression was given below;

$$\frac{d\eta}{d\tau} = k_f \lambda(q) \frac{(a_{N_2})^{0.5}\left[\frac{(a_{H_2})^{0.375}}{(a_{NH_3})^{0.25}}\right] - \frac{1}{Ka}\left[\frac{(a_{NH_3})^{0.75}}{(a_{H_2})^{1.125}}\right]}{1 + K_{H_2}(a_{H_2})^{0.3} + K_{NH_3}(a_{NH_3})^{0.2}} \qquad (4.7)$$

Rossetti et al. designed this expression for both reactant feed ratio (H_2/N_2) of 3 and 1.5. So, the authors could show the effect of decreasing of feed ratio for ammonia synthesis reaction in terms of increasing of conversion at same operating conditions.

4.4.2 The Effect of Reactant Feed Ratio on Reactor Volume and Process Cost

The idea of decreasing the cost of the ammonia production process can be real with decreasing the reactant feed ratio (H_2/N_2). A British patent showed that, Ru catalysts show higher activities when H_2/N_2 feed ratio is selected as 1.5 compared the traditional H_2/N_2 feed ratio of 3 [17]. After that, Rossetti et al. showed the same idea experimentally. Rossetti et al [16] do not show only the feed ratio comparison for Ru

catalysts but also compared Ru catalysts with Fe catalyst. In this manner, constructing the equilibrium curves for H_2/N_2 feed ratio 1.5 and 3.0 can give us an understanding about the activity of the Ru catalyst. Figure 15 showed that, the equilibrium curve of H_2/N_2 feed ratio of 1.5 is the left side of the H_2/N_2 feed ratio of 3. This means that, at same operating temperature, the conversion value of H_2/N_2 feed ratio of 1.5 is higher than H_2/N_2 feed ratio of 3.0. In such energy intensive systems, increasing the ammonia synthesis reaction conversion has an important role in terms of decreasing the cost of the process.

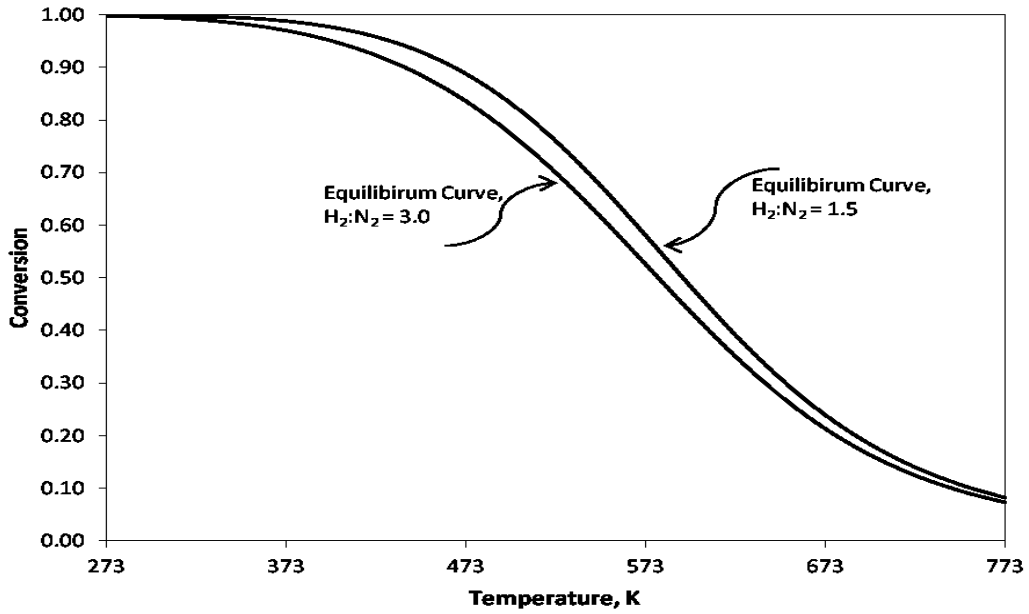

Figure 16. Behavior of Equilibrium Curve of Ammonia Synthesis Reaction with Different Feed Ratios

Figure 16 shows the equilibrium curve behaviors of H_2/N_2 feed ratios of 1.5 and 3.0. Calculations of equilibrium curves with respect to temperature are drawn using data of Rossetti et al. Besides the equilibrium curve calculations, preliminary reactor design calculations were performed using Modified Temkin reaction rate for ammonia synthesis and determined the reactor volumes for different feed ratios and different inlet temperatures. The summary of the reactor volume calculations are given in Table 3.

Table 3. Effect on reactor volume of feed ratio (H_2/N_2) change from 3.0 to 1.5 in ammonia synthesis reaction

H_2/N_2 Feed Ratio	Inlet Temperature, K	Conversion	Volume of Reactor, L
1.5	573	0.32	43.30
1.5	623	0.30	35.64
1.5	673	0.30	40.95
3.0	573	0.21	33.85
3.0	573	0.27	205.98
3.0	623	0.21	33.59
3.0	673	0.21	2789

As seen in Table 3, the reactor volumes for different feed ratios are in the same order of magnitude. But, conversion values of H_2/N_2 feed ratio of 1.5 are one and a half times higher than H_2/N_2 feed ratio of 3.0 at same temperatures. In addition to this, if we would like to increase the conversion value from 0.21 to 0.27 for H_2/N_2 feed ratio of 3.0 at 573 K, required reactor volume increases from 33.85 L to 205.98 L. In other words, according to preliminary ammonia synthesis reactor volume calculations, increasing the conversion amount at traditional operating reactant stoichiometry brings an additional reactor volume with respect to new concept of H_2/N_2 feed ratio of 1.5.

Another solution for decreasing the cost of ammonia synthesis process can be cold feed injection technology. Generally, commercial ammonia synthesis reactors have intercooling systems. After reactants passed through the first catalyst bed, this gas composition including a portion of reactant and product goes through the heat exchanger (cooler) to get rid of some extra energy. In cold injection technology, a determined amount of reactant is sprayed over the gas composition when cooling operation carries on. Spray cold reactant to gas composition have two main advantages. The first one is about the sensible heat of gas composition. The required energy duty of cooler can be decreased by cold feed injection method due to temperature gradient. The second advantage is about the conversion. When cold reactant feed is sprayed through the gas composition, molar fraction of the product, ammonia, decreases and this naturally is a reason of increasing the reaction rate of ammonia synthesis at same temperature.

In this thesis study, the effect of cold feed injection and intermediate heat exchange on reaction rate is investigated. In Figure 17, reaction rates are found larger in the presence of cold feed injection technology.

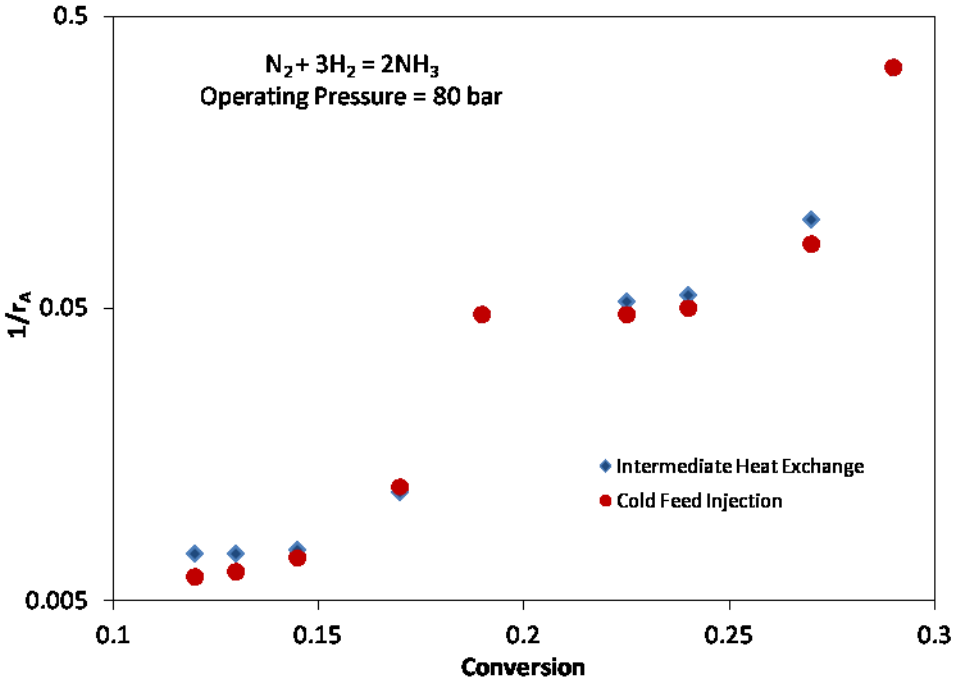

Figure 17. The design plot of ammonia synthesis reactor in the presence of two different cooling technologies.

All the calculations and graphs regarding to ammonia synthesis reactor calculation can be found in Appendix A.1 part of the thesis.

4.4.3 ChemCAD Ammonia Synthesis Loop Simulations

Ammonia synthesis reactor requires recycling of unreacted raw material due to the low conversions. 30 % of the reactants can be converted into ammonia per pass in a reactor. Remaining reactants are recycled.

On the other hand, ammonia synthesis reactors are operated at high pressures. One of the main cost items for ammonia production process is compression cost. In Figure 18, main steps for ammonia synthesis loop are given. Different alternatives are proposed in this figure for compressing the reactants and/or products. In Figure

18, dry and pure synthesis gas goes through the ammonia converter (a) then ammonia is condensed in the separator (b). After that, unreacted synthesis gas is recycled to the loop via compressors. Compressor section contains two compressors. While the first compressor (d) compresses the dry and pure synthesis gas to ammonia synthesis loop, the other one (e) compresses the unreacted gases to the loop.

If synthesis gas has some impurities such as CO_2 and water for ammonia synthesis, the place of the separator and the ammonia converter change (Figure 18B). The main reason is that ammonia is a very powerful chemical for absorbing gas impurities such as CO_2 and water. In this way, synthesis gas is cleaned via product ammonia but the quality of the ammonia decreases. This type of synthesis loop has two main disadvantages. The first disadvantage is that, ammonia separation in the separator is harder with respect to Figure 18A synthesis loop due to dilution of ammonia with fresh synthesis gas. The second problem is the concentration of ammonia at the inlet of the converter.

A new synthesis loop shown in Figure 18C is developed to overcome these problems. This ammonia synthesis loop is known as “four-nozzle compressor ammonia synthesis loop”. In this loop, a new design of compressor arrangement is used. In this design, the compression duties of compressors are separated from each other. The compressor (d) is only responsible for the compression of fresh synthesis gas and the compressor (e) is responsible for compression of pure synthesis gas. In this way, the extra energy which is wasted in the classic compressor design in Figure 18B is gained via new compressor design.

At very high operating pressures such as 25 MPa, using Figure 18D design can be more efficient. In this design, a new cooler (c) is added to the system after ammonia converter. At higher pressures, a great portion of ammonia can be liquefied at separator (c) via cooling water and air. In this situation, the amount of recycled gas decreases and the cost of the compression decreases. On the other hand, because of getting a great portion of ammonia in separator (c), the quality of the product increases with respect to design B and C.

In this manner, decreasing the compression cost of the process is one of the main purposes for companies. At early stages of Haber-Bosch process, energy requirement for 1 ton ammonia was 90 GJ. Nowadays, this value is decreased to 30 GJ per ton of ammonia. In order to decrease the energy requirements to lower values, some breakthroughs in ammonia synthesis technology are still needed. As mentioned earlier, ruthenium metal is highly active for ammonia synthesis at milder conditions with respect to the traditional magnetite catalyst. Using ruthenium catalyst instead of magnetite catalyst, process can be operated at low temperatures and pressures. This improvement brings reduction in the operating costs. Another improvement which comes with ruthenium catalyst is using below the stoichiometric ratio. According to recent studies, ruthenium can exhibit better catalytic performance for ammonia synthesis at lower hydrogen presence in the reactor than stoichiometric ratio of N_2:H_2=1:3. This idea has not been used up to now by the industry due to the cost of ruthenium catalyst. Ruthenium catalyst is approximately 10^4 times more expensive than magnetite catalyst.

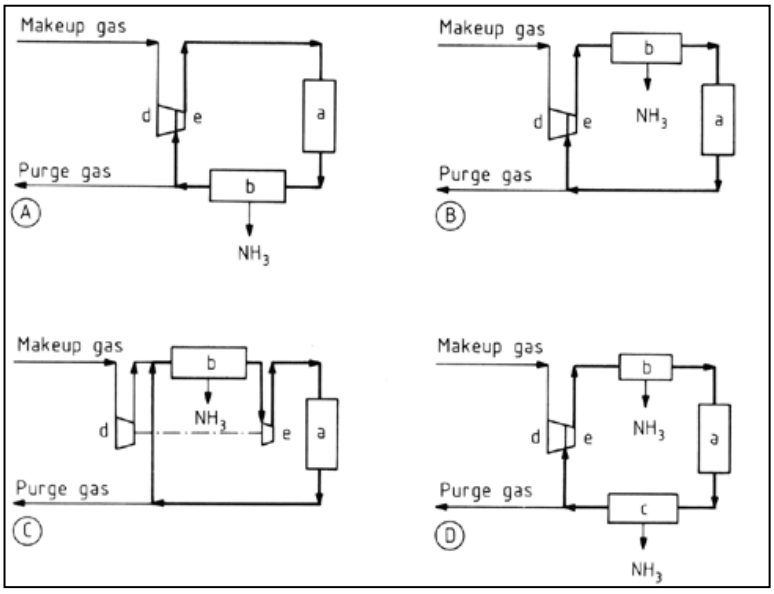

Figure 18. Different Types of Ammonia Synthesis Loops [87]

a) Ammonia converter, b) ammonia separator via condensation and chillers, c) ammonia separator via cooling water or air, d) fresh synthesis gas compressor, e) recycle gas compressor

In this part of the thesis, the relation between the compressor duty of the ammonia synthesis process and the type of the synthesis loop was investigated. In order to do this investigation the characteristics of different synthesis loops were examined via CHEMCAD, chemical engineering unit operations simulation program was used. Additionally a relationship between the compressor work and reaction conversion was established.

The result of the change of compressor work with respect to reaction conversion was given in Figure 19. There is a close relationship between the recycle amount of unreacted H_2 and N_2 and the compressor duty. When, the conversion of the reactor increases, amount of unreacted gases decrease. Therefore, amount of recycled gas and compressor duty decrease. One of the main cost items of the ammonia production is the compressor duty.

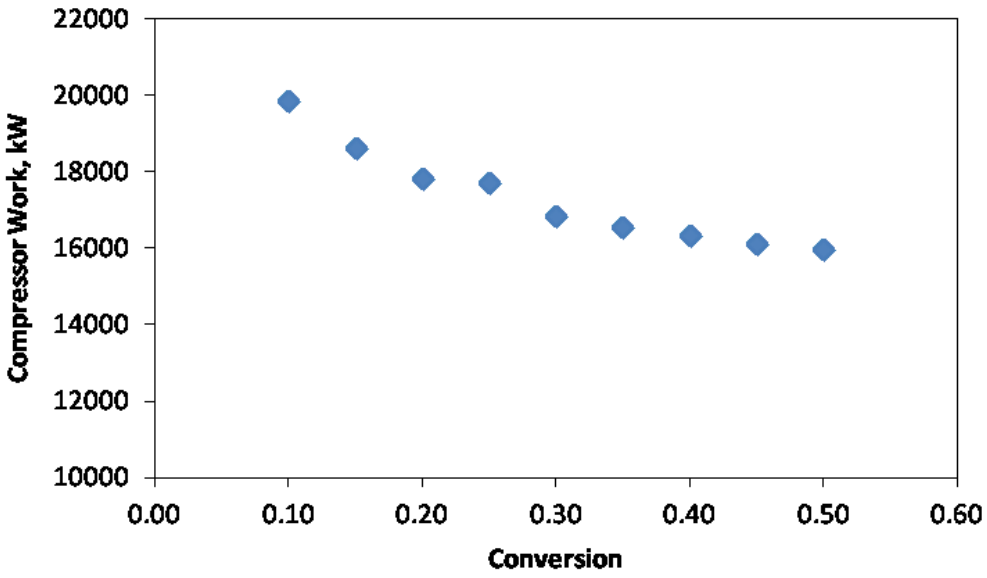

Figure 19. Changing of Compressor Work with respect to Ammonia Synthesis Reaction Conversion

The CHEMCAD simulation results of the ammonia reactor recycle configurations shown in Figure 18 are given in Table 4. Details of the simulation calculations and parameters are given in Appendix A.2. As seen from the table, even when, produced

ammonia amounts are same with same reactor conversion values, compressor duty of synthesis loops are very different.

Table 4. Comparison of Compressor Duties of Different Ammonia Synthesis Loops

	Compressor Work, kW	Produced Ammonia, kmol/h
Loop A	16852.5	357.6
Loop B	69863	339.5
Loop C	81574	339.5
Loop D	24439	347

CHAPTER 5

EXPERIMENTAL

5.1 Synthesis of Ruthenium Based Catalysts

1 wt % Ru/CNT, Ru/Vulcan, Ru/SBA-15 and Ru/SiO_2 catalysts were prepared via incipient wetness method. Appropriate amount of support material was weighed. Then the needed amount of ruthenium nitrosyl nitrate (Sigma-Aldrich) salt was dissolved in 2-3 ml/g water to bring about incipient wetness and added to the supports to prepare slurry. The slurry was mixed for a while. Finally, Ru/CNT, Ru/SBA-15 and Ru/SiO_2 catalysts were dried at 373 K in furnace overnight and reduced with H_2 in chemisorption manifold at 623 K.

Similarly, Na-Ru/Vulcan catalyst containing 1 wt. % Na and 1 wt. % Ru was prepared via incipient wetness co-impregnation method. First an apropriate amount of Vulcan was weighed. Then the needed amount of $NaNO_3$ (Merck) and ruthenium nitrosyl nitrate (Sigma-Aldrich) salts were dissolved in 2-3 ml/g water to bring about incipient wetness and added to the supports to prepare slurry. The slurry was mixed for a while. Finally, Na-Ru/Vulcan catalyst was dried at room temperature overnight and reduced with H_2 in chemisorption manifold at 623 K

5.2 Characterization of Ru-Based Catalysts

5.2.1 H_2 Chemisorption

The H_2 chemisorption measurement was done in a high vacuum manifold. Figure 21 shows the schematic representation of chemisorption manifold. The required steps for H_2 chemisorption experiments are given below (Figure 20):

Reduction of the catalyst:

1. About 200 mg catalyst is put into the sample cell.
2. Sample cell is connected to high vacuum manifold via high vacuum fittings.
3. Manifold is evacuated for app. 5 minutes then vacuum pump valve is closed in order to check if there is any leak into the system.
4. After the leak test, the system is evacuated again and 760 torr of helium gas is introduced to the manifold.
5. Sample cell is heated up to 423 K and kept at that temperature for 30 min.
6. Helium is evacuated and 100 torr of H_2 is admitted to the manifold.
7. Then sample cell is heated up to 623 K at a rate of 6 K/min.
8. After temperature is 623 K, the manifold is evacuated and 100 torr of H_2 is sent on to sample cell and waited for approximately 30 min.
9. After 30 min, H_2 gas inside the manifold and sample cell is evacuated and 500-600 torr H_2 gas is introduced to the system for 3 times with same 30 min. waiting and evacuation procedure.
10. After these steps, reduction of the catalyst is done. After that, sample cell is evacuated overnight at room temperature.

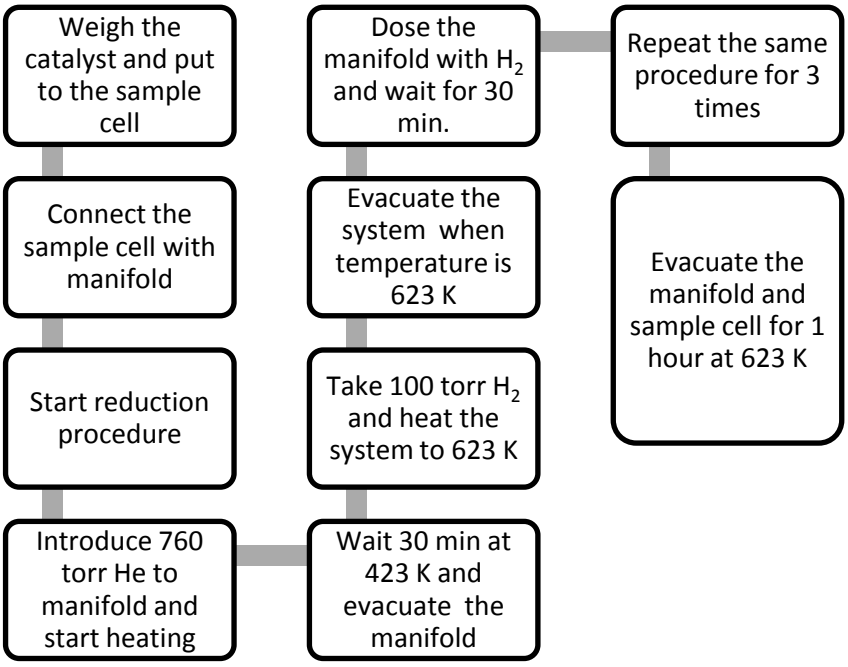

Figure 20. Reduction procedure of Ru catalysts at chemisorption manifold

After evacuation over night, total chemisorption measurement procedure is applied.

Total and weak adsorption:

In order to determine the dispersion of the metal over support total adsorption and weak adsorption procedures are applied to the catalyst. Dispersion of the catalyst is determined from the intercepts of the total and weak adsorption isotherms. So, total and weak adsorption measurements are recorded from low pressures to high pressures. The steps of measurements are given below (Figure 22):

1. Dead volume measurement is done in order to find the total empty volume in the presence of the catalyst. Approximately 50 torr of helium gas is sent to the manifold, the pressure is recorded. The pressure after opening the sample cell valve is also recorded. The use of ideal gas law allows one to calculate the total volume after expansion.
2. Helium gas is evacuated. Sample valve is closed and H_2 gas is introduced to the system. The pressure is recorded.

3. Sample valve is opened; system is allowed to reach thermal and chemical equilibrium for 10 min.
4. After, pressure is stabilized, pressure is recorded and valve is closed again pressure reading is recorded.
5. After the first H_2 chemisorption measurement is completed, more H_2 was introduced in the manifold while the sample valve is closed.
6. This procedure is repeated from 1 torr pressure to 600 torr pressure. After total isotherm measurement is done, manifold is evacuated for 10 min at room temperature to remove the weakly adsorbed hydrogen species over the catalyst.
7. Then weak adsorption measurement is done from 1 torr pressure to 600 torr pressure via same procedure with total adsorption.

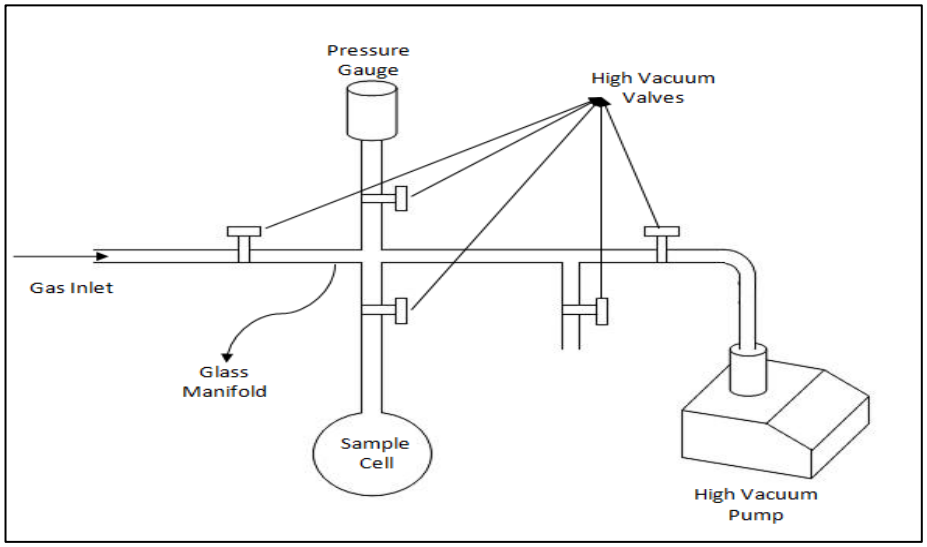

Figure 21. Schematic representation of chemisorption manifold

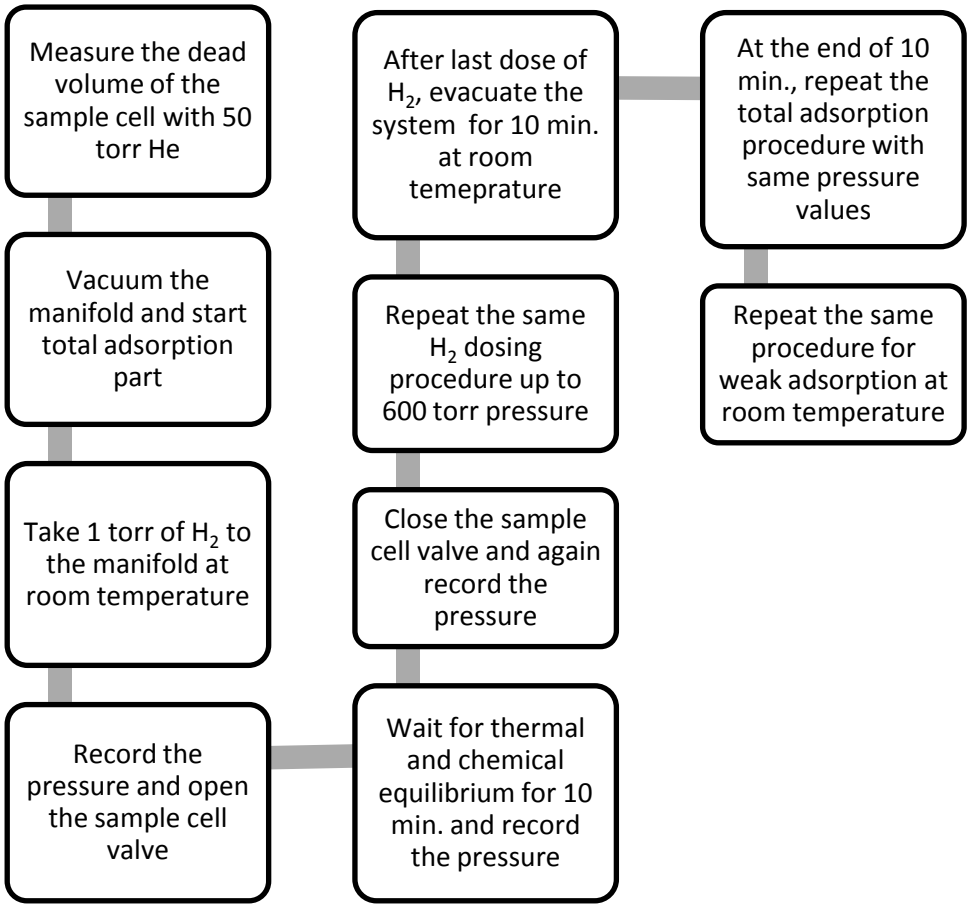

Figure 22. H_2 chemisorption procedure of Ru catalysts at chemisorption manifold

The effect of evacuation time for cleaning of the Ru surface after reduction was also examined. In the first set of experiments, Ru catalysts were evacuated for 2 hours at 623 K, and then H_2 chemisorption experiment was done. In the second set of experiments, Ru catalysts similarly were reduced and evacuated overnight at room temperature. As a result of the study, it is observed that the catalysts which evacuated overnight had higher H_2 uptake values.

During the adsorption measurements, there are kinetic limitations imposed by the pore mouth dimensions relative to the mean free path of the molecule. The isotherms do not necessarily represent the equilibrium conditions, since the time allowed for the process is shorter than required for equilibrium. By choosing a shorter time for the isotherm measurements, it is intended to establish the

adsorption/desorption equilibrium over the metal surface and stop the experiment before excessive amount of spillover occurred.

5.2.2 TEM Images

Surface morphologies and particle size distributions of Ru/SBA-15, Ru/SiO_2 and Ru/CNT catalysts are investigated using JEOL 2100 F high resolution transmission electron microscopy. In order to obtain TEM images of the catalysts, Ru/SBA-15, Ru/CNT and Ru/SiO_2 samples were dissolved in ethanol. The suspensions are kept overnight at room temperature. Then, samples are transferred to a Cu grid. The Cu grid was inserted to TEM and observation was done.

CHAPTER 6

RESULTS AND DISCUSSION

6.1 Results of Adsorption Studies

In this study, in order to reveal the H_2 adsorption characteristics over Ru metal, H_2 chemisorption experiments were performed. The dispersions of the metals were determined from strongly bound hydrogen amounts. Over the next paragraphs, the determination of the strong hydrogen amounts is briefly described.

In H_2 chemisorption measurements, H_2 uptake amount vs. pressure graphs were obtained. Strongly bound hydrogen is an arbitrary statement accepted in the literature for chemisorbed hydrogen that cannot be evacuated after 10 min of vacuum. Its determination requires the measurement of total hydrogen adsorption isotherm on a clean surface, and weak hydrogen adsorption isotherm collected after the strong hydrogen isotherm followed by evacuation for 10 min. The pressure ranges of the graphs were selected as from 0 torr pressure to 700 torr pressures. There are two main reasons of selecting the pressure ranges: The first reason is the determination of Ru metal dispersions of the catalyst at low pressure range. The second reason is the observation of adsorption characteristics of H_2 over Ru based catalysts at relatively (up to 700 torr) high pressures.

Low range H_2 adsorption experiments were performed in order to determine the dispersion of the precious metals. Dispersion of the supported noble metal catalysts are determined by the subtraction of the intercepts of total adsorption isotherm and weak adsorption isotherm. H_2 adsorption measurements were

performed at high pressure range (50 – 700 torr) due to observe the adsorption mechanism of the H_2 molecules over a supported nobel metal catalyst.

6.2 Dispersion Determination

6.2.1 H_2 Chemisorption

Ru/SiO_2

Chemisorption measurement of %1 wt. Ru/SiO_2 was given in Figure 23. The total H_2 uptake up to 620 torr pressure was measured as 475 μmol $H_2/g_{catalyst}$. The H/Ru ratio was calculated as 9.

When behavior of total adsorption isotherm was examined, there are two distinct regions: 1st region is up to 100 torr H_2 pressure. The 2nd region is between 100 torr and 700 torr. In the first region, a sharp increase was observed and the H_2 uptake was measured as 225 μmol $H_2/g_{catalyst}$. After 100 torr pressure, a gradual increase was observed. The H_2 uptake in the second region of the total adsorption isotherm was measured as 225 μmol/$g_{catalyst}$.

When weak adsorption isotherm was examined, a gradual increase with pressure increase was clearly observed. Total H_2 uptake for weak adsorption isotherms at 620 torr pressure was determined as approximately 150 μmol $H_2/g_{catalyst}$.

In order to determine the dispersion of the Ru/SiO_2 catalyst, low pressure range of H_2 adsorption graph was given in Figure 24. When total and weak adsorption isotherms of Ru/SiO_2 catalyst was examined at low pressure range in order to determine the dispersion of the catalyst, the intercept value of the total adsorption isotherm cannot be determined clearly. Because, the behavior of the total adsorption isotherm did not exhibit a distinct linearity at low pressure range. In addition to this, there were not any measured weak adsorption isotherm value at 0 – 30 torr. Therefore, the dispersion value obtained by using the intercept values as shown in Figure 24 cannot be said as clearly correct. If the dispersion of the Ru/SiO_2

catalyst was determined as seen from the intercepts of the Figure 24, the dispersion of the catalyst was determined as approximately 5%.

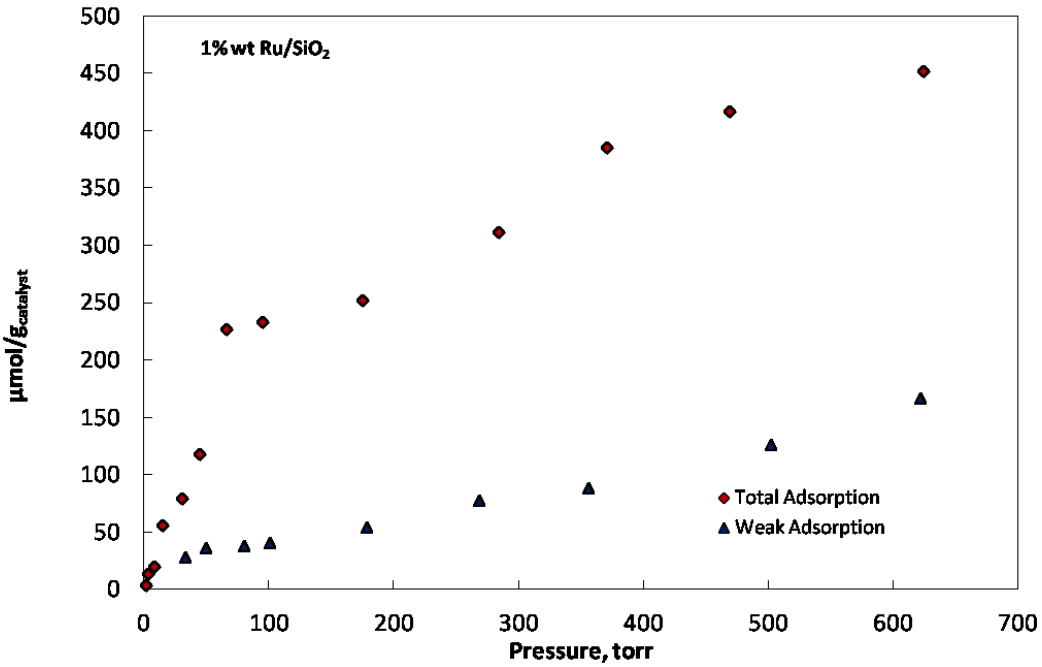

Figure 23. H_2 adsorption isotherms for 1% wt. Ru/SiO_2 at room temperature

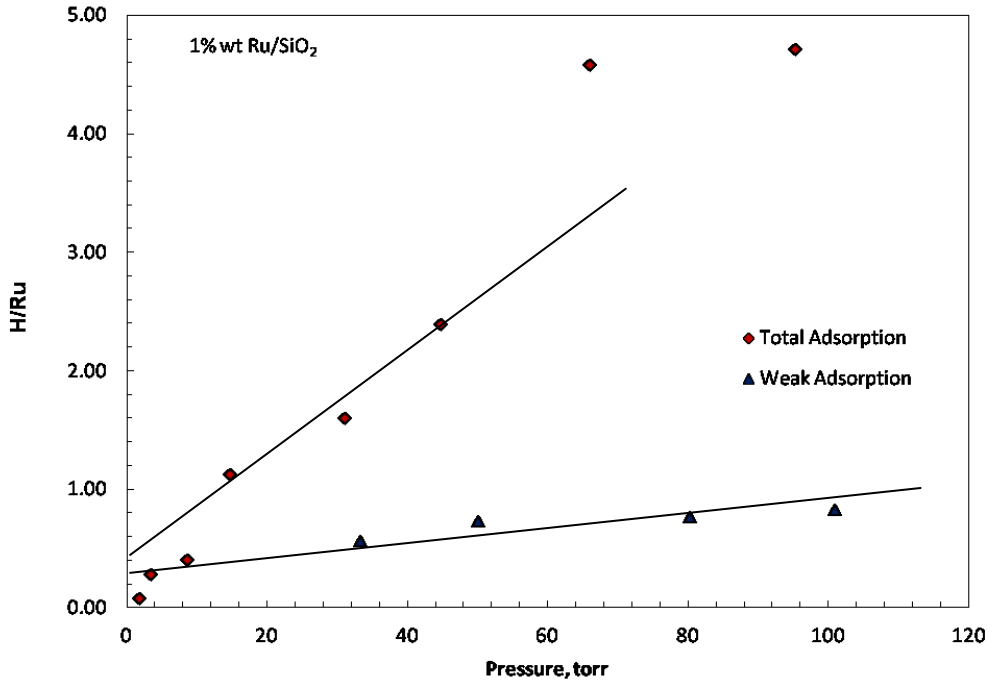

Figure 24. H_2 adsorption isotherm of 1% wt. Ru/SiO_2 at low pressure range

Ru/SBA-15

The H_2 chemisorption measurement of 1% wt. Ru/SBA-15 was given in Figure 25. The total H_2 uptake in total adsorption isotherm was measured as 1000 $\mu mol/g_{catalyst}$ in the presence of 475 torr H_2 pressure. H/Ru ratio for total adsorption isotherm was calculated as 20. The behaviors of total and weak adsorption isotherms are similar. The weakly H_2 uptake over Ru/SBA-15 catalyst was obtained as 775 $\mu mol/g_{catalyst}$ at 475 torr H_2 pressure and room temperature.

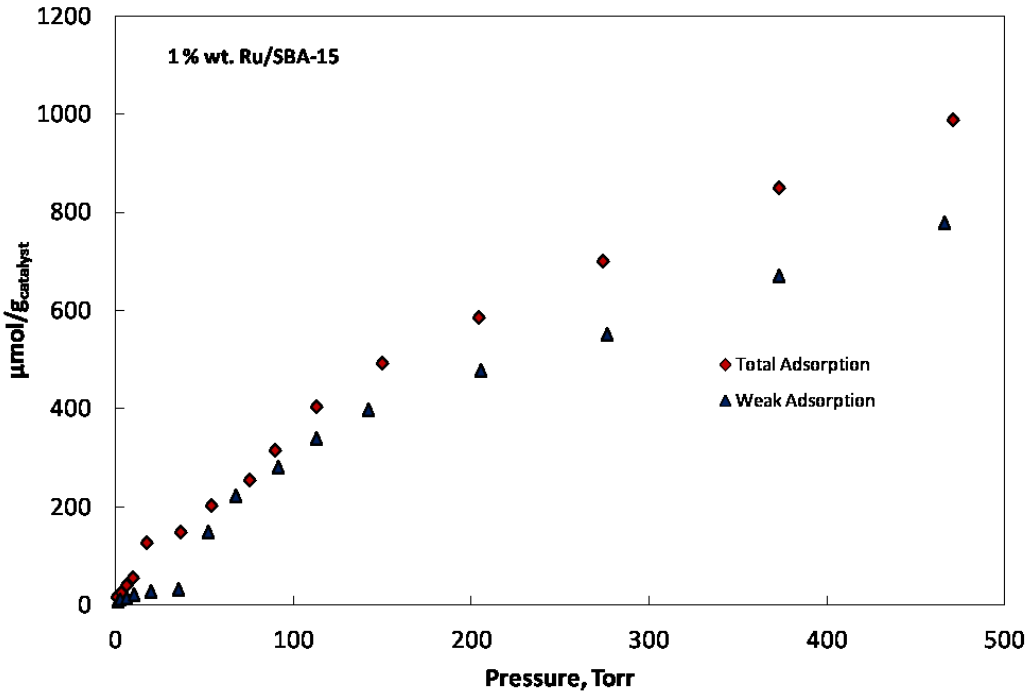

Figure 25. H_2 adsorption isotherms for %1 wt. Ru/SBA-15 at room temperature

The low pressure range of H_2 chemisorption isotherms of Ru/SBA-15 was shown in Figure 26. Using Figure 26, metal dispersion of the catalyst was determined as 10% via H_2 chemisorption.

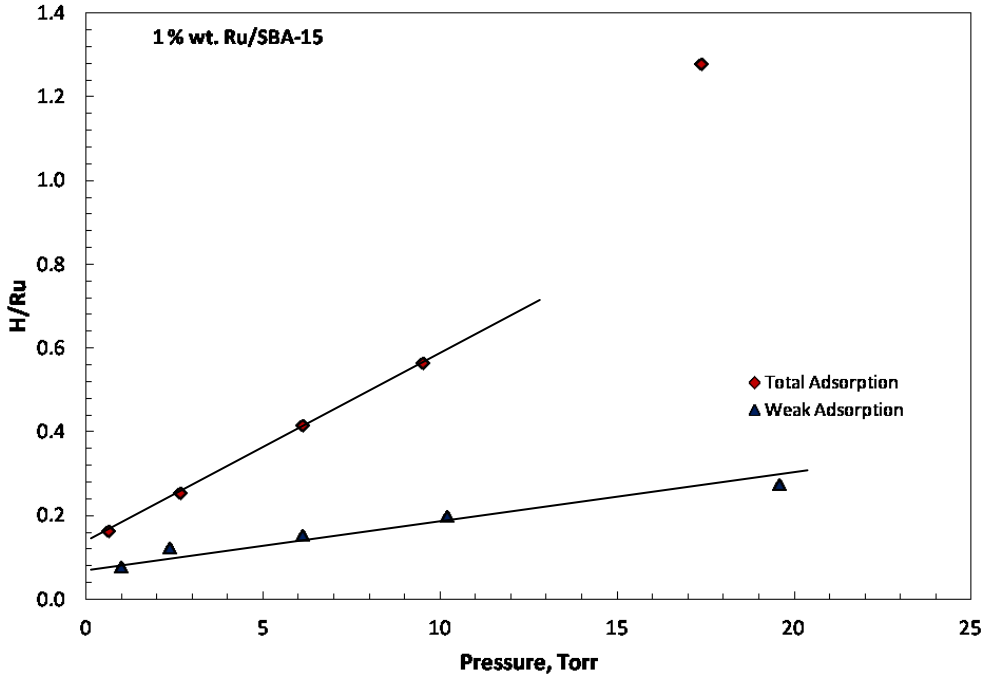

Figure 26. H_2 Adsorption Isotherm of 1 % wt. Ru/SBA-15 at Low Pressure Range

Ru/CNT

Mean free path can be defined as the average distance just before colliding with another gas molecule [92]. During the adsorption of H_2 over Ru/CNT, the adsorption kinetics imposed by the Knudsen diffusivity plays an important role. Because Ru metal particles are mainly located inside carbon nanotubes. When the pore diameter and mean free path of the molecules are close to each other, probability of penetration of molecules inside pores increases. The mean free path of a gas molecule can be determined via Eqn. 4.1 given below;

$$\lambda = \frac{k_B T}{\sqrt{2}\pi d^2 P} \qquad (4.1)$$

where T is temperature, P is pressure, k_B (= 1.380×10^{-23} J/K) is Boltzman constant and d is diameter of gas molecule.

H_2 chemisorption isotherms of 1 % wt. Ru/CNT were given in Figure 27. The total H_2 uptake measured at 500 torr H_2 pressure was 520 μmol $H_2/g_{catalyst}$. The H/Ru

ratio was determined as 10. When total adsorption isotherm of Ru/CNT catalyst was examined, two different behaviors were observed with increasing pressure. . Between 0 – 80 torr pressure range, it is observed that there is a gradual increase in H_2 uptake, but it has a small value and H/Ru was determined as 0.8 which is a smaller value than unity. At 80 torr, a sharp increase is observed from 40 µmol H_2 to 300 µmol H_2 per 1 g catalyst. After that sharp increase, a gradual increase was observed in H_2 adsorption isotherm from 300 µmol/$g_{catalyst}$ to 520 µmol H_2/$g_{catalyst}$.

The weak adsorption isotherm of Ru/CNT had a gradual increase behavior. The H_2 uptake at 500 torr H_2 pressure was measured as 240 µmol H_2/$g_{catalyst}$. When H_2 adsorption graph and relationship between total adsorption and weak adsorption isotherms were examined, a close relationship between the total and weak adsorption isotherms was observed in the low pressure range. The possible reasons of this behavior were discussed in discussion part.

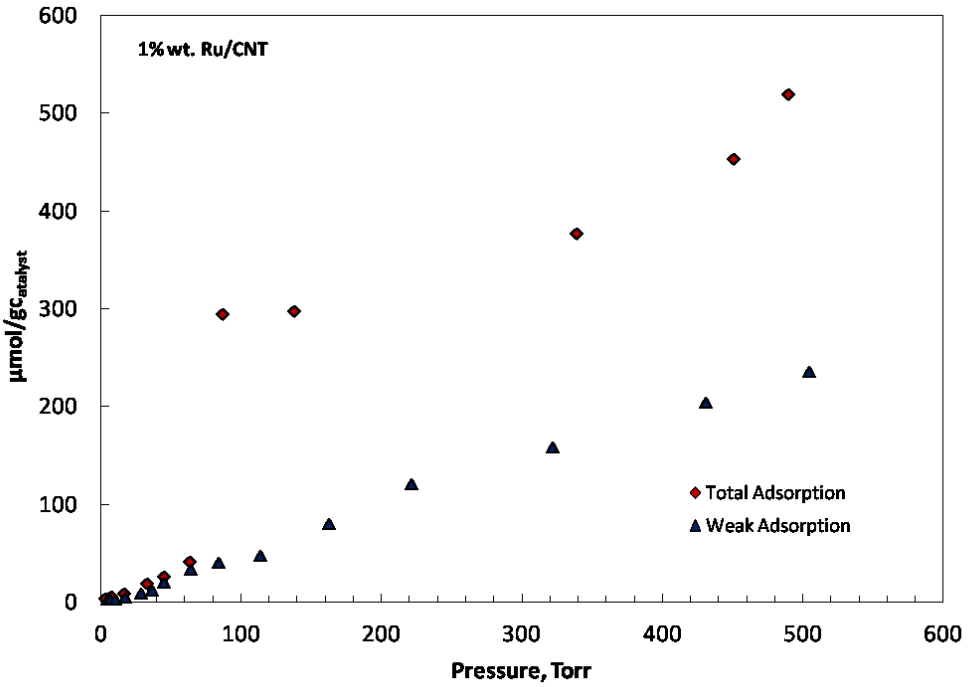

Figure 27. H_2 adsorption isotherm for %1 wt. Ru/CNT at room temperature

In order to determine the dispersion of the Ru/CNT catalyst, low range pressure H_2 chemisorption graph was given in Figure 28. The dispersion of the catalyst was determined as 1.5%.

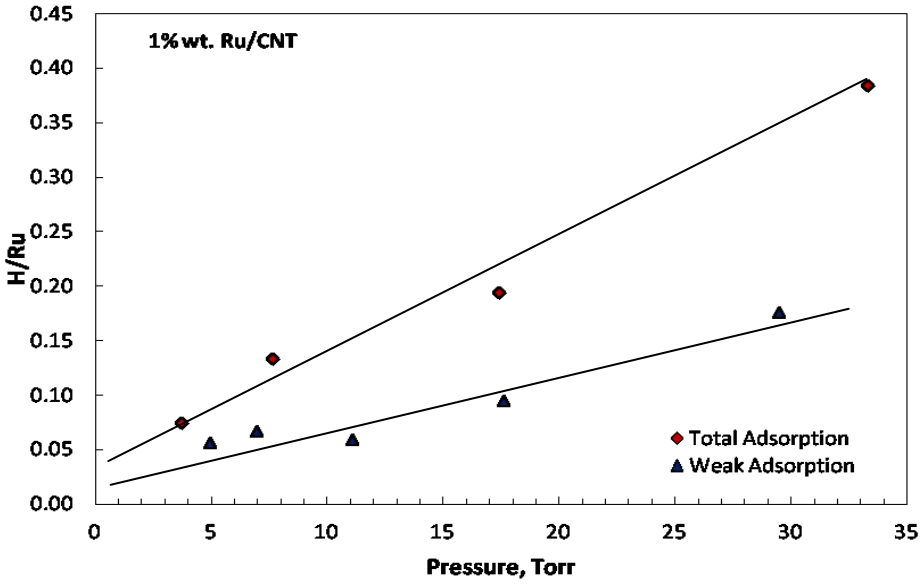

Figure 28. H_2 Adsorption Isotherm of 1 wt.% Ru/CNT at Low Pressure Range

Ru/Vulcan

The chemisorption experiment result of 1% wt. Ru/Vulcan catalyst was given in Figure 29. When Figure 29 was examined, the total H_2 uptake was measured as 110 μmol $H_2/g_{catalyst}$ at 580 torr H_2 pressure. H/Ru ratio was determined as 2. Total and weak adsorption isotherms of Ru/Vulcan catalyst had similar behaviors.

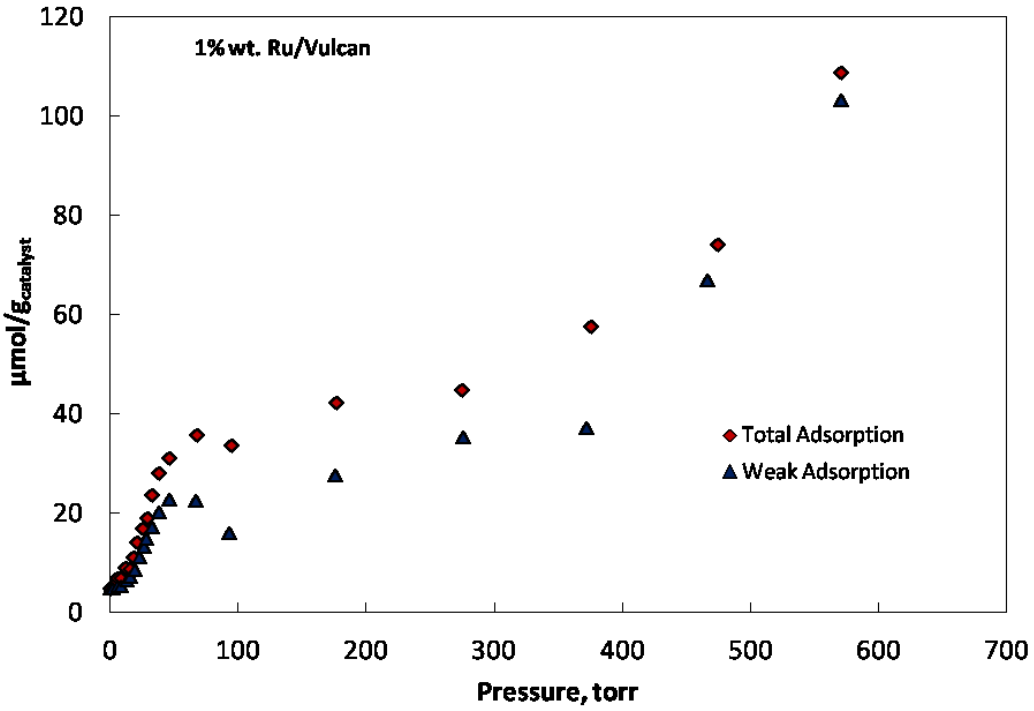

Figure 29. H_2 adsorption isotherm for %1 wt. Ru/Vulcan at room temperature

Dispersion of Ru/Vulcan catalyst was calculated as 27% from Figure 30. The dispersion determination was conducted in a different manner compared to other catalysts. When Figure 29 was examined carefully, it can be observed that there is a saturation between 80 and 300 torr pressures. At low pressure range, dispersion cannot be determined, because total and weak adsorption isotherms overlapped with each other.

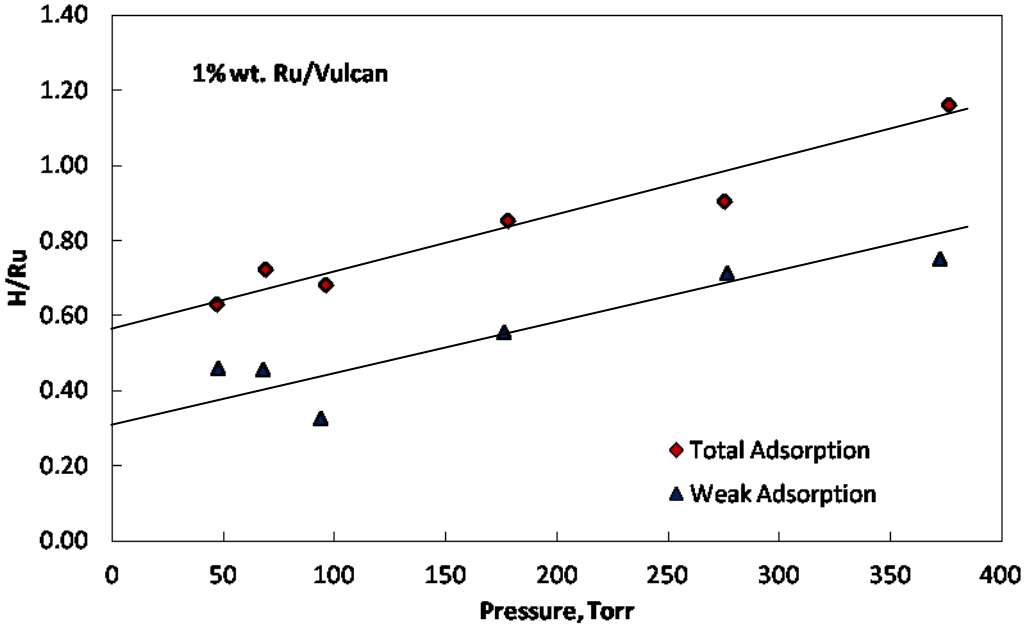

Figure 30. H_2 Adsorption Isotherm of 1 % wt. Ru/Vulcan between 50 and 400 torr pressure range

Na-Ru/Vulcan

Results of H_2 chemisorption experiment of Na-Ru/Vulcan (including 1 wt. % Na and 1 wt. % Ru) was given in Figure 31. H_2 uptake of Na-Ru/Vulcan catalyst was found as 180 μmol $H_2/g_{catalyst}$ at 575 torr pressure. H/Ru ratio was determined as 3.

The behaviors of total and weak adsorption isotherms were observed as similar at low pressure range. In other words, total adsorption isotherm and weak adsorption isotherm were overlapped each other as seen in Figure 32. After 200 torr pressure, the difference between the total and weak adsorption pressure increased with increasing pressure. Therefore, dispersion of the Na-Ru/Vulcan catalyst cannot be calculated.

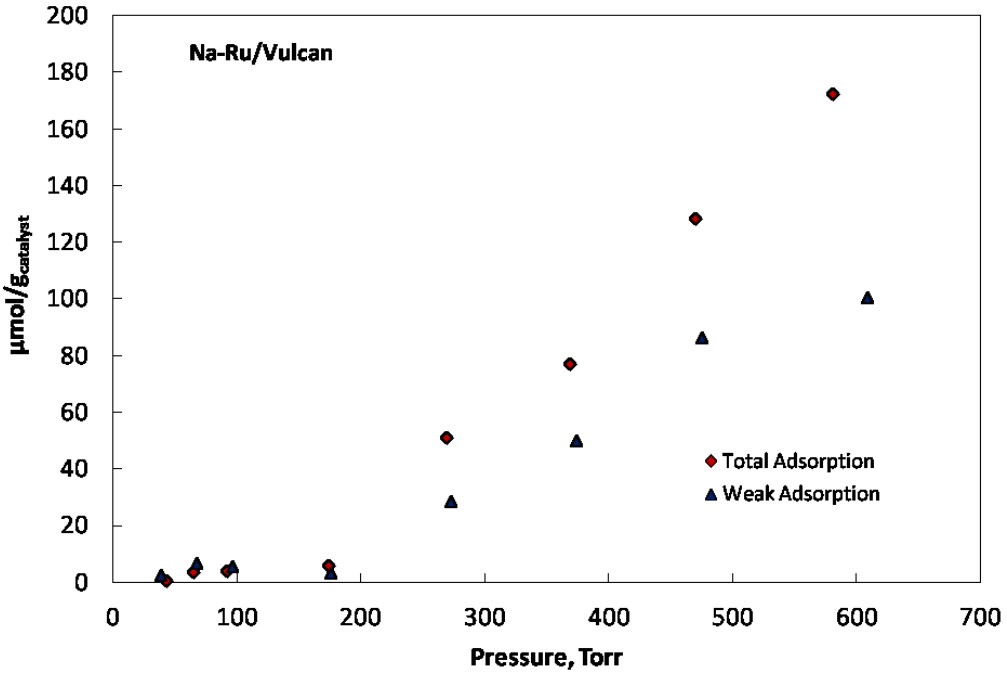

Figure 31. H_2 Adsorption Isotherm of 1 wt. % Na-Ru/Vulcan at room temperature

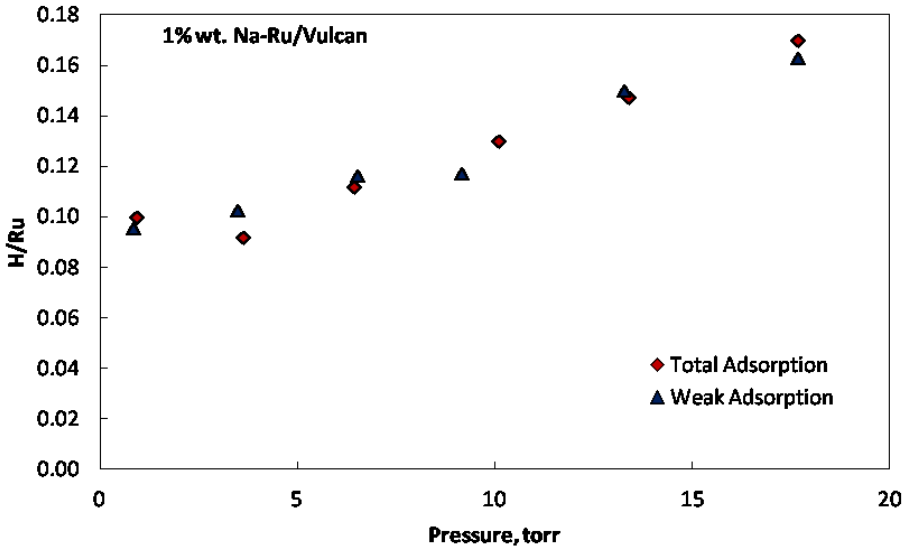

Figure 32. H_2 Adsorption Isotherm of 1 wt.% Na-Ru/Vulcan at Low Pressure Range

6.2.2 Transmission Electron Microscopy Images

TEM images of Ru/SiO_2 were given in Figure 33. Ru particles over SiO_2 support are dispersed with different sizes. The range of sizes of Ru particles varies

between 1 to 11 nm if all the particles are assumed as spherical. The most available particle size over SiO_2 support is 6-7 nm diameters. The particle size distribution graph of Ru/SiO_2 catalyst is given in Figure 33 (c). In Figure 33 (b), Crystal fringes of Ru metal is given. Lattice fringe of the Ru metal is reported as 0.27 nm in literature [93]. The lattice fringes of Ru metal were measured as 0.26 nm for Ru/SiO_2.

a)

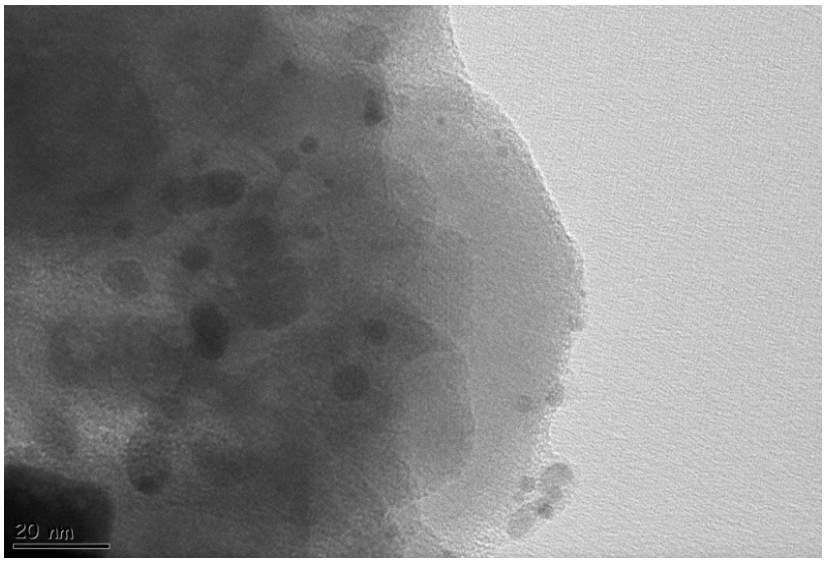

b)

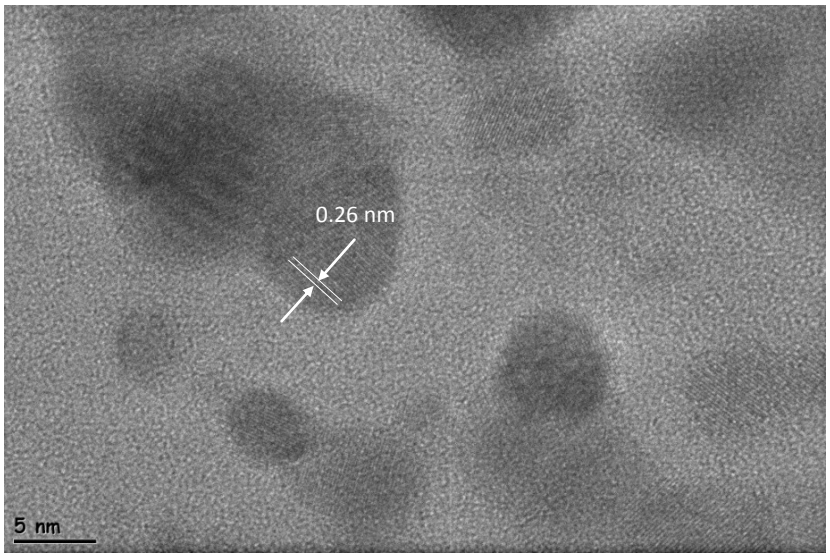

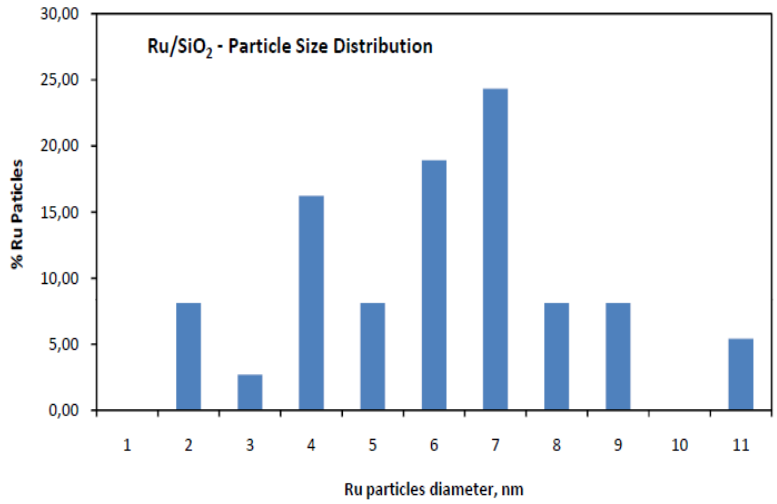

Figure 33. TEM image of 1% wt. Ru/SiO_2 catalyst a) dispersed particles over SiO_2 support, b) Crystal fringes of Ru metal over SiO_2, c) Particle size distribution

In Figure 34, TEM image of Ru/SBA-15 catalyst was given. As seen in TEM image, the ordered structure of SBA-15 can easily be seen with a pore diameter of approximately 8 nm. Figure 34 and other TEM images of Ru/SBA-15 catalyst showed that size distribution of Ru metal particles located over the SBA-15 support varied between 7 nm to 19 nm. Some large particles having 31 nm diameters exist over SBA-15.

a)

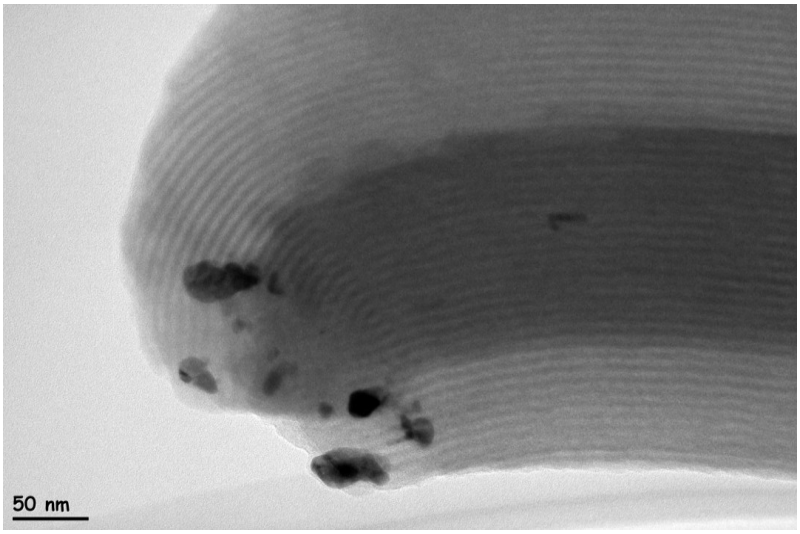

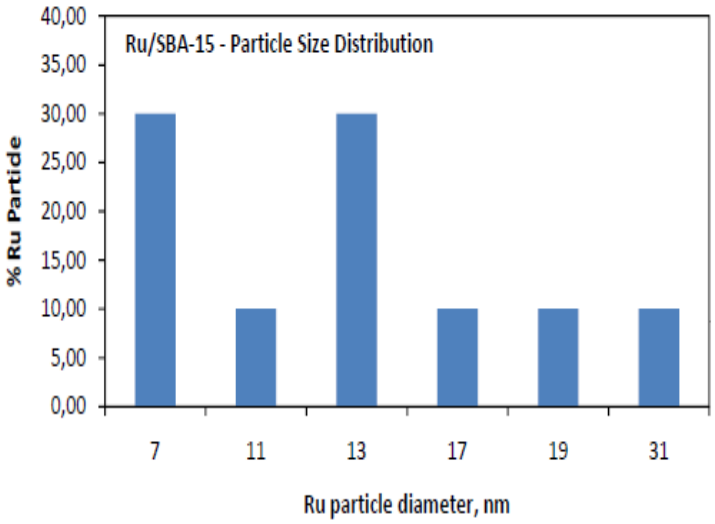

b)

Figure 34. a) TEM image of 1% wt. Ru/SBA-15 catalyst, b) Particle size distribution of Ru/SBA-15

In addition to mentioned Ru particles over SBA-15 catalyst, Ru particle which is located inside SBA-15 pores was detected by EDX spectrum. When TEM image of Ru/SBA-15 was examined, well distributed Ru particles can be observed in the middle of SBA-15 support. The EDX spectrum of Ru/SBA-15 catalyst is given in Figure 35.

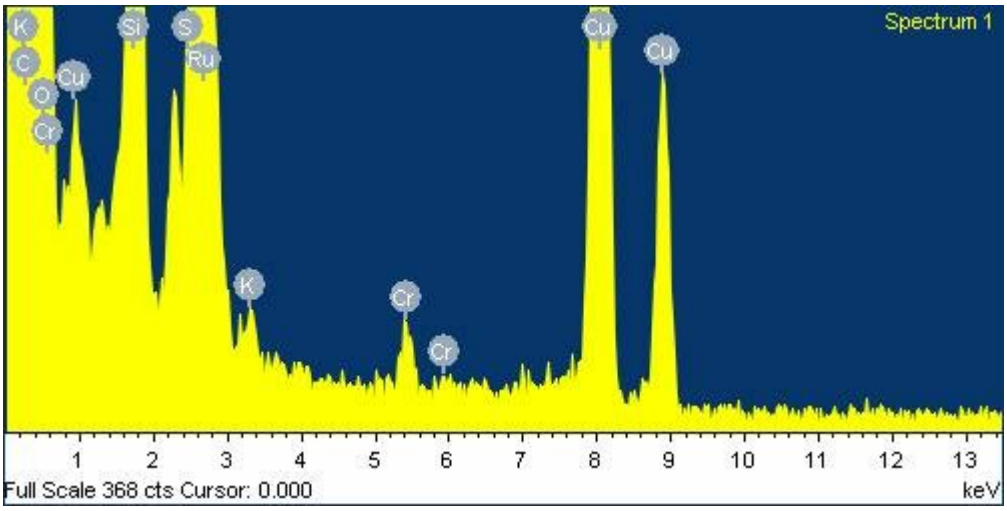

Figure 35: EDX Spectrum of Ru/SBA-15 catalyst

TEM images of the Ru/CNT catalyst are shown in Figure 36. Figure 36 (a) showed the structure of the carbon nanotubes. The diameter of the carbon nanotubes is determined between 50 - 120 nm diameters. When the diameter of the CNTs and the image of the CNTs were investigated, CNTs can be classified as multi walled carbon nanotubes.

The average particle size of Ru was determined as 3 – 4 nm from Figure 36 (b). The range of Ru particle sizes is observed between 1 nm to 5 nm. When Figure 36 (b) was examined, all of the Ru particles are located inside the CNT. This is somewhat a controversial assignment. But the absence of any particles extending out of the edge of the CNT indicates that Ru particles are in the subsurface of the nanotubes.

a) 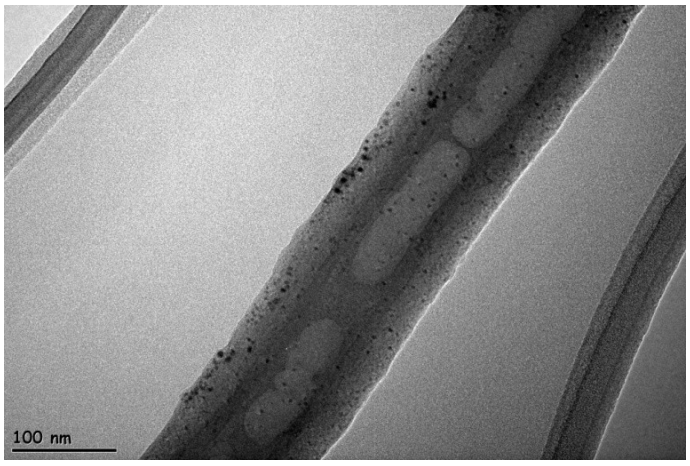

b) 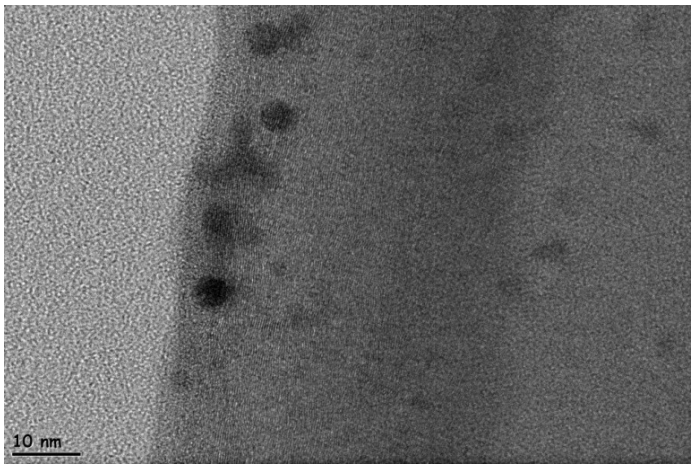

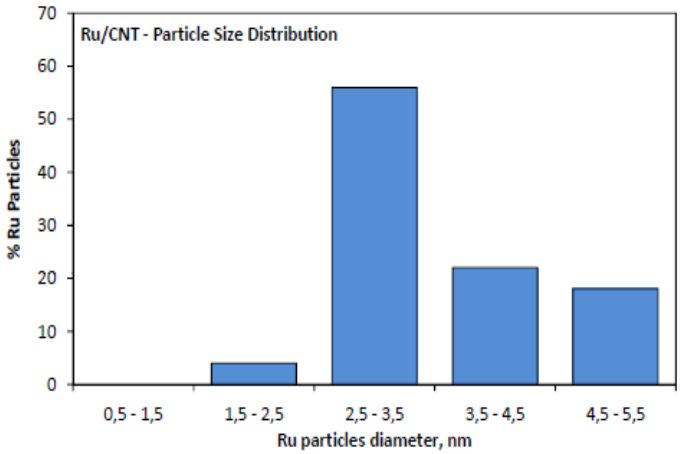

c)

Figure 36. TEM images of 1% Ru/CNT catalyst a) Ru particles and Multiwalled Carbon Nanotubes, b) Crystal fringes of Ru metal over MWCNT, c) Particle size distribution

Table 5. H_2 chemisorption % Ru metal dispersion results of the catalysts

	Total H[a] ($\mu mol/g_{cat}$)	Weak H[a] ($\mu mol/g_{cat}$)	Strong H[a] ($\mu mol/g_{cat}$)	% Dispersion by hydrogen chemisorption	% Dispersion by TEM[c]
Ru/SBA-15	240	200	40	10	7.1
Ru/SiO_2	460	380	80	5	16.7
Ru/CNT	600	480	120	1.5	28.6
Ru/Vulcan	70	26	44	27	Not Available
Na-Ru/Vulcan	9	0	9	Cannot be measured	Not Available

[a] Total, strong and weakly adsorbed hydrogen amount are determined at monolayer coverage

The results of H_2 chemisorption and TEM images are summarized in Table 5. When Table 5 was examined, the dispersion values which are determined via two different methods are in agreement for Ru/SBA-15 samples. On the contrary, there is a big difference for the values measured for Ru/CNT and Ru/SiO_2.

When H_2 chemisorption behavior of Ru/CNT catalyst was examined, it was observed that the significant amount of H_2 uptake started after 80 torr pressure (Figure 27). Up to 80 torr, H_2 uptake was measured as 40 µmol $H_2/g_{catalyst}$. On the

other hand, TEM picture of Ru/CNT catalyst exhibited that, big portion of Ru particles are located in the inner side of the CNT support.

When H_2 uptake values of all catalyst were investigated, Ru/SBA-15 catalyst had the highest H_2 uptake amount at high pressure range. This result can be explained as the surface area of the support. The surface areas of the supports are given in Table 6 indicate a correlation between the surface areas of the supports and the H_2 uptake of the catalysts.

Table 6. Relationship between H_2 uptake of the catalysts and surface area of supports

	Surface Area of the catalyst, m^2/g	**Surface Area of the support, m^2/g**	**H/Ru ratio calculated from total adsorption isotherms**
Ru/SBA-15	374	649	20
Ru/SiO_2	34	217	9
Ru/CNT	22	17	10
Ru/Vulcan	172	240	2

H/Ru ratio of Ru/SBA-15, Ru/SiO_2, Ru/CNT and Ru/Vulcan catalysts are greater than unity indicating a strongly bound hydrogen on the support surface. After the saturation of Ru particles adsorbed hydrogen species diffused out from the surface of Ru particle to support surface [74,78].

The mean free path of H_2 molecules at room temperature and 80 torr pressure is calculated as 1.2 μm. It can be a reasonable value for transport of H_2 molecules into the CNT pores. The mean diameter of CNTs is determined as 50 nm. In this situation, the reason of difference in the dispersion value of Ru/CNT catalyst can be speculated as the transport resistance of the H_2 molecules into the CNT pores under the conditions that equilibrium is not achieved.

The dispersion of the Na-Ru/Vulcan catalyst cannot be determined via H_2 chemisorption method. The main reason of this situation is the overlapping of total

and weak adsorption isotherms. Similar behavior was observed for Ru/Vulcan catalyst at low pressure range. But, between 50 – 400 torr pressures, a saturation region was observed for Ru/Vulcan catalyst and dispersion of the catalyst could be determined. A similar saturation region for Na-Ru/Vulcan catalyst through the whole pressure range was looked for, but it could not be found. As seen in Figure 32, total and weak adsorption isotherms overlap. In other words, strongly bound hydrogen adsorption cannot be measured on Na-Ru/Vulcan catalyst. At higher pressures, total and weak adsorption isotherms differ slightly. The reason of this behavior may be explained by increasing the pressure of the H_2 over Ru metal. As pressure of H_2 increases, the probability of dissociation over Ru metal increases despite Na atoms.

6.1 Spillover Measurements

The spillover measurements were carried out with Ru/Vulcan and Na-Ru/Vulcan catalysts. It is reported that spillover process is a diffusion process [78]. The spillover measurements of Ru/Vulcan and Na-Ru/Vulcan were given in Figure 37 and 38.

In order to calculate the coefficient of diffusion, point source diffusion differential equation was used. The solution of point source diffusion differential equation for a semi-infinite line source was given below:

$$C = C_e \left[1 - \frac{8}{\pi^2} \exp\left(-\frac{\pi^2 Dt}{b^2}\right)\right] \qquad (2.14)$$

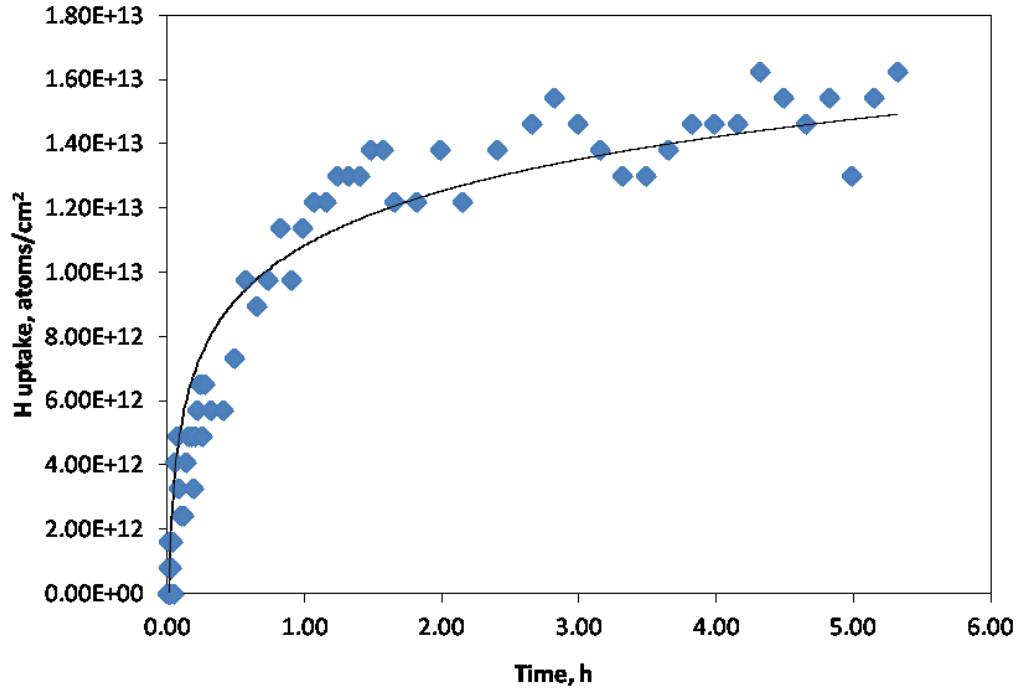

Figure 37: Spillover measurement of Ru/Vulcan at room temperature and 375 torr

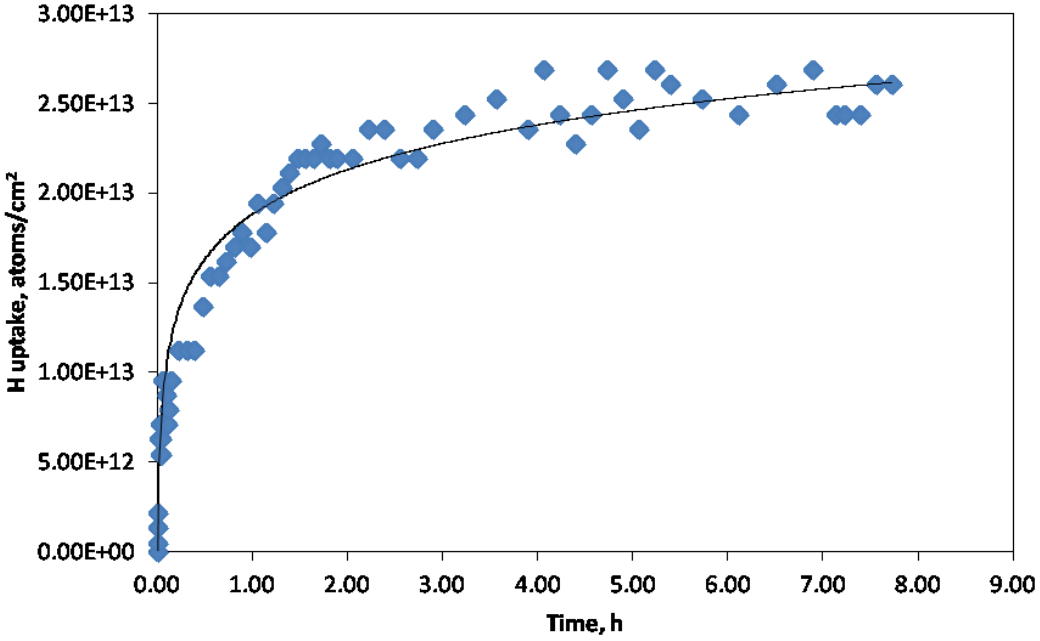

Figure 38: Spillover measurement of Na-Ru/Vulcan at room temperature and 375 torr

When spillover measurement plots of Ru/Vulcan and Na-Ru/Vulcan were examined, both processes reached the equilibrium approximately within 6 hours. The total H uptake for Ru/Vulcan and Na-Ru/Vulcan catalysts were measured as 1.5 x 10^{13} H atoms/cm^2 and 2.5 x 10^{13} H atoms/cm^2, respectively.

After detailed calculations (calculations are given in Appendix A.4), the coefficient of diffusion for Ru/Vulcan was determined as 1.39 x 10^{-14} cm^2/sec. Similarly, for Na-Ru/Vulcan catalyst, it was found as 1.23 x 10^{-14} cm^2/sec. The coefficient of diffusions for low pressure range and other related results were summarized in Table 7.

There are lots of contributions in the literature for coefficient of diffusion for different catalyst and support system. For example, Sermon et al. reported the coefficient of diffusion on WO_3 and MoO_3 as 10^{-16} cm^2/sec and 10^{-13} cm^2/sec, respectively [94]. at room temperature. In addition to this, at 100 ^oC, Fleisch and Abermann published the diffusion coefficient over carbon and SiO_2 support as 10^{-14} cm^2/sec [95]. At 400 ^oC, Kramer and Andre calculated the coefficient of diffusion on alumina support as 10^{-15} cm^2/sec [69]. When our results are compared to literature results, it can be said that the results are reasonable. The value of coefficient of diffusion differs between 10^{-13} and 10^{-16} cm^2/sec.

When calculation method of diffusion coefficient was examined, one of the most important parameter is the particle density. It directly influences the amount of H_2 uptake and number of diffused out hydrogen species from the active center. In our catalyst, the particle density per cm^2 was calculated as 4.75 x 10^9. The reported particle density values from the literature are between 10^{10} to 10^{13} per cm^2 of support. The reason of this slight disagreement with literature can be explained as the dispersion of the catalyst. While the dispersion of our Ru/Vulcan catalyst is about 27%, the same value for used catalysts are change between 40% - 80% [69]

Table 7. Comparison of Spillover Measurement of Ru/Vulcan and Na-Ru/Vulcan Catalysts

Catalyst Name	**Ru/Vulcan**	**Na-Ru/Vulcan**
Metal Percent	1% wt. Ru	1% wt. Na – 1% wt. Ru
Dispersion	0.27	
Mean Particle Diameter, nm	3.70	
Mean Distance between Particles, nm	145	
Particle Density, particle/cm^2	4.75×10^{9}	
Equilibrium Coverage, atoms/cm^2	1.45×10^{13} 9.00×10^{12}	2.50×10^{13} 4.50×10^{12}
Coefficient of Diffusion, cm^2/sec	1.39×10^{-14} 1.51×10^{-15}	

CHAPTER 7

CONCLUSIONS

The aim of this study was to investigate the H_2 chemisorption characteristics of Ru based ammonia synthesis catalysts. Total H_2 chemisorption measurements of Ru/SiO_2, Ru/SBA-15, Ru/CNT, Ru/Vulcan and Na-Ru/Vulcan catalysts indicated that H_2 uptake amount is a function of surface area of support material. The dispersions of the catalyst were determined via two characterization methods which are H_2 chemisorption and TEM. The dispersion values of Ru/SBA-15 catalyst determined via two different techniques are in agreement with each other. But, the dispersion values of Ru/SiO_2 and Ru/CNT catalysts are in disagreement. The dispersion values of Ru/SiO_2 and Ru/CNT catalysts determined via TEM technique were found as 20 and 3 times more with respect to H_2 chemisorption technique. The structure of the support materials and location of Ru particle has a key role in this situation.

H_2 spillover measurements over Ru/Vulcan and Na-Ru/Vulcan at same conditions showed that H_2 uptake of Na-Ru/Vulcan catalyst is higher than Ru/Vulcan catalyst. But, H_2 adsorption process reached equilibrium faster in the presence of Ru/Vulcan catalyst.

REFERENCES

[1] http://www.fertilizer.org/ifa/Home-Page/SUSTAINABILITY/Climate-change/A-historical-perspective.html- last accessed 21/09/2010

[2] www.fertilizer.org/ifa/ifadata/search, retrieved 27 August 2009

[3] Patrick Heffer, Medium-Term Outlook for World Agriculture and Fertilizer Demand 2008/09 – 2013/14 (Paris: IFA, June 2009), p. 25.

[4] A. Ozaki, K. Aika: "Catalytic Activation of Dinitrogen," in R. H. Anderson, M. Boudart (eds.): Catalysis: Science and Technology, vol. 1, Springer Verlag, Berlin–Heidelberg–New York 1981, pp. 87 – 158.

[5] J. R. Jennings (ed.): Catalytic Ammonia Synthesis, Plenum Press, New York and London 1991, pp. 20

[6] http://www.ruf.rice.edu/~natelson/research.html last accessed 21.06.2012

[7] G. Ertl, Catalysis Reviews, Science and Engineering, 21 (1980) 201

[8] P. Stolze and J. K. Norskov, Physical Review Letters, 55 (1985), 2502

[9] K. Aika, H. Hori, A. Ozaki, Journal of Catalysis, 27 (1972), 424

[10] K. Aika, A. Ozaki, Journal of Catalysis, 16 (1970), 97

[11] C. J. H. Jacobsen, S. Dahl, P. L. Hansen, E. Törnqvist, L. Jensen, H. Topsoe, D.V. Prip, P.B. Moenshaug, I. Chorkendorff, Journal of Molecular Catalysis A: Chemical, 163 (2000), 19

[12] T.W. Hansen, P.L. Hansen, S. Dahl, C.J.H. Jacobsen, Catalyst Letters 84, 1-2 (2002),7

[13] K. Honkala, A. Hellman, I.N. Remediakis, A. Logadottir, A. Carlsson, S. Dahl, C.H. Christensen, J.N. Norskov, Science, 307 (2005), 555

[14] W. Raróg-Pilecka, E. Miskiewicz, D. Szmigiel, Z. Kowalczyk, Journal of Catalysis 231 (2005), 11.

[15] X.L. Zhenh, S.J. Zhang, J. Xu, K.M. Wei, Carbon 40 (2002), 2597

[16] I. Rossetti, N. Pernicone, F. Ferrero, L. Forni, Industrial and Engineering Chemistry Research, 45 (2006), 4150

[17] US Patent, No: 4,163,775, British Petroleum, Process for the synthesis of ammonia using catalysts supported on graphite containing carbon (1979)

[18] Retrieved from http://onlinelibrary.wiley.com/doi/10.1002/14356007.o02_o11/pdf pp.190, last accessed 24.08.2012

[19] Gary Maxwell, Synthetic Ammonia Products: A Practical Guide to the Products and Processes, Plenum Publishers, 2004, New York

[20] Retrieved from http://onlinelibrary.wiley.com/doi/10.1002/14356007.a02_143.pub3/full pp. 107, lastaccessed 24.08.2012

[21] Retrieved from http://onlinelibrary.wiley.com/doi/10.1002/14356007.a02_143.pub3/full pp. 108, last accessed 24.08.2012

[22] http://en.wikipedia.org/wiki/World_population last accessed 17/06/2012

[23] G.J. Leigh, The World's Greatest Fix: A History of Nitrogen and Agriculture, Oxford University Press, 2004, New York, pg. 123

[24] Retrieved from http://onlinelibrary.wiley.com/doi/10.1002/14356007.a02_143.pub3/full pp. 109, last accessed 24.08.2012

[25] Fritz Haber, Nobel Lecture, Retrieved from http://www.nobelprize.org/nobel_prizes/chemistry/laureates/1918/haber-lecture.html in 25.06.2012

[26] J.W. Erisman, M.A. Sutton, J. Galloway, Z. Klimont, W. Winiwarter, Nature Geoscience, 1 (2008) 636-639

[27] Retrieved from http://onlinelibrary.wiley.com/doi/10.1002/14356007.o02_o11/full pp. 127, last accessed 24.08.2012

[28] http://www.nobelprize.org/nobel_prizes/chemistry/laureates/2007/ last accessed 19/06/2012

[29] Retrieved from http://www.topsoe.com/business_areas/ammonia/processes/~/media/PDF%20files/Ammonia/Topsoe_radial_flow_converters.ashx last accessed 23/11/2012

[30] Retrieved from http://www.uhde.eu/competence/technologies/fertiliser/ammonia urea/75/94/ammonia-conversion.html last accessed 23/11/2012

[31] M. A. Hasnat, M.R. Karim, M. Machida, Catalysis Communications, 10 (2009), 1975

[32] A. Skodra and M. Stoukides, Solid State Ionics, 180 (2009), 1332

[33] G. N. Schrauzer and T.D. Guth, Journal of American Chemical Society, 99 (1977), 7189

[34] M. Yamauchi, R. Abe, T. Tsukuda, K. Kato, M. Takata, Journal of American Chemical Society, 133 (2011), 1150

[35] H. Miyama, N. Fujii, Y. Nagae, Chemical Physics Letters, 74 (1980), 523

[36] Q. Li, K. Domen, S. Naito, T. Onishi, K. Tamaru, Chemistry Letters, 3 (1983), 321

[37] M.E. Vol'pin and V. B. Shur, Dokl. Akad. Nauk SSSR, 156 (1964), 1102

[38] A.E.Shilov, Catalysis with organized molecular systems, page 171-182 in Perspectives In Catalysis, J.M. Thomas and K. I. Zamaraev, eds, Blackwell Scientific, Cambridge, 1992.

[39] T. H. Rod, A. Logadottir, J. K. Norskov, Journal of Chemical Physics, 112, (2000), 5343

[40] B. Hinnemann and J.K. Norskov, Topics in Catalysis, 37 (2006), 55

[41] N. Schindelin, C. Kisker, J.L. Schlessman, J.B. Howard, D.C. Rees, Nature 387 (1997), 370

[42] M. Temkin and V. Phyzev, Acta Physicochim, 12 (1940) 327

[43] P. Stoltze and J.K. Norskov, Physical Chemistry Letters, 55 (1985) 2502

[44] P. Stoltze and J.K. Norskov, Journal of Catalysis, 110 (1988) 1

[45] J.A. Dumesic and A.A. Trevino, Journal of Catalysis, 116 (1989) 119

[46] Buzzi Ferraris G., Donati G., Rejna F., Carra S., Chemical Engineering Science, 29 (1974), 1621.

[47] O. Hinrichsen, F. Rosowski, M. Muhler, G. Ertl, Chemical Engineering Science, 51 (1996), 1683

[48] A. Logadottir and J.K. Norskov, Journal of Catalysis, 220 (2003), 273

[49] S. Dahl, A. Logadottir, C.J.H. Jacobsen, J.K. Norskov, Applied Catalysis A-General, 222 (2001), 19

[50] A. Hellman, K. Honkala, I.N. Remediakis, A. Logadottir, A. Carlsson, S. Dahl, C.H. Christensen, J.K. Norskov, Surface Science, 603 (2009), 1731

[51] B.R. McClaine, T. Becue, C. Lock, R.J. Davis, Journal of Molecular Catalysis A: Chemical, 163 (2000), 105

[52] Y.V. Larichev, B.L. Moroz, V.I. Zaikovskii, S.M. Yunusov, E.S. Kalyuzhnaya, V.B. Shur, V.I. Bukhtiyarov, Journal of Physical Chemistry C, 111 (2007), 9427

[53] Y.V. Larichev, Journal of Physical Chemistry C, 112 (2008), 14776

[54] D. Szmigiel, W. Rarog-Pilecka, E. Miskiewicz, E. Maciejewska, Z. Kaszkur, J.W. Sobczak, Z. Kowalczyk, Catalysis Letters, 100 (2005), 79

[55] E. Truszkiewicz, W. Rarog-Pilecka, K. Schmidt-Szałowski, S. Jodzis, E. Wilczkowska, D. Łomot, Z. Kaszkur, Z. Karpinski, Z. Kowalczyk, Journal of Catalysis, 265 (2009), 181

[56] W. Raróg-Pilecka, E. Miskiewicz, S. Jodzis a, J. Petryk, D. Łomot, Z. Kaszkur, Z. Karpinski, Z. Kowalczyk, Journal of Catalysis, 239 (2006), 313

[57] X. Yang, W. Zhang, C. Xia, X. Xiong, X. Mu, B. Hu, Catalysis Communications, 11 (2010), 867

[58] Q.Xu, J. Lin, J. Li, X. Fu, Y. Liang, D. Liao, Catalysis Communications, 8 (2007), 1881

[59] X. Luo, R. Wang, J. Ni, J. Lin, B. Lin, X. Xu, K. Wei, Catalysis Letters, 133 (2009), 382

[60] T.W. Hansen, J.B. Wagner, P.L. Hansen, S. Dahl, H. Topsoe, C.J.H. Jacobsen, Science, 294 (2001), 1508

[61] B. Veisz, Z. Kiraly, L. Toth, B. Pecz, Chemical Materials, 14, (2002), 2882

[62] Z. You, K. Inazu, K. Aika, T. Baba, Journal of Catalysis, 251 (2007), 321

[63] X. Yang, L. Tang, C. Xia, X. Xiong, X. Mu, B. Hu, Chinese Journal of Catalysis, 33 (2012), 447

[64] K. Aika, H. Hori, A. Ozaki, Journal of Catalysis, 27 (1972), 424

[65] A.J. Robell, E.V. Ballou, M. Boudart, The Journal of Physical Chemistry, 68 (1964), 2748

[66] J.M. Sinfelt and P.J. Lucchessi, Journal of American Chemical Society, 85 (1963), 3365

[67] S. Khoobiar, Journal of Physical Chemistry, 68 (1964), 411

[68] W.C. Conner and J.L. Falconer, Chemistry Reviews, 95 (1995), 759

[69] R. Kramer and M. Andre, Journal of Catalysis, 58 (1979), 287

[70] D.O. Uner, N. Savargoankar, M. Pruski, T.S. King, Dynamics of Surface and Reaction Kinetics in Heterogeneous Catalysis (Editor: G.F. Froment and K.C. Waugh), Elsevier (1997), 315

[71] D. Uner, Industrial & Engineering Chemistry Research, 37 (1998), 2239

[72] D. Uner, M. Pruski, T.S. King, Topics in Catalysis, 2 (1995), 58

[73] C. Pedrero, T. Waku, E. Iglesia, Journal of Catalysis, 233 (2005), 241

[74] N. Kumar, T.S. King, R.D. Vigil, Chemical Engineering Science, 55 (2000) 4973

[75] N. Savargoankar, R.L. Narayan, M. Pruski, D.O. Uner, T.S. King, Journal of Catalysis, 178 (1998), 26

[76] Nitrogen, 193 (1991) 17 – 21

[77] J. P. Shirez, J. R. LeBlanc, Kellogg Ammonia Club Meeting, San Francisco 1989.

[78] S.E. Siporin and R.J. Davis, Journal of Catalysis, 225 (2004), 359

[79] N. Satoh, J.I. Hayashi, H. Hattori, Applied Catalysis A: General, 202 (2000), 207

[80] P.C.H. Mitchell, A.J. Ramirez-Cuesta, S.F. Parker, J. Tomkinson, D. Thompsett, Journal of Physical Chemistry B, 107 (2003), 6838

[81] L. Wang and R.T. Yang, Journal of Physical Chemistry C, 112 (2008), 12486

[82] L.Wang, F. Yang, M. Miller, R.T. Yang, Industrial & Engineering Chemistry Research, 48 (2009) 2920

[83] Q. Li and A. D. Lueking, The Journal of Physical Chemistry C, 115, 4273

[84] R. Bhowmick, S. Rajasekaran, D. Friebel, Cara Beasley, L. Jiao, H. Ogasawara, H. Dai, B. Clemens, A. Nilsson, The Journal of American Chemical Society, 133 (2011), 5580

[85] R. Prins, Chemical Reviews, 112 (2012), 2714

[86] KBR Technology, Global Ammonia Market Update Presentation, Technology Conference in Dubai, 5 – 6 October 2009

[87] Retrieved from http://onlinelibrary.wiley.com/doi/10.1002/0471238961.0113131503262116.a01.pub3/full last accessed 24.08.2012

[88] http://www.easychem.com.au/monitoring-and-management/maximising-production/industrial-uses-of-ammonia last accessed 14.07.2012

[89] ICCA, IEA & DECHEMA, Catalysis Roadmap Subject Matter Workshop, Backrounder Paper

[90] Retrieved from http://onlinelibrary.wiley.com/doi/10.1002/14356007.o02_o11/pdf pp.173-207, last accessed 24.08.2012

[91] http://en.wikipedia.org/wiki/Henry_Louis_Le_Chatelier last accessed 21.06.2012

[92] R.J. Silbey, R.A. Alberty, M.G. Bawendi, Physical Chemistry, 4th Edition, Wiley, New Jersey, 2005,

[93] http://www.webelements.com/ruthenium/crystal_structure.html last accessed 29.07.2012

[94] P.A. Sermon, G.C. Bond, Journal of Chemical Society, Faraday Transections 1, 72 (1976), 730

[95] T. Fleisch and R. Abermann, Journal of Catalysis, 50 (1977), 268

APPENDICES

A.1. ADIABATIC AMMONIA SYNTHESIS REACTOR DESIGN CALCULATIONS

1. Cp Constants of N_2, H_2 and NH_3

Material	***a***	***b x 10²***	***c x 10⁵***	***d x 10⁹***
Nitrogen	28.883	-0.157	0.808	-2.871
Hydrogen	29.088	-0.192	0.400	-0.870
Ammonia	24.619	3.75	-0.138	

$C_p = a + bT + cT^2 + dT^3, T\ is\ in\ degrees\ K\ and\ C_p\ in \frac{J}{mol - K}$

Ref : S.Sandler, Chemical, and Engineering Thermodynamics, 3rd Edition, 1999, John Wiley and Sons

$$\Delta C_p = \left(24.619 - \frac{3}{2} * 29.088 - \frac{1}{2} * 28.882\right) + \left(3.75 \times 10^{-2} + \frac{3}{2} * 0.192 \times 10^{-2} + \frac{1}{2} * 0.157 \times 10^{-2}\right) T + \left(-0.138 \times 10^{-5} - \frac{3}{2} * 0.400 \times 10^{-5} - \frac{1}{2} * 0.808 \times 10^{-5}\right) T^2 + \left(\frac{3}{2} * 0.870 \times 10^{-9} + \frac{1}{2} * 2.871 \times 10^{-9}\right) T^3$$

$$\Delta C_p = -33.454 + 4.11 \times 10^{-2} T - 1.14 \times 10^{-5} T^2 + 2.74 \times 10^{-9} T^3$$

$$\Delta H_T = \Delta H^o_{298} + \int_{298}^{T} \Delta C_p dT$$

$$\Delta H_T = \left[\Delta H^o_{f,NH3} - \left(\frac{3}{2} * \Delta H^o_{f,H2} + \frac{1}{2} * \Delta H^o_{f,N2}\right)\right] + \int_{298}^{T} [-33.454 + 4.11 \times 10^{-2} T - 1.14 \times 10^{-5} T^2 + 2.74 \times 10^{-9} T^3] dT$$

$$\Delta H_T = (-46100) + (-33.454T) + \left(\frac{4.11 \times 10^{-2}}{2} T^2\right) + \left(\frac{-1.14 \times 10^{-5}}{3} T^3\right) + \left(\frac{2.74 \times 10^{-9}}{4} T^4\right)$$

$$\Delta H_T = -46100 - 33.45 * T + 2.06 \times 10^{-2} * T^2 - 3.80 \times 10^{-6} * T^3 + 6.85 \times 10^{-10} * T^4$$

$$\Delta G^o_{rxn} = \Delta G^o_{f,NH3} - \left[\frac{3}{2} * \Delta G^o_{f,H2} - \frac{1}{2} * \Delta G^o_{f,N2}\right]$$

$$\Delta G^o_{rxn} = -16500$$

$$\Delta G^o_{rxn} = -16500 \frac{J}{mol}$$

$$\Delta G^o_{rxn} = -R * T * \ln K_{298}$$

$$\ln K_{298} = \frac{-\Delta G^o_{rxn}}{R * T}$$

$$\ln K_{298} = \frac{16500}{8.314 \times 298}$$

$$\ln K_{298} = 6.66$$

Relating Equilibrium Constant with Temperature

$$\ln K_T = \ln K_{298} + \int_{298}^{T} \frac{\Delta H_T}{RT^2} dT$$

$$\ln K_T = 6.66 + \int_{298}^{T} \frac{-46100 - 33.45 * T + 2.06 \times 10^{-2} * T^2 - 3.80 \times 10^{-6} * T^3 + 6.85 \times 10^{-10} * T^4}{8.314 * T^2} dT$$

$$\ln K_T = 6.66 + \int_{298}^{T} [-\frac{5544.9}{T^2} - \frac{4.02}{T} + 2.48 \times 10^{-3} - 4.57 \times 10^{-7} T + 8.24 \times 10^{-11} T^2] dT$$

$$\ln K_T = 6.66 + \left(\frac{5544.9}{T} - 4.02 \ln T + 2.48 \times 10^{-3} T - 2.29 \times 10^{-7} T^2 + 2.75 \times 10^{-11} T^3\right)_{298}^{T}$$

$$\ln K_T = 6.66 + 5544.9\left(\frac{1}{T} - \frac{1}{298}\right) - 4.02(\ln T - \ln 298) + 2.48 \times 10^{-3}(T - 298) - 2.29 \times 10^{-7}(T^2 - 298^2) + 2.75 \times 10^{-11}(T^3 - 298^3)$$

$$\ln K_T = 6.66 + \frac{5544.9}{T} - 18.61 - 4.02 \ln T + 22.90 + 2.48 \times 10^{-3} T - 0.74 - 2.29 \times 10^{-7} T^2 + 0.02 + 2.75 \times 10^{-11} T^3 - 0.0073$$

$$\ln K_T = 10.22 + \frac{5544.9}{T} - 4.02 \ln T + 2.48 \times 10^{-3} T - 2.29 \times 10^{-7} T^2 + 2.75 \times 10^{-11} T^3$$

Relating Equilibrium Constant with Equilibrium Conversion

$$\frac{1}{2} N_2 + \frac{3}{2} H_2 \rightleftharpoons NH_3$$

$$K_T = K_y \times K_\phi \times P_T^{(\text{products} - \text{reactants})}$$

$$K_y = \frac{y_{NH_3}^{\upsilon_{NH_3}}}{y_{N_2}^{\upsilon_{N_2}} y_{H_2}^{\upsilon_{H_2}}} = \frac{y_{NH_3}}{(y_{N_2})^{0.5}(y_{H_2})^{1.5}}$$

$$K_y = \frac{\phi_{NH_3}^{\upsilon_{NH_3}}}{\phi_{N_2}^{\upsilon_{N_2}} \phi_{H_2}^{\upsilon_{H_2}}} = \frac{\phi_{NH_3}}{(\phi_{N_2})^{0.5}(\phi_{H_2})^{1.5}}$$

Inlet Molar Flow Rates of Reactants and Products

Nitrogen : $F_{N_{2o}}$

Hydrogen : $F_{H_{2o}}$ ($F_{H_{2o}} = 3 * F_{N_{2o}}$)

Ammonia : $F_{NH_{3o}}$

Molar Fraction of Each Compound at Equilibrium

$$y_{N_2} = \frac{F_{N_2}}{F_T} = \frac{F_{N_{2o}}(1 - X_e)}{F_{N_{2o}}(4 - 2X_e)} = \frac{\mathbf{(1 - X_e)}}{\mathbf{(4 - 2X_e)}}$$

$$y_{H_2} = \frac{F_{H_2}}{F_T} = \frac{F_{N_{2o}}(3 - 3X_e)}{F_{N_{2o}}(4 - 2X_e)} = \frac{\mathbf{(3 - 3X_e)}}{\mathbf{(4 - 2X_e)}}$$

$$y_{NH_3} = \frac{F_{NH_3}}{F_T} = \frac{2F_{N_{2o}}X_e}{F_{N_{2o}}(4 - 2X_e)} = \frac{\mathbf{2X_e}}{\mathbf{(4 - 2X_e)}}$$

$$K_y = \frac{\left(\frac{2X_e}{4 - 2X_e}\right)}{\left(\frac{1 - X_e}{4 - 2X_e}\right)^{0.5}\left(\frac{3 - 3X_e}{4 - 2X_e}\right)^{1.5}} = \frac{2X_e(4 - 2X_e)}{3^{1.5}(1 - X_e)^2}$$

Fugacity Coefficients of Each Component @80 bar and 300 – 1000 K

$$K_\phi = \frac{\phi_{NH_3}}{\phi_{N_2}^{0.5}\phi_{H_2}^{1.5}}$$

Combination of Terms of Equilibrium Constant

$$K_T = \frac{2X_e(4-2X_e)}{3^{1.5}(1-X_e)^2}\frac{\phi_{NH_3}}{{\phi_{N_2}}^{0.5}{\phi_{H_2}}^{1.5}}\frac{1}{80}$$

Adiabatic Energy Balance

General Adiabatic Energy Balance Equation

$$\sum_{inlet} F_i C_{p_i} dT + \sum_{outlet} F_i C_{p_i} dT = (-\Delta H_R) F_{A_0} X_A$$

- ***Reactor 3 (Inlet)***

$$\sum_{inlet} F_i C_{p_i} dT = \int_{T_{i3}}^{298} F_{N_2} C_{P_{N2}} dT + \int_{T_{i3}}^{298} F_{H_2} C_{P_{H2}} dT + \int_{T_{i3}}^{298} F_{NH_3} C_{P_{NH3}} dT$$

$$F_{N_2} \int_{Ti3}^{298} \left(3{,}28 + 5{,}93 \times 10^{-4}T + \frac{4000}{T^2}\right) dT$$

$$+ F_{H_2} \int_{Ti3}^{298} \left(3{,}249 + 4{,}22 \times 10^{-4}T + \frac{8300}{T^2}\right) dT$$

$$+ F_{NH_3} \int_{Ti3}^{298} \left(3{,}5778 + 3{,}02 \times 10^{-3}T - \frac{18600}{T^2}\right) dT$$

$$F_{N_2}\left[3{,}28(298 - T_{i3}) + 2{,}965 \times 10^{-4}\left(298^2 - {T_{i3}}^2\right) - 4000\left(\frac{1}{298} - \frac{1}{T_{i3}}\right)\right]$$

$$+ F_{H_2}\left[3{,}249(298 - T_{i3}) + 2{,}11 \times 10^{-4}\left(298^2 - {T_{i3}}^2\right) - 8300\left(\frac{1}{298} - \frac{1}{T_{i3}}\right)\right]$$

$$+ F_{NH_3}\left[3{,}5778(298 - T_{i3}) + 1{,}51 \times 10^{-3}\left(298^2 - {T_{i3}}^2\right) + 18600\left(\frac{1}{298} - \frac{1}{T_{i3}}\right)\right]$$

$$F_{N_2}\left[977{,}44 - 3{,}28T_{i3} + 26{,}33 - 2{,}965 \times 10^{-4}{T_{i3}}^2 - 13{,}42 + \frac{4000}{T_{i3}}\right]$$
$$+ F_{H_2}\left[968{,}202 - 3{,}249T_{i3} + 18{,}74 - 2{,}11 \times 10^{-4}{T_{i3}}^2 - 27{,}85 + \frac{8300}{T_{i3}}\right]$$
$$+ F_{NH_3}\left[1066{,}2 - 3{,}5778T_{i3} + 134{,}1 - 1{,}51 \times 10^{-3}{T_{i3}}^2 + 62{,}42 - \frac{18600}{T_{i3}}\right]$$

$$F_{N_2}\left[990{,}35 - 3{,}28T_{i3} - 2{,}965 \times 10^{-4}{T_{i3}}^2 + \frac{4000}{T_{i3}}\right]$$
$$+ F_{H_2}\left[959{,}09 - 3{,}249T_{i3} - 2{,}11 \times 10^{-4}{T_{i3}}^2 + \frac{8300}{T_{i3}}\right]$$
$$+ F_{NH_3}\left[1262{,}72 - 3{,}5778T_{i3} - 1{,}51 \times 10^{-3}{T_{i3}}^2 - \frac{18600}{T_{i3}}\right]$$

REACTOR 3		
Species	**Inlet, kmol/s**	**Outlet, kmol/s**
N_2	4,36	3,82
H_2	13,07	11,46
NH_3	2,04	3,12

$$\left(4{,}36\frac{kmol}{s}\right)\left(8{,}314\frac{kJ}{kmol-K}\right)\left(990{,}35-3{,}28T_{i3}-2{,}965\times10^{-4}{T_{i3}}^{2}+\frac{4000}{T_{i3}}\right)$$
$$+\left(13{,}07\frac{kmol}{s}\right)\left(8{,}314\frac{kJ}{kmol-K}\right)\left(959{,}09-3{,}249T_{i3}-2{,}11\times10^{-4}{T_{i3}}^{2}+\frac{8300}{T_{i3}}\right)$$
$$+\left(2{,}04\frac{kmol}{s}\right)\left(8{,}314\frac{kJ}{kmol-K}\right)\left(1262{,}72-3{,}5778T_{i3}-1{,}51\times10^{-3}{T_{i3}}^{2}-\frac{18600}{T_{i3}}\right)$$

$$35899{,}2-118{,}9T_{i3}-0{,}011{T_{i3}}^{2}+\frac{144996{,}2}{T_{i3}}+104218{,}5-353{,}1T_{i3}-0{,}023{T_{i3}}^{2}$$
$$+\frac{901911}{T_{i3}}+21416{,}4-60{,}7T_{i3}-0{,}026{T_{i3}}^{2}-\frac{315466{,}4}{T_{i3}}$$

$$161534{,}1-532{,}7T_{i3}-0{,}06{T_{i3}}^{2}+\frac{731440{,}8}{T_{i3}}$$

- ***Reactor 3 (Outlet)***

$$\sum_{outlet}F_iC_{p_i}dT=\int_{298}^{700}F_{N_2}C_{P_{N2}}dT+\int_{298}^{700}F_{H_2}C_{P_{H2}}dT+\int_{298}^{700}F_{NH_3}C_{P_{NH3}}dT$$

$$=F_{N_2}\int_{298}^{700}\left(3{,}28+5{,}93\times10^{-4}T+\frac{4000}{T^2}\right)dT$$
$$+F_{H_2}\int_{Ti3}^{700}\left(3{,}249+4{,}22\times10^{-4}T+\frac{8300}{T^2}\right)dT$$
$$+F_{NH_3}\int_{298}^{700}\left(3{,}5778+3{,}02\times10^{-3}T-\frac{18600}{T^2}\right)dT$$

$$= F_{N_2}\left[3{,}28(700-298)+2{,}965\times10^{-4}(700^2-298^2)-4000\left(\frac{1}{700}-\frac{1}{298}\right)\right]$$
$$+F_{H_2}\left[3{,}249(700-298)+2{,}11\times10^{-4}(700^2-298^2)\right.$$
$$\left.-8300\left(\frac{1}{700}-\frac{1}{298}\right)\right]$$
$$+F_{NH_3}\left[3{,}5778(700-298\,)+1{,}51\times10^{-3}(700^2-298^2)\right.$$
$$\left.+18600\left(\frac{1}{700}-\frac{1}{298}\right)\right]$$

$$F_{N_2}[1318{,}6+119+7{,}7]+F_{H_2}[1306{,}1+84{,}7+16]$$
$$+F_{NH_3}[1438{,}3+605{,}8-35{,}8]$$

$$=\left(3{,}82\frac{kmol}{s}\right)\left(8{,}314\frac{kJ}{kmol-K}\right)(1445{,}3)$$
$$+\left(11{,}46\frac{kmol}{s}\right)\left(8{,}314\frac{kJ}{kmol-K}\right)(1406{,}8)$$
$$+\left(3{,}12\frac{kmol}{s}\right)\left(8{,}314\frac{kJ}{kmol-K}\right)(2008{,}3)$$

$$=232034{,}3\frac{kJ}{s}$$

- ***<u>Combining the Equations:</u>***

$$161534{,}1-532{,}7T_{i3}-0{,}06{T_{i3}}^2+\frac{731440{,}8}{T_{i3}}+232034{,}3=(-\Delta H_R)F_{A_3}X_A$$

$$393568{,}4-532{,}7T_{i3}-0{,}06{T_{i3}}^2+\frac{731440{,}8}{T_{i3}}$$
$$=\left(46110\frac{kJ}{kmol}\right)\left(4{,}36\frac{kmol}{s}\right)(0{,}29-0{,}19)$$

$$373464{,}4-532{,}7T_{i3}-0{,}06{T_{i3}}^2+\frac{731440{,}8}{T_{i3}}=0$$

$$T_{i_3}=655\ K$$

- ***Reactor 2 (Inlet)***

$$\sum_{inlet} F_i C_{p_i} dT = \int_{T_{i2}}^{298} F_{N_2} C_{P_{N2}} dT + \int_{T_{i2}}^{298} F_{H_2} C_{P_{H2}} dT + \int_{T_{i2}}^{298} F_{NH_3} C_{P_{NH3}} dT$$

$$F_{N_2} \int_{Ti2}^{298} \left(3{,}28 + 5{,}93 \times 10^{-4} T + \frac{4000}{T^2}\right) dT$$

$$+ F_{H_2} \int_{Ti2}^{298} \left(3{,}249 + 4{,}22 \times 10^{-4} T + \frac{8300}{T^2}\right) dT$$

$$+ F_{NH_3} \int_{Ti2}^{298} \left(3{,}5778 + 3{,}02 \times 10^{-3} T - \frac{18600}{T^2}\right) dT$$

$$F_{N_2} \left[3{,}28(298 - T_{i2}) + 2{,}965 \times 10^{-4}\left(298^2 - {T_{i2}}^2\right) - 4000\left(\frac{1}{298} - \frac{1}{T_{i2}}\right)\right]$$

$$+ F_{H_2} \left[3{,}249(298 - T_{i2}) + 2{,}11 \times 10^{-4}\left(298^2 - {T_{i2}}^2\right) - 8300\left(\frac{1}{298} - \frac{1}{T_{i2}}\right)\right]$$

$$+ F_{NH_3} \left[3{,}5778(298 - T_{i2}) + 1{,}51 \times 10^{-3}\left(298^2 - {T_{i2}}^2\right) + 18600\left(\frac{1}{298} - \frac{1}{T_{i2}}\right)\right]$$

$$F_{N_2}\left[977{,}44 - 3{,}28T_{i2} + 26{,}33 - 2{,}965 \times 10^{-4}{T_{i2}}^2 - 13{,}42 + \frac{4000}{T_{i2}}\right]$$
$$+ F_{H_2}\left[968{,}202 - 3{,}249T_{i2} + 18{,}74 - 2{,}11 \times 10^{-4}{T_{i2}}^2 - 27{,}85 + \frac{8300}{T_{i2}}\right]$$
$$+ F_{NH_3}\left[1066{,}2 - 3{,}5778T_{i2} + 134{,}1 - 1{,}51 \times 10^{-3}{T_{i2}}^2 + 62{,}42 - \frac{18600}{T_{i2}}\right]$$

$$F_{N_2}\left[990{,}35 - 3{,}28T_{i2} - 2{,}965 \times 10^{-4}{T_{i2}}^2 + \frac{4000}{T_{i2}}\right]$$
$$+ F_{H_2}\left[959{,}09 - 3{,}249T_{i2} - 2{,}11 \times 10^{-4}{T_{i2}}^2 + \frac{8300}{T_{i2}}\right]$$
$$+ F_{NH_3}\left[1262{,}72 - 3{,}5778T_{i2} - 1{,}51 \times 10^{-3}{T_{i2}}^2 - \frac{18600}{T_{i2}}\right]$$

REACTOR 2		
Species	**Inlet, kmol/s**	**Outlet, kmol/s**
N_2	4,73	4,36
H_2	14,20	13,07
NH_3	1,29	2,04

$$\left(4{,}73\frac{kmol}{s}\right)\left(8{,}314\frac{kJ}{kmol-K}\right)\left(990{,}35-3{,}28T_{i2}-2{,}965\times10^{-4}{T_{i2}}^{2}+\frac{4000}{T_{i3}}\right)$$
$$+\left(14{,}20\frac{kmol}{s}\right)\left(8{,}314\frac{kJ}{kmol-K}\right)\left(959{,}09-3{,}249T_{i2}-2{,}11\times10^{-4}{T_{i2}}^{2}+\frac{8300}{T_{i2}}\right)$$
$$+\left(1{,}29\frac{kmol}{s}\right)\left(8{,}314\frac{kJ}{kmol-K}\right)\left(1262{,}72-3{,}5778T_{i2}-1{,}51\times10^{-3}{T_{i2}}^{2}-\frac{18600}{T_{i2}}\right)$$

$$38945{,}7-129T_{i2}-0{,}012{T_{i2}}^{2}+\frac{157301}{T_{i2}}+113229-383{,}6T_{i2}-0{,}025{T_{i2}}^{2}$$
$$+\frac{979888}{T_{i3}}+13542{,}7-38{,}4T_{i2}-0{,}016{T_{i2}}^{2}-\frac{199486{,}1}{T_{i2}}$$

$$165717{,}4-551T_{i2}-0{,}053{T_{i2}}^{2}+\frac{937702{,}9}{T_{i2}}$$

- ***Reactor 2 (Outlet)***

$$\sum_{outlet}F_iC_{p_i}dT=\int_{298}^{750}F_{N_2}C_{P_{N_2}}dT+\int_{298}^{750}F_{H_2}C_{P_{H_2}}dT+\int_{298}^{750}F_{NH_3}C_{P_{NH3}}dT$$

$$=F_{N_2}\int_{298}^{750}\left(3{,}28+5{,}93\times10^{-4}T+\frac{4000}{T^2}\right)dT$$
$$+F_{H_2}\int_{298}^{750}\left(3{,}249+4{,}22\times10^{-4}T+\frac{8300}{T^2}\right)dT$$
$$+F_{NH_3}\int_{298}^{750}\left(3{,}5778+3{,}02\times10^{-3}T-\frac{18600}{T^2}\right)dT$$

$$= F_{N_2}\left[3{,}28(750-298)+2{,}965\times10^{-4}(750^2-298^2)-4000\left(\frac{1}{750}-\frac{1}{298}\right)\right]$$
$$+F_{H_2}\left[3{,}249(750-298)+2{,}11\times10^{-4}(750^2-298^2)\right.$$
$$\left.-8300\left(\frac{1}{750}-\frac{1}{298}\right)\right]$$
$$+F_{NH_3}\left[3{,}5778(750-298\,)+1{,}51\times10^{-3}(750^2-298^2)\right.$$
$$\left.+18600\left(\frac{1}{750}-\frac{1}{298}\right)\right]$$

$$F_{N_2}[1482{,}6+140{,}5+8{,}1]+F_{H_2}[1468{,}6+99{,}9+16{,}8]$$
$$+F_{NH_3}[1617{,}2+715{,}3-37{,}6]$$

$$=\left(4{,}36\frac{kmol}{s}\right)\left(8{,}314\frac{kJ}{kmol-K}\right)(1631{,}2)$$
$$+\left(13{,}07\frac{kmol}{s}\right)\left(8{,}314\frac{kJ}{kmol-K}\right)(1585{,}3)$$
$$+\left(2{,}04\frac{kmol}{s}\right)\left(8{,}314\frac{kJ}{kmol-K}\right)(2294{,}9)$$

$$=270317{,}2\frac{kJ}{s}$$

- ***<u>Combining the Equations:</u>***

$$165717{,}4-551T_{i2}-0{,}053{T_{i2}}^2+\frac{937702{,}9}{T_{i2}}+270317{,}2=(-\Delta H_R)F_{A_2}X_A$$

$$436034{,}4-551T_{i2}-0{,}053{T_{i2}}^2+\frac{937702{,}9}{T_{i2}}$$
$$=\left(46110\frac{kJ}{kmol}\right)\left(4{,}73\frac{kmol}{s}\right)(0{,}19-0{,}12)$$

$$420767{,}6-551T_{i2}-0{,}053{T_{i2}}^2+\frac{937702{,}9}{T_{i2}}=0$$

$$T_{i_2}=717\ K$$

- ***Reactor 1 (Inlet)***

$$\sum_{inlet} F_i C_{p_i} dT = \int_{T_{i1}}^{298} F_{N_2} C_{P_{N_2}} dT + \int_{T_{i1}}^{298} F_{H_2} C_{P_{H_2}} dT$$

$$F_{N_2} \int_{Ti1}^{298} \left(3{,}28 + 5{,}93 \times 10^{-4} T + \frac{4000}{T^2}\right) dT$$

$$+ F_{H_2} \int_{Ti1}^{298} \left(3{,}249 + 4{,}22 \times 10^{-4} T + \frac{8300}{T^2}\right) dT$$

$$F_{N_2} \left[3{,}28(298 - T_{i1}) + 2{,}965 \times 10^{-4}\left(298^2 - {T_{i1}}^2\right) - 4000\left(\frac{1}{298} - \frac{1}{T_{i1}}\right)\right]$$

$$+ F_{H_2} \left[3{,}249(298 - T_{i1}) + 2{,}11 \times 10^{-4}\left(298^2 - {T_{i1}}^2\right) - 8300\left(\frac{1}{298} - \frac{1}{T_{i1}}\right)\right]$$

$$F_{N_2} \left[977{,}44 - 3{,}28 T_{i1} + 26{,}33 - 2{,}965 \times 10^{-4} {T_{i1}}^2 - 13{,}42 + \frac{4000}{T_{i1}}\right]$$

$$+ F_{H_2} \left[968{,}202 - 3{,}249 T_{i1} + 18{,}74 - 2{,}11 \times 10^{-4} {T_{i1}}^2 - 27{,}85 + \frac{8300}{T_{i1}}\right]$$

$$F_{N_2} \left[990{,}35 - 3{,}28 T_{i1} - 2{,}965 \times 10^{-4} {T_{i1}}^2 + \frac{4000}{T_{i1}}\right]$$

$$+ F_{H_2} \left[959{,}09 - 3{,}249 T_{i1} - 2{,}11 \times 10^{-4} {T_{i1}}^2 + \frac{8300}{T_{i1}}\right]$$

REACTOR 1		
Species	**Inlet, kmol/s**	**Outlet, kmol/s**
N_2	5,38	4,73

H_2	16,14	14,20
NH_3	0,00	1,29

$$\left(5{,}38\frac{kmol}{s}\right)\left(8{,}314\frac{kJ}{kmol-K}\right)\left(990{,}35-3{,}28T_{i1}-2{,}965\times10^{-4}{T_{i1}}^{2}+\frac{4000}{T_{i3}}\right)$$
$$+\left(16{,}14\frac{kmol}{s}\right)\left(8{,}314\frac{kJ}{kmol-K}\right)\left(959{,}09-3{,}249T_{i1}-2{,}11\right.$$
$$\left.\times10^{-4}{T_{i1}}^{2}+\frac{8300}{T_{i1}}\right)$$

$$44297{,}7-146{,}7T_{i1}-0{,}013{T_{i1}}^{2}+\frac{178917{,}3}{T_{i1}}+128698{,}3-436T_{i1}-0{,}028{T_{i1}}^{2}$$
$$+\frac{1113760}{T_{i3}}$$

$$172996-582{,}7T_{i1}-0{,}041{T_{i1}}^{2}+\frac{1292677{,}3}{T_{i1}}$$

- ***Reactor 1 (Outlet)***

$$\sum_{outlet}F_iC_{p_i}dT=\int_{298}^{800}F_{N_2}C_{P_{N2}}dT+\int_{298}^{800}F_{H_2}C_{P_{H2}}dT+\int_{298}^{800}F_{NH_3}C_{P_{NH3}}dT$$

$$=F_{N_2}\int_{298}^{800}\left(3{,}28+5{,}93\times10^{-4}T+\frac{4000}{T^2}\right)dT$$
$$+F_{H_2}\int_{298}^{800}\left(3{,}249+4{,}22\times10^{-4}T+\frac{8300}{T^2}\right)dT$$
$$+F_{NH_3}\int_{298}^{800}\left(3{,}5778+3{,}02\times10^{-3}T-\frac{18600}{T^2}\right)dT$$

$$= F_{N_2}\left[3{,}28(800-298)+2{,}965\times10^{-4}(800^2-298^2)-4000\left(\frac{1}{800}-\frac{1}{298}\right)\right]$$
$$+F_{H_2}\left[3{,}249(800-298)+2{,}11\times10^{-4}(800^2-298^2)\right.$$
$$\left.-8300\left(\frac{1}{800}-\frac{1}{298}\right)\right]$$
$$+F_{NH_3}\left[3{,}5778(800-298\,)+1{,}51\times10^{-3}(800^2-298^2)\right.$$
$$\left.+18600\left(\frac{1}{800}-\frac{1}{298}\right)\right]$$

$$F_{N_2}[1646{,}6+163{,}4+8{,}4]+F_{H_2}[1631+116{,}3+17{,}5]$$
$$+F_{NH_3}[1796{,}1+832{,}3-39{,}2]$$

$$=\left(4{,}73\frac{kmol}{s}\right)\left(8{,}314\frac{kJ}{kmol-K}\right)(1818{,}4)$$
$$+\left(14{,}20\frac{kmol}{s}\right)\left(8{,}314\frac{kJ}{kmol-K}\right)(1764{,}8)$$
$$+\left(1{,}29\frac{kmol}{s}\right)\left(8{,}314\frac{kJ}{kmol-K}\right)(2589{,}2)$$

$$=307628{,}5\frac{kJ}{s}$$

- ***<u>Combining the Equations:</u>***

$$172996-582{,}7T_{i1}-0{,}041{T_{i1}}^2+\frac{1292677{,}3}{T_{i1}}+307628{,}5=(-\Delta H_R)F_{A_1}X_A$$

$$480624{,}5-582{,}7T_{i1}-0{,}041{T_{i1}}^2+\frac{1292677{,}3}{T_{i1}}$$
$$=\left(46110\frac{kJ}{kmol}\right)\left(5{,}38\frac{kmol}{s}\right)(0{,}12-0{,}00)$$

$$450855{,}9-582T_{i1}-0{,}041{T_{i1}}^2+\frac{1292677{,}3}{T_{i1}}=0$$

$$T_{i_1}=740\ K$$

Ammonia Synthesis Reaction – Adiabatic Energy Balance with Addition of Fresh Feed

- ***Reactor 1***

REACTOR 1					
Species	**Inlet, kmol/s**	**Outlet, kmol/s**	**Inlet Temperature, K**	**Outlet Temperature, K**	**Amount of Feed Added, kmol/s**
N_2	5,38	4,73	740	800	0,112
H_2	16,14	14,20			0,336
NH_3	0,00	1,29			---

- ***Reactor 2***

REACTOR 2					
Species	**Inlet, kmol/s**	**Outlet, kmol/s**	**Inlet Temperature, K**	**Outlet Temperature, K**	**Amount of Feed Added, kmol/s**
N_2	4,84	4,36	717	750	0,117
H_2	14,54	13,07			0,351
NH_3	1,29	2,25			---

- ***Reactor 3***

REACTOR 3				
Species	**Inlet, kmol/s**	**Outlet, kmol/s**	**Inlet Temperature, K**	**Outlet Temperature, K**
N_2	4,48	3,82	655	700
H_2	13,42	11,46		
NH_3	2,25	3,57		

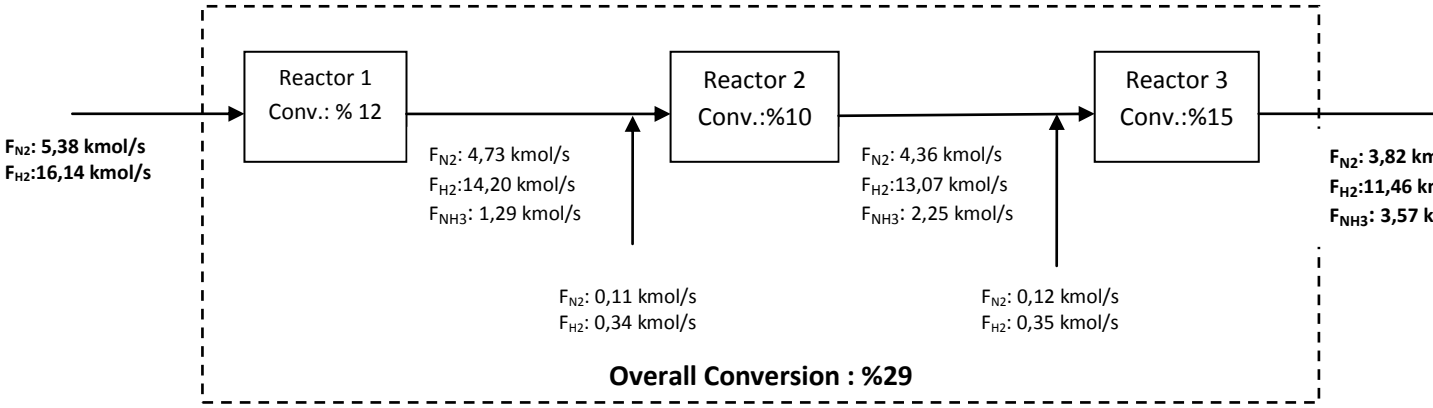

APPENDIX A.2

A.2. DETAILED RESULTS OF CHEMCAD AMMONIA SYNTHESIS LOOP SIMULATIONS

AMMONIA SYNTHESIS LOOP - FIGURE 17A

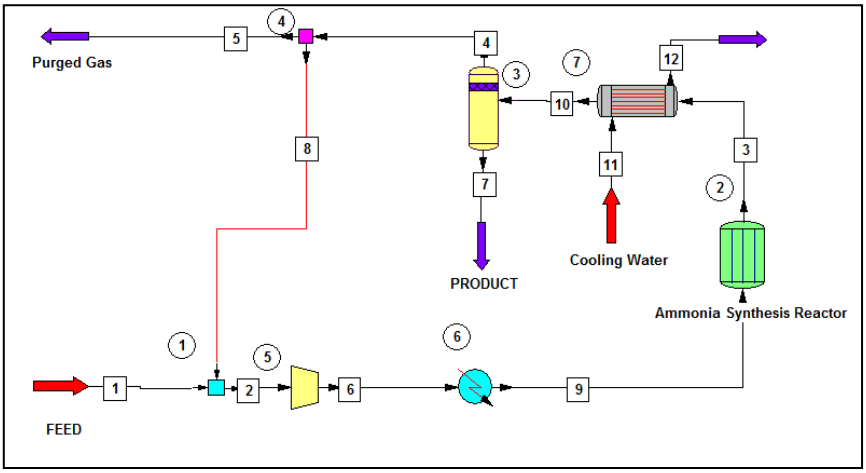

Stream No.	1	2	3	4
Temp K	500.0000	170.6994	774.0211	102.3113
Pres atm	100.0000	5.0000	99.0000	1.0000
Enth kJ/h	5.9329E+006	-2.1973E+007	7.0565E+007	-2.9378E+007
Vapor mole fraction	1.0000	1.0000	1.0000	1.0000
Total kmol/h	1000.0000	6385.2038	6027.4236	5669.6433
Flowrates in kmol/h				
Nitrogen	200.0000	596.3004	417.4103	417.4102
Hydrogen	800.0000	5788.9035	5252.2329	5252.2329
Ammonia	0.0000	0.0000	357.7803	0.0000
Water	0.0000	0.0000	0.0000	0.0000

Stream No.	5	6	7	8
Temp K	102.3113	504.3933	102.3113	102.3113
Pres atm	1.0000	100.1000	1.0000	1.0000
Enth kJ/h	-1.4689E+006	3.8686E+007	-2.9714E+007	-2.7909E+007
Vapor mole fraction	1.0000	1.0000	0.00000	1.0000
Total kmol/h	283.4822	6385.2038	357.7803	5386.1609
Flowrates in kmol/h				
Nitrogen	20.8705	596.3004	0.0001	396.5397
Hydrogen	262.6117	5788.9035	0.0000	4989.6211
Ammonia	0.0000	0.0000	357.7802	0.0000
Water	0.0000	0.0000	0.0000	0.0000

Stream No.	9	10	11	12
Temp K	673.0000	298.0000	298.0000	318.8552
Pres atm	100.0000	99.0000	1.0000	1.0000
Enth kJ/h	7.0565E+007	-1.6759E+007	-1.5878E+010	-1.5790E+010
Vapor mole fraction	1.0000	1.0000	0.00000	0.00000
Total kmol/h	6385.2038	6027.4236	55509.2983	55509.2983

Flowrates in kmol/h				
Nitrogen	596.3004	417.4103	0.0000	0.0000
Hydrogen	5788.9035	5252.2329	0.0000	0.0000
Ammonia	0.0000	357.7803	0.0000	0.0000
Water	0.0000	0.0000	55509.2983	55509.2983

AMMONIA SYNTHESIS LOOP - FIGURE 17B

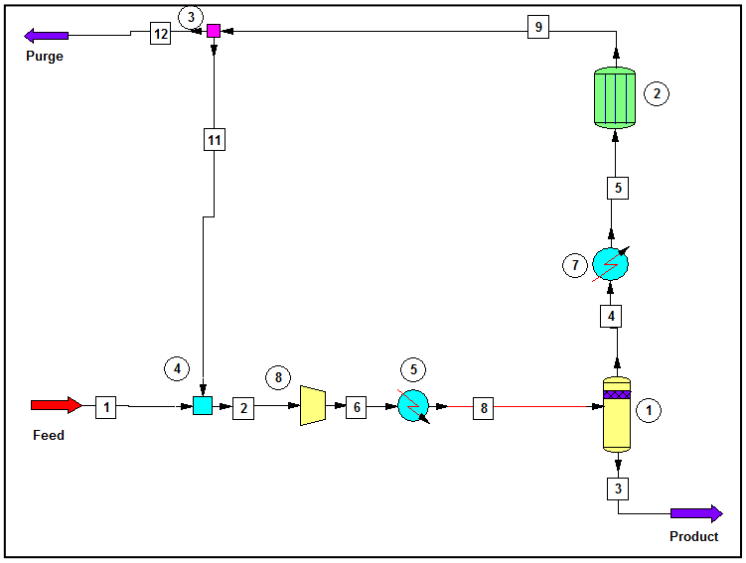

Stream No.	1	2	3	4
Temp K	500.0000	739.0989	200.0000	200.0000
Pres atm	100.0000	5.0000	100.0000	100.0000
Enth kJ/h	5.9329E+006	7.2551E+007	-2.5483E+007	-1.7968E+007
Vapor mole fraction	1.0000	1.0000	0.00000	1.0000
Total kmol/h	1000.0000	6722.8325	339.8537	6381.9631
Flowrates in kmol/h				
Nitrogen	200.0000	596.8557	0.1286	596.7011
Hydrogen	800.0000	5776.7097	0.1910	5775.5305
Ammonia	0.0000	349.2670	339.5341	9.7316

Stream No.	5	6	8	9
Temp K	673.0000	1855.3615	200.0000	774.0207
Pres atm	100.0000	100.0000	100.0000	99.0000
Enth kJ/h	7.0124E+007	3.2403E+008	-4.3453E+007	7.0125E+007
Vapor mole fraction	1.0000	1.0000	0.94945	1.0000
Total kmol/h	6381.9631	6722.8325	6722.8325	6024.0340
Flowrates in kmol/h				
Nitrogen	596.7011	596.8557	596.8557	417.7428
Hydrogen	5775.5305	5776.7097	5776.7097	5238.6419
Ammonia	9.7316	349.2670	349.2670	367.6495

Stream No.	11	12
Temp K	774.0207	774.0207
Pres atm	99.0000	99.0000
Enth kJ/h	6.6618E+007	3.5062E+006
Vapor mole fraction	1.0000	1.0000
Total kmol/h	5722.8323	301.2017
Flowrates in kmol/h		
Nitrogen	396.8557	20.8871
Hydrogen	4976.7096	261.9321
Ammonia	349.2670	18.3825

AMMONIA SYNTHESIS LOOP - FIGURE 17C

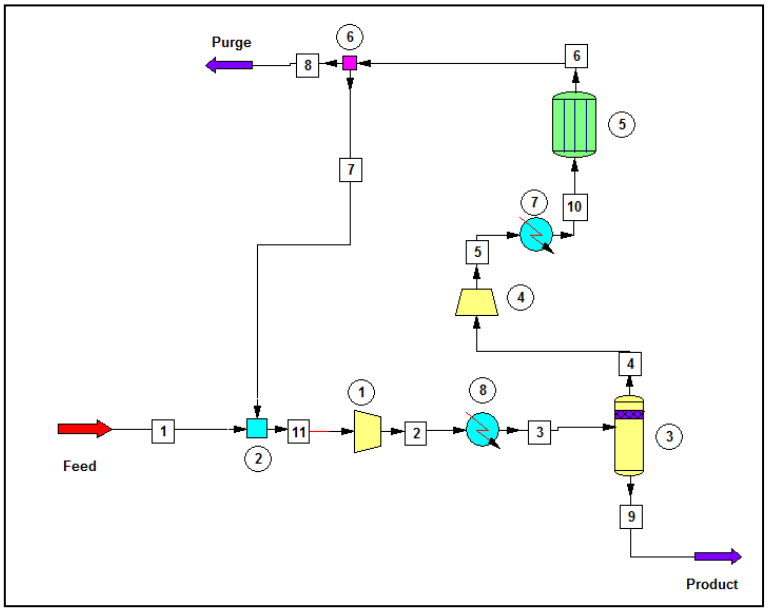

FLOW SUMMARIES

Stream No.	1	2	3	4
Temp K	500.0000	1856.2173	200.0000	175.0000
Pres atm	100.0000	100.0000	100.0000	10.0000
Enth kJ/h	5.9329E+006	3.2350E+008	-4.3111E+007	-2.1517E+007
Vapor mole fraction	1.0000	1.0000	0.94995	1.0000
Total kmol/h	1000.0000	6707.1543	6707.1543	6367.6276
Flowrates in kmol/h				
Nitrogen	200.0000	597.2013	597.2013	597.1917
Hydrogen	800.0000	5764.8578	5764.8578	5764.8512
Ammonia	0.0000	345.0951	345.0951	5.5847

Stream No.	5	6	7	8
Temp K	411.7944	774.2203	774.2203	774.2203
Pres atm	100.0000	99.0000	99.0000	99.0000
Enth kJ/h	2.1003E+007	7.0139E+007	6.6632E+007	3.5070E+006
Vapor mole fraction	1.0000	1.0000	1.0000	1.0000
Total kmol/h	6367.6276	6009.9474	5709.4496	300.4974
Flowrates in kmol/h				
Nitrogen	597.1917	418.3533	397.4356	20.9177
Hydrogen	5764.8512	5228.3338	4966.9171	261.4167
Ammonia	5.5847	363.2602	345.0971	18.1630

Stream No.	9	10	11
Temp K	175.0000	673.0000	739.1869
Pres atm	10.0000	100.0000	5.0000
Enth kJ/h	-2.6214E+007	7.0139E+007	7.2565E+007
Vapor mole fraction	0.00000	1.0000	1.0000
Total kmol/h	339.5263	6367.6276	6709.4497
Flowrates in kmol/h			
Nitrogen	0.0096	597.1917	597.4356
Hydrogen	0.0065	5764.8512	5766.9171
Ammonia	339.5102	5.5847	345.0971

AMMONIA SYNTHESIS LOOP - FIGURE 17D

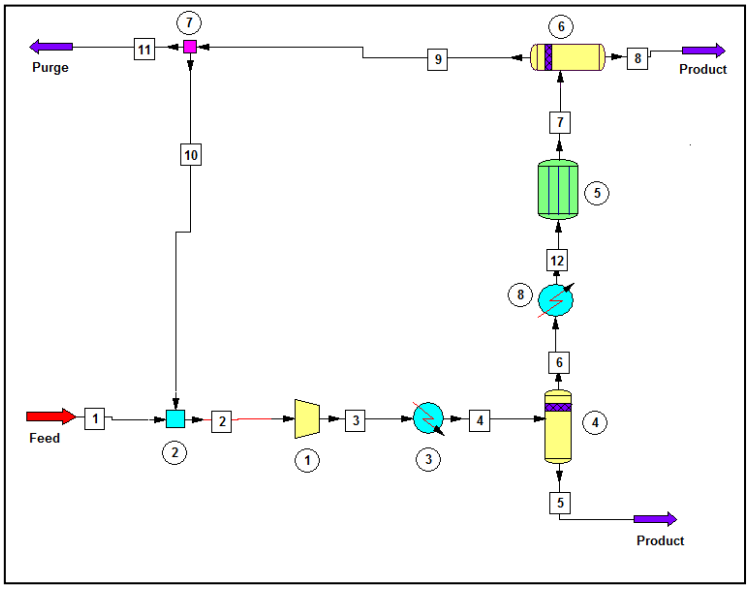

FLOW SUMMARIES

Stream No.	1	2	3	4
Temp K	500.0000	491.1318	1322.2408	298.0000
Pres atm	100.0000	5.0000	100.0000	100.0000
Enth kJ/h	5.9329E+006	5.6609E+006	3.2489E+007	-1.7286E+005
Vapor mole fraction	1.0000	1.0000	1.0000	1.0000
Total kmol/h	1000.0000	1042.9165	1042.9165	1042.9165
Flowrates in kmol/h				
Nitrogen	200.0000	207.2577	207.2577	207.2577
Hydrogen	800.0000	832.2997	832.2997	832.2997
Ammonia	0.0000	3.3591	3.3591	3.3591

Stream No.	5	6	7	8
Temp K	200.0000	200.0000	889.9801	200.0000
Pres atm	100.0000	100.0000	99.0000	1.0000
Enth kJ/h	-1.2018E+005	-3.0521E+006	1.1463E+007	-4.4252E+006
Vapor mole fraction	0.00000	1.0000	1.0000	0.00000
Total kmol/h	1.6034	1041.3131	917.1101	58.7796
Flowrates in kmol/h				
Nitrogen	0.0013	207.2564	145.1549	0.0005
Hydrogen	0.0008	832.2989	645.9940	0.0003
Ammonia	1.6013	1.7578	125.9611	58.7788

Stream No.	9	10	11	12
Temp K	200.0000	200.0000	200.0000	673.0000
Pres atm	1.0000	1.0000	1.0000	100.0000
Enth kJ/h	-5.4404E+006	-2.7202E+005	-5.1684E+006	1.1462E+007
Vapor mole fraction	1.0000	1.0000	1.0000	1.0000
Total kmol/h	858.3304	42.9165	815.4139	1041.3131
Flowrates in kmol/h				
Nitrogen	145.1544	7.2577	137.8967	207.2564
Hydrogen	645.9937	32.2997	613.6940	832.2989
Ammonia	67.1823	3.3591	63.8232	1.7578

APPENDIX A.3

A.3 AN EXAMPLE OF H_2 REDUCTION PROCEDURE FOR CHEMISORPTION (Na-Ru/Vulcan)

Step 1: Weighing the catalyst and connection to manifold.

- 0.3319 g Na-Ru/Vulcan catalyst was weighed and connected to the manifold via vacuum tight special connection.
- After that, leak test procedure was applied. Manifold was evacuated after a while and vacuum valve was closed. The pressure change was observed. Before the leak test, the baseline pressure measurement was read as 4.12×10^{-2} torr and after closed the valve pressure was measured as 6.38×10^{-2}. It can be said that leak rate is so small and experiment can be done.

Step 2: Heating Procedure

- At room temperature 680 torr He gas was taken to the manifold and heating was started. The aim of heating up to 150 ^{o}C of sample cell in the presence of He gas almost atmosphere pressure was to get rid of water molecules over the catalyst.
- The sample cell was heated up to 150 ^{o}C in 1.5 hour time interval and sample cell was waited at 150 ^{o}C for 30 minutes. When system came to 150 ^{o}C in, pressure was read as 709 torr.
- After water was gone away from the catalyst via evacuation of the manifold at 150 ^{o}C, approximately 140 torr of H_2 was taken to the manifold and sample cell again was started to heating up to 350 ^{o}C. The data of H_2 decrease with respect to time and temperature are tabulated below:

Time, sec.	Pressure, torr	Temperature, ^{o}C
0	179	176
15	141	
60	140,1	180
300	133,8	188

420	125,4	
600	118,5	200
720	113,4	
900	107,5	217
1080	105,9	
1200	105,3	237
1800	106,7	293

Step 3: High Temperature H_2 Reduction Procedure

- When system was reached to 350 ^oC, manifold was evacuated.
- Then, fresh H_2 was taken into system and sent to the sample cell. The details of the pressure chance can be seen in below;

Time, sec.	Pressure, torr	Temperature, ^oC
0	503	355
15	399.5	
30	398.8	357
60	397.0	
120	395.7	361
150	394.8	
240	394.4	
600	392.4	372
900	391.4	378
1200	391.1	
1500	390.8	371
1800	390.6	371

- Similar H_2 reduction procedure was applied for four times to the catalyst in two hours period.
- After H_2 reduction procedure, manifold was evacuated at reduction temperature (360 ^oC) for 2 hours.

- Finally, heating system was closed and manifold will be evacuated overnight.

APPENDIX A.4.

A.4. DETAILS OF POINT SOURCE DIFFUSION CALCULATIONS

Derivation Details of the Corresponding Equations for Calculating the Amount of Spiltover Hydrogen

The general partial derivative of transient diffusion problem is

$$\frac{\partial C}{\partial t} = D\frac{\partial^2 C}{\partial x^2}$$

The solution for this equation in a semi-infinite region for a point source with the given initial and boundary conditions were given below:

I.C. C = 0 when x > a at t = 0

B.C. $C = C_e$ when x = a at t > 0

The general solution for the equation for this second partial derivative is for a point source is

$$C = C_e\sqrt{\frac{a}{x}}\left[1 - erf\left(\frac{x-a}{4Dt^{-\frac{1}{2}}}\right)\right]$$

In order to calculate the total amount of spiltover hydrogen, change of concentration with respect to x when x=a should be integrated from t=0 to $t = t_{equilibirum}$

$$M = 4aC_e\sqrt{\pi Dt}$$

According to Kramer and Andre, there are lots of point source over the support. So, when spillover process carries on from metal to support surface, the concentration profile of each point source interfere with each other.

In this situation, solution of the derivative equation was done with respect to line source mechanism. In other words, the name of the solution can be said as “uniform initial distribution – variable surface concentration”

The solution of the given equation was done with regard to defined initial and boundary conditions given below:

Initial Condition ,	I.C.	t = 0, C = C_e	0 < x <b
Boundary Condition,	B.C. 1	t ≥ 0, C = C_1	x = 0
Boundary Condition,	B.C. 2	t ≥ 0, C = C_2	x = b

The general solution for this expression is

$$C = C_1 + (C_2 - C_1)\frac{x}{b} + \frac{2}{\pi}\sum_{0}^{\infty}\frac{C_2\cos n\pi - C_1}{n} sin\frac{n\pi x}{b}\exp\left(-\frac{Dn^2\pi^2 t}{b^2}\right) + \frac{4C_o}{\pi}\sum_{0}^{\infty}\frac{1}{2m+1} sin\frac{(2m+1)\pi x}{b}\exp\left(-\frac{D(2m+1)^2\pi^2 t}{b^2}\right)$$

If M_t denotes the total amount of diffusing substance which has entered the support plane at time t, and M_∞ the corresponig quantity after infinite time, then

$$\frac{M_t}{M_\infty} = 1 - \sum_{n=0}^{\infty}\frac{8}{(2n+1)^2\pi^2}\exp\{-D(2n+1)^2\pi^2 t/b^2\}$$

Calculation of Coefficient of Diffusion of Ru/Vulcan at 375 Torr

The solution of differential equation of Point Source Diffusion is given below if the system comes to equilibrium:

$$c = c_e\left[1 - \frac{8}{\pi^2}\exp\left(-\frac{\pi^2 Dt}{b^2}\right)\right]$$

where, *c* is the H uptake per cm^2 of support. c_e is the equilibrium concentration when system comes to equilibrium. *D* is the coefficient of diffusion and *b* is the mean distance between the particles.

If this fit is applicable for the graph, then we can calculate the coefficient of diffusivity.

At 1 hour:

$$c = 1.05 \times 10^{13}\ \frac{H\ atoms}{cm^2}$$

$$c_e = 1.45 \times 10^{13} \frac{H\ atoms}{cm^2}$$

$$a = 145\ nm$$

$$1.05 \times 10^{13} = 1.45 \times 10^{13} \left[1 - \frac{8}{\pi^2} \exp\left(-\frac{\pi^2 D(3600)}{(1.45 \times 10^{-5})^2}\right)\right]$$

$$D = 1.39 \times 10^{-14} \frac{cm^2}{sec}$$

The calculation details of *a, c, c_e* are given at the end of this report.

Calculation of Dispersion and Mean Particle Diameter of Ru particle over Ru/Vulcan catalyst

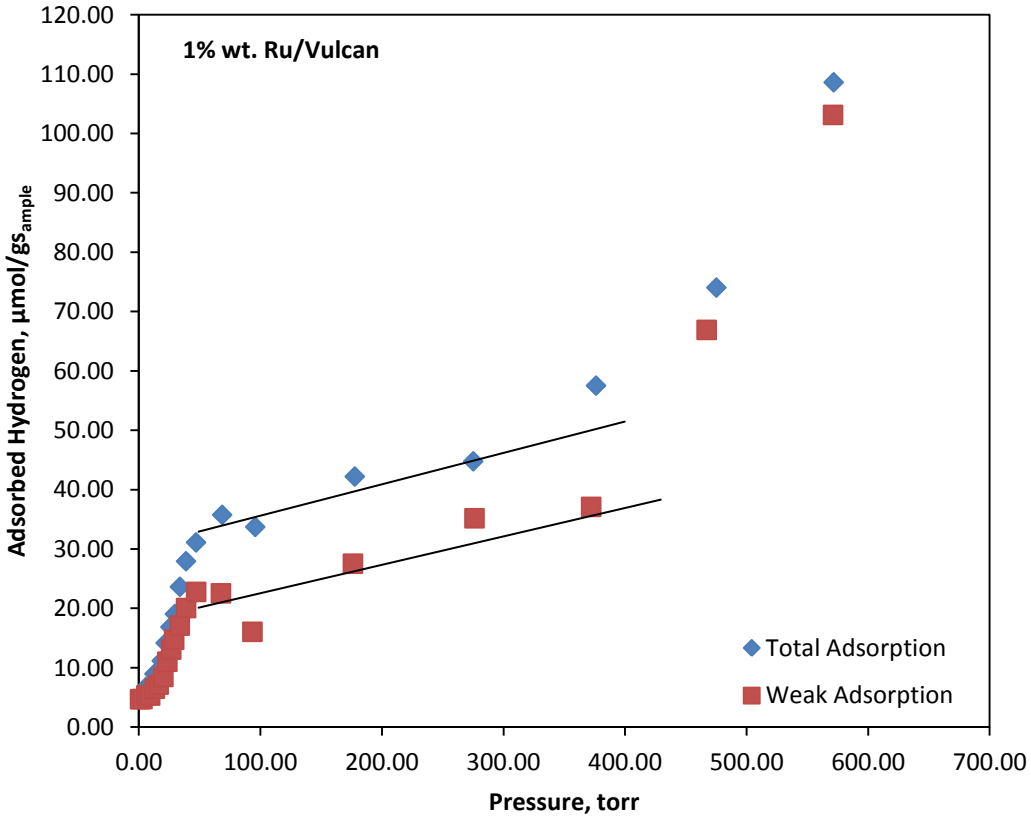

$$Intercept\ Difference = Total\ Adsorption - Weak\ Adsorption$$

$$Intercept\ Difference = 31.5\ \frac{\mu mol}{gcat} - 18.0\ \frac{\mu mol}{gcat} = 13.5 \frac{\mu mol}{gcat}$$

$$\%\ Dispersion$$

$$= \left(13.5 \frac{\mu mol\ H_2}{gcat}\right)\left(\frac{1\ gcat}{0.01\ g\ Ru}\right)\left(\frac{101.07\ g\ Ru}{1\ mol\ Ru}\right)\left(\frac{1\ mol\ Ru}{10^6\ \mu mol\ Ru}\right)\left(\frac{2\ \mu mol\ H}{1\ \mu mol\ H_2}\right) * 100$$

$$\%\ Dispersion = 27.2\ \%$$

$$Mean\ Particle\ Diameter = \frac{100}{Dispersion} = \frac{100}{27.2} = 3.7\ nm$$

Calculation of Average Number of Ru particles located 1 cm^2 of Support (Vulcan) Surface

$$App.Surface\ Area\ of\ Catalyst$$

$$= (1\ g\ catalyst) * \left(\frac{241\ m^2}{1\ g\ catalyst}\right) * \left(\frac{1 \times 10^4\ cm^2}{1\ m^2}\right)$$

$$= 2.41 \times 10^6\ cm^2$$

$$Number\ of\ Ru\ Atoms\ over\ Support$$

$$= (1\ g\ catalyst) * \left(\frac{0.01\ g\ Ru}{1\ g\ catalyst}\right) * \left(\frac{1\ mol\ Ru}{101.07\ g\ Ru}\right) * \left(\frac{27.2}{100}\right)$$

$$* \left(\frac{6.02 \times 10^{23}\ Ru}{1\ mol\ Ru}\right) = 1.45 \times 10^{19}\ Ru$$

- <u>Calculation of Number of Ru atoms in a Spherical Ru Particle</u>

$$Atomic\ Volume\ of\ Ru = 8.3 \frac{cm^3}{mol} \times \frac{1\ mol}{6.02\ \times 10^{23}} = 1.379\ \times 10^{-23} \frac{cm^3}{Ru\ atom}$$

$$Volume\ of\ a\ Ru\ Particle\ (spherical) = \frac{4}{3}\pi * r^3$$

$$= \frac{4}{3} * \pi * \left(\frac{3.7\ \text{nm}}{2} \times \frac{10^{-7}\ \text{cm}}{1\ \text{nm}}\right)^3 = 2.873 \times 10^{-20}\ \frac{cm^3}{Ru\ particle}$$

$$Number\ of\ Ru\ atoms\ in\ a\ Ru\ Particle = \frac{3.635 \times 10^{-20}\ \frac{cm^3}{Ru\ particle}}{2.873\ \times 10^{-23}\frac{cm^3}{Ru\ atom}}$$

$$= 1265\ \frac{Ru\ atom}{Ru\ particle}$$

Calculation of Number of Ru Particle in 1 cm^2 Support Surface (Particle Density)

$$Number\ of\ Ru\ Atoms\ over\ Support$$

$$= \frac{1\ g\ support}{241\ m^2} \times \frac{1.45 \times 10^{19}\ Ru\ Atom}{1\ g\ support} \times \frac{1\ m^2}{10^4\ cm^2}$$

$$= 6.02\ \times 10^{12}\ \frac{Ru\ atoms}{cm^2}$$

$$Number\ of\ Ru\ Particles\ over\ Support$$

$$= 6.02\ \times 10^{12}\ \frac{Ru\ atoms}{cm^2} \times \frac{1\ Ru\ Particle}{1265\ Ru\ atom}$$

$$= 4.75 \times 10^9 \frac{Ru\ particle}{cm^2}$$

Calculation of Mean Distances Between Particles

Assume that, all Ru particles are in square order with respect to each other over 1 cm^2 support:

$$Number\ of\ Ru\ Particle\ in\ 1\ edge = \sqrt{4.75 \times 10^9} = 6.9 \times 10^4$$

If the distance between each particle is a;

$$Mean\ Distance\ Between\ Metal\ Particles = a = \frac{1\ cm}{4.8 \times 10^4} = 1.45 \times 10^{-5} cm$$

$$= 145\ nm$$

APPENDIX A.5.

A.5. MICROKINETIC ANALYSIS OF AMMONIA SYNTHESIS REACTION

A.5.1 FORTRAN Code For Microkinetic Model

```
PROGRAM MICROKINETIC_AMMONIA_RUTHENIUM
INTEGER,PARAMETER :: IKIND=SELECTED_REAL_KIND (p=8,r=80)
INTEGER,PARAMETER :: INT=SELECTED_INT_KIND(18)
REAL (KIND=IKIND) :: T,R,DELT,KF10,KR10,KF20,KR20,KF30,KR30,KF40,KR40,KF50,KR50,KF60,KR60,A
REAL (KIND=IKIND) ::
V0,VCAT,PHI,RHOCAT,CT,YN2,YH3,YNH3,KF1,KR1,KF2,KR2,KF3,KR3,KF4,KR4,KF5,KR5,KF6,KR6,RATE_CHECK
REAL (KIND=IKIND) ::
DTHETAN,DTHETAH,DTHETANH,DTHETANH2,DTHETANH3,CN2,CH2,CNH3,DCN2,DCH2,DCNH3
REAL (KIND=IKIND) ::
THETAN,THETAH,THETANH,THETANH2,THETANH3,THETAV,W,THETANN,THETAHN,THETANHN,THETANH2
N,THETANH3N,THETAVN
 REAL (KIND=IKIND) :: CN2N,CH2N,CNH3N,TIME,T1,T2,B,C,SYSTIME
 CHARACTER(LEN=22) :: LINE
INTEGER (KIND=INT) :: N,ITER
        PRINT*,"INPUT # OF TIME STEPS"

 READ*,N

        PRINT*, "Processing..."
   CALL CPU_TIME(T1)
        IFLAG1=0; IFLAG2=0; IFLAG3=0; IFLAG4=0; IFLAG5=0; IFLAG6=0; IFLAG7=0; IFLAG8=0; IFLAG9=0;
ITFLAG=0

!       CONSTANTS

T=523       ! Operating Temperature, K
R=8.314     ! Gas Constant, J/(mol*K)
TIME=0              ! Total Time, s
 DELT=1E-13   ! Time Stepping, s
KF10=56e-3   ! Rate Constant Forward 1, 1/(Pa*s)
KR10=2e10    ! Rate Constant Reverse 1, 1/s
KF20=6e13    ! Rate Constant Forward 2, 1/s
KR20=15e13   ! Rate Constant Reverse 2, 1/s
KF30=47e12   ! Rate Constant Forward 3, 1/s
KR30=18e12   ! Rate Constant Reverse 3, 1/s
KF40=33e12   ! Rate Constant Forward 4, 1/s
KR40=93e11   ! Rate Constant Reverse 4, 1/s
KF50=24e12   ! Rate Constant Forward 5, 1/s
KR50=21e2    ! Rate Constant Reverse 5, 1/(Pa*s)
KF60=55e1    ! Rate Constant Forward 6, 1/(Pa*s)
KR60=25e12   ! Rate Constant Reverse 6, 1/s
V0=3e-4      ! Volumetric Flowrate, m^3/s
VCAT=0.0001  ! Reactor Volume, m^3
PHI=0.34     ! Catalyst Porosity
RHOCAT=3650  ! Catalyst Density

CT=1448      ! Total Inlet Concentration, mol/m^3
YN2=0.25     ! Inlet Mole Fraction N2
YH2=0.75     ! Inlet Mole Fraction H2
YNH3=0       ! Inlet Mole Fraction NH3
A=0.03              ! TOF Conversion Number
W=0.001             ! Catalyst Weight

LINE="----------------------"
```

```
!           INITIALIZATION
OPEN(8,FILE='Concentrations.txt',STATUS='REPLACE')
OPEN(9,FILE='Coverages.txt',STATUS='REPLACE')
CN2=CT*YN2   ! Initial Nitrogen Concentration, mol/m^3
CH2=CT*YH2   ! Initial Hydrogen Concentration, mol/m^3
CNH3=CT*YNH3 ! Initial Ammonia Concentration, mol/m^3
THETAV=1
THETAN=0
THETAH=0
THETANH=0
   THETANH2=0
   THETANH3=0


!           RATE CONSTANTS

   KF1=KF10*EXP(-33000/(R*T))  ! Rate Constant Forward 1
           KR1=KR10*EXP(-137000/(R*T)) ! Rate Constant Reverse 1
   KF2=KF20*EXP(-111000/(R*T)) ! Rate Constant Forward 2
           KR2=KR20*EXP(-74100/(R*T))  ! Rate Constant Reverse 2
   KF3=KF30*EXP(-60400/(R*T))  ! Rate Constant Forward 3
           KR3=KR30*EXP(-8600/(R*T))   ! Rate Constant Reverse 3
   KF4=KF40*EXP(-17200/(R*T))  ! Rate Constant Forward 4
           KR4=KR40*EXP(-64600/(R*T))  ! Rate Constant Reverse 4
   KF5=KF50*EXP(-83700/(R*T))  ! Rate Constant Forward 5
           KR5=KR50*EXP(-0/(R*T))                  ! Rate Constant Reverse 5
   KF6=KF60*EXP(-0/(R*T))              ! Rate Constant Forward 6
           KR6=KR60*EXP(-82000/(R*T))          ! Rate Constant Reverse 6

           RATE_CHECK=KF1*CN2*R*T*(THETAV**2)-KR1*(THETAN**2) ! Rate Limiting Step
   WRITE(8,100) "LOG(TIME) (s)","LOG(CN2) (mol/m^3)","LOG(CH2) (mol/m^3)","LOG(CNH3) (mol/m^3)"
   WRITE(9,101) "LOG(TIME)
(s)","LOG(THETAN)","LOG(THETAH)","LOG(THETANH)","LOG(THETANH2)","LOG(THETANH3)","LOG(THETAV)"
           WRITE(8,200) (LINE,J=1,4)
   WRITE(9,201) (LINE,J=1,7)


!           EULER SOLVER

           DO ITER=1,N

           CALL
CBATCH(DCN2,DCH2,DCNH3,A,VCAT,THETAN,THETAH,THETANH3,THETAV,W,KF1,KR1,T,KF6,KR6,KF5,KR5,C
N2,CH2,CNH3)
   CALL
DTHETA(CN2,CH2,CNH3,THETAN,THETAH,THETANH,THETANH2,THETANH3,THETAV,KF1,KR1,KF2,KR2,KF3,K
R3,KF4,KR4,KF5,KR5,KF6,KR6,T,&
   DTHETAN,DTHETAH,DTHETANH,DTHETANH2,DTHETANH3)
           CALL
EULER(THETAN,THETANN,THETAH,THETAHN,THETANH,THETANHN,THETANH2,THETANH2N,THETANH3,TH
ETANH3N,THETAVN,&

CN2,CH2,CNH3,CH2N,CN2N,CNH3N,DCN2,DCH2,DCNH3,DTHETAN,DTHETAH,DTHETANH,DTHETANH2,DTHET
ANH3,DELT)

   TIME=TIME+DELT

!           PRINT-OUT BLOCK

           IF(ITER>1.AND.ITER<=100) THEN
                   IF(MOD(ITER,5)==0) THEN
                   WRITE(8,300) LOG10(TIME),LOG10(CN2N),LOG10(CH2N),LOG10(CNH3N)
           WRITE(9,400)
LOG10(TIME),LOG10(THETANN),LOG10(THETAHN),LOG10(THETANHN),LOG10(THETANH2N),LOG10(THETANH
3N),LOG10(THETAVN)
           ENDIF
           ELSE IF(ITER>100.AND.ITER<=1000) THEN
           IF(MOD(ITER,100)==0) THEN
                   WRITE(8,300) LOG10(TIME),LOG10(CN2N),LOG10(CH2N),LOG10(CNH3N)
```

```
            WRITE(9,400)
LOG10(TIME),LOG10(THETANN),LOG10(THETAHN),LOG10(THETANHN),LOG10(THETANH2N),LOG10(THETANH
3N),LOG10(THETAVN)
            ENDIF
   ELSE IF(ITER>1000.AND.ITER<=100000) THEN
            IF(MOD(ITER,10000)==0) THEN
                        WRITE(8,300) LOG10(TIME),LOG10(CN2N),LOG10(CH2N),LOG10(CNH3N)
            WRITE(9,400)
LOG10(TIME),LOG10(THETANN),LOG10(THETAHN),LOG10(THETANHN),LOG10(THETANH2N),LOG10(THETANH
3N),LOG10(THETAVN)
            ENDIF
   ELSE IF(ITER>100000.AND.ITER<=10000000) THEN
            IF(ITFLAG==0) THEN
                        DELT=DELT*10_IKIND
         ITFLAG=1
      ENDIF
            IF(MOD(ITER,100000)==0) THEN
                        WRITE(8,300) LOG10(TIME),LOG10(CN2N),LOG10(CH2N),LOG10(CNH3N)
            WRITE(9,400)
LOG10(TIME),LOG10(THETANN),LOG10(THETAHN),LOG10(THETANHN),LOG10(THETANH2N),LOG10(THETANH
3N),LOG10(THETAVN)
            ENDIF
            ELSE IF(ITER>10000000.AND.ITER<=1000000000) THEN
            IF(ITFLAG==1) THEN
            DELT=DELT*100_IKIND
                                    ITFLAG=2
      ENDIF
            IF(MOD(ITER,1000000)==0) THEN
                        WRITE(8,300) LOG10(TIME),LOG10(CN2N),LOG10(CH2N),LOG10(CNH3N)
            WRITE(9,400)
LOG10(TIME),LOG10(THETANN),LOG10(THETAHN),LOG10(THETANHN),LOG10(THETANH2N),LOG10(THETANH
3N),LOG10(THETAVN)
            ENDIF
   ELSE IF(ITER>1000000000.AND.ITER<=1000000000) THEN
            IF(ITFLAG==2) THEN
            DELT=DELT*100_IKIND
                                    ITFLAG=3
      ENDIF
                        IF(MOD(ITER,10000000)==0) THEN
                        WRITE(8,300) LOG10(TIME),LOG10(CN2N),LOG10(CH2N),LOG10(CNH3N)
            WRITE(9,400)
LOG10(TIME),LOG10(THETANN),LOG10(THETAHN),LOG10(THETANHN),LOG10(THETANH2N),LOG10(THETANH
3N),LOG10(THETAVN)
            ENDIF
            ELSE
            IF(ITFLAG==3) THEN
            DELT=DELT*1000_IKIND
                                    ITFLAG=4
      ENDIF
            IF(MOD(ITER,100000000)==0) THEN
                        WRITE(8,300) LOG10(TIME),LOG10(CN2N),LOG10(CH2N),LOG10(CNH3N)
            WRITE(9,400)
LOG10(TIME),LOG10(THETANN),LOG10(THETAHN),LOG10(THETANHN),LOG10(THETANH2N),LOG10(THETANH
3N),LOG10(THETAVN)
            ENDIF
   ENDIF

            CALL
SWAP(THETAN,THETANN,THETAH,THETAHN,THETANH,THETANHN,THETANH2,THETANH2N,THETANH3,THE
TANH3N,THETAV,THETAVN,&
   CN2,CH2,CNH3,CH2N,CN2N,CNH3N)

!           REPORT BLOCK

            B=ITER
            C=N
            IF (IFLAG1==1) GOTO 20
            IF(B/C*100.GT.10) THEN
   PRINT*,"%10"
```

```
   IFLAG1=1
   GOTO 10
   ENDIF
20          IF (IFLAG2==1) GOTO 21
            IF(B/C*100.GT.20) THEN
   PRINT*,"%20"
   IFLAG2=1
   GOTO 10
   ENDIF
21          IF (IFLAG3==1) GOTO 22
            IF(B/C*100.GT.30) THEN
   PRINT*,"%30"
   IFLAG3=1
            GOTO 10
   ENDIF
22          IF (IFLAG4==1) GOTO 23
            IF(B/C*100.GT.40) THEN
   PRINT*,"%40"
   IFLAG4=1
            GOTO 10
   ENDIF
23          IF (IFLAG5==1) GOTO 24
            IF(B/C*100.GT.50) THEN
   PRINT*,"%50"
   IFLAG5=1
            GOTO 10
   ENDIF
24          IF (IFLAG6==1) GOTO 25
            IF(B/C*100.GT.60) THEN
   PRINT*,"%60"
   IFLAG6=1
            GOTO 10
   ENDIF
25          IF (IFLAG7==1) GOTO 26
            IF(B/C*100.GT.70) THEN
   PRINT*,"%70"
   IFLAG7=1
            GOTO 10
   ENDIF
26          IF (IFLAG8==1) GOTO 27
            IF(B/C*100.GT.80) THEN
   PRINT*,"%80"
   IFLAG8=1
            GOTO 10
   ENDIF
27          IF (IFLAG9==1) GOTO 10
            IF(B/C*100.GT.90) THEN
   PRINT*,"%90"
   IFLAG9=1
            GOTO 10
   ENDIF

10          ENDDO

100         FORMAT(4(A19,1X))
101         FORMAT(7(A19,1X))
200         FORMAT(4(A19,1X))
201         FORMAT(7(A19,1X))
300         FORMAT(4(F18.5,1X,1H'))
400         FORMAT(7(F18.5,1X,1H'))

            CALL CPU_TIME(T2)
   SYSTIME=T2-T1
   IF(SYSTIME>=60.AND.SYSTIME<=3600) THEN
   SYSTIME=SYSTIME/60_IKIND
            PRINT*, "Solved in:",SYSTIME,"minutes."
   ELSE IF(SYSTIME>=3600) THEN
   SYSTIME=SYSTIME/3600_IKIND
   PRINT*,"Solved in:",SYSTIME,"hours."
```

```
   ELSE
   PRINT*,"Solved in:",SYSTIME,"seconds."
   ENDIF

            END PROGRAM MICROKINETIC_AMMONIA_RUTHENIUM


!           SUBPROGRAMS
!           ------------------------------------------------------------------------------------------------------------------------

!           SUBPROGRAM FOR CALCULATING THE DERIVATIVES OF CONCENTRATIONS FOR A BATCH
REACTOR

   SUBROUTINE
CBATCH(DCN2,DCH2,DCNH3,A,VCAT,THETAN,THETAH,THETANH3,THETAV,W,KF1,KR1,T,KF6,KR6,KF5,KR5,C
N2,CH2,CNH3)
   INTEGER,PARAMETER :: IKIND=SELECTED_REAL_KIND (p=8,r=80)
   REAL (KIND=IKIND) :: DCN2,DCH2,DCNH3,A,VCAT,THETAN,THETAH,THETANH3,THETAV,W
   REAL (KIND=IKIND) :: KF1,KR1,T,KF6,KR6,KF5,KR5,CN2,CH2,CNH3,R

   R=8.314_IKIND

            DCN2=A/VCAT*(-KF1*CN2*R*T*(THETAV**2)+KR1*(THETAN**2))*W
            DCH2=3*A/VCAT*(-KF6*CH2*R*T*(THETAV**2)+KR6*(THETAH**2))*W
            DCNH3=2*A/VCAT*(KF5*THETANH3-KR5*THETAV*CNH3*R*T)*W

   RETURN
   END

!           ------------------------------------------------------------------------------------------------------------------------


!           SUBPROGRAM FOR CALCULATING THE DERIVATIVES OF FRACTIONAL COVERAGES

            SUBROUTINE
DTHETA(CN2,CH2,CNH3,THETAN,THETAH,THETANH,THETANH2,THETANH3,THETAV,&

KF1,KR1,KF2,KR2,KF3,KR3,KF4,KR4,KF5,KR5,KF6,KR6,T,DTHETAN,DTHETAH,DTHETANH,DTHETANH2,DTHET
ANH3)
   INTEGER,PARAMETER :: IKIND=SELECTED_REAL_KIND (p=8,r=80)
   REAL (KIND=IKIND) :: CN2,CH2,CNH3,THETAN,THETAH,THETANH,THETANH2,THETANH3,THETAV
   REAL (KIND=IKIND) :: KF1,KR1,KF2,KR2,KF3,KR3,KF4,KR4,KF5,KR5,KF6,KR6,T,R
            REAL (KIND=IKIND) :: DTHETAN,DTHETAH,DTHETANH,DTHETANH2,DTHETANH3

   R=8.314_IKIND

            DTHETAN=KF1*CN2*R*T*(THETAV**2)-KR1*(THETAN**2)-
2*KF2*(THETAN)*(THETAH)+2*KR2*(THETANH)*(THETAV)
            DTHETANH=2*KF2*(THETAN)*(THETAH)-2*KR2*(THETANH)*(THETAV)-
2*KF3*(THETANH)*(THETAV)+2*KR3*(THETANH2)*(THETAV)
            DTHETANH2=2*KF3*(THETANH)*(THETAH)-2*KR3*(THETANH2)*(THETAV)-
2*KF4*(THETANH2)*(THETAH)+2*KR4*(THETANH3)*(THETAV)
            DTHETANH3=2*KF4*(THETANH2)*(THETAH)-2*KR4*(THETANH3)*(THETAV)-
2*KF5*(THETANH3)+2*KR5*CNH3*R*T*(THETAV)

            DTHETAH=-2*KF2*(THETAN)*(THETAH)+2*KR2*(THETANH)*(THETAV)-
2*KF3*(THETANH)*(THETAH)+2*KR3*(THETANH2)*(THETAV)&
   -2*KF4*(THETANH2)*(THETAH)+2*KR4*(THETANH3)*(THETAV)+3*KF6*CH2*R*T*(THETAV**2)-
3*KR6*(THETAH**2)

            THETAV=1_IKIND-THETAN-THETAH-THETANH-THETANH2-THETANH3

   RETURN
   END


!           ------------------------------------------------------------------------------------------------------------------------

!           SUBPROGRAM FOR EULER'S METHOD
```

```
            SUBROUTINE
EULER(THETAN,THETANN,THETAH,THETAHN,THETANH,THETANHN,THETANH2,THETANH2N,THETANH3,TH
ETANH3N,THETAVN,&

CN2,CH2,CNH3,CH2N,CN2N,CNH3N,DCN2,DCH2,DCNH3,DTHETAN,DTHETAH,DTHETANH,DTHETANH2,DTHET
ANH3,DELT)

            INTEGER,PARAMETER :: IKIND=SELECTED_REAL_KIND (p=8,r=80)
   REAL (KIND=IKIND) ::
THETAN,THETANN,THETAH,THETAHN,THETANH,THETANHN,THETANH2,THETANH2N,THETANH3
   REAL (KIND=IKIND) :: THETANH3N,THETAVN,CN2,CH2,CNH3,CH2N,CN2N,CNH3N,DCN2,DCH2,DCNH3
            REAL (KIND=IKIND) :: DTHETAN,DTHETAH,DTHETANH,DTHETANH2,DTHETANH3,DELT


            CN2N=CN2+DELT*DCN2
            CH2N=CH2+DELT*DCH2
   CNH3N=CNH3+DELT*DCNH3
   THETANN=THETAN+DELT*DTHETAN
   THETAHN=THETAH+DELT*DTHETAH
   THETANHN=THETANH+DELT*DTHETANH
   THETANH2N=THETANH2+DELT*DTHETANH2
   THETANH3N=THETANH3+DELT*DTHETANH3
   THETAVN=1_IKIND-THETANN-THETAHN-THETANHN-THETANH2N-THETANH3N

   RETURN
   END

!           ----------------------------------------------------------------------------------------------------------------------

!           SUBPROGRAM FOR SWAPPING NEW AND OLD VALUES AFTER EULER'S METHOD

            SUBROUTINE
SWAP(THETAN,THETANN,THETAH,THETAHN,THETANH,THETANHN,THETANH2,THETANH2N,THETANH3,THE
TANH3N,THETAV,THETAVN,&
   CN2,CH2,CNH3,CH2N,CN2N,CNH3N)

   INTEGER,PARAMETER :: IKIND=SELECTED_REAL_KIND (p=8,r=80)
   REAL (KIND=IKIND) ::
THETAN,THETANN,THETAH,THETAHN,THETANH,THETANHN,THETANH2,THETANH2N,THETANH3
   REAL (KIND=IKIND) :: THETANH3N,THETAV,THETAVN,CN2,CH2,CNH3,CH2N,CN2N,CNH3N

   THETAN=THETANN; THETAH=THETAHN; THETANH=THETANHN; THETANH2=THETANH2N;
THETANH3=THETANH3N; THETAV=THETAVN
   CN2=CN2N; CH2=CH2N; CNH3=CNH3N

   RETURN
   END

!           ----------------------------------------------------------------------------------------------------------------------
```

A.5.2 Reactor Modeling using Microkinetic Analysis for Ammonia Synthesis Reaction Mechanism

In a catalytic reaction, many events regarding to chemical conversion occur at the catalyst surface. Global rate equations and/or macro-kinetic equations of reaction give lots of information about the reaction and for reactor modeling. In order to define the details of the reactions on catalytic surfaces, microkinetic modeling is

needed. The surface intermediates, and specific reaction rates can be determined more accurately with microkinetic modeling.

One of the main problems of the catalytic ammonia synthesis reaction was reported as the dissociation of N_2 over catalyst. In this study, microkinetic analysis of ammonia synthesis reaction in the presence of Ru catalysts was modeled. The model was run in a batch reactor at industrial operating conditions such as 100 bar and 673 K. The results of the surface coverages of all intermediates are determined.

A.5.3 Microkinetic Analysis of Ammonia Synthesis Reaction over Ru Catalyst

Microkinetic model based on the mechanism given in Table 5 was implemented in a batch reactor over Ru catalyst at 100 bar pressure and various temperatures (298 K – 673 K). Batch reactor volume and the amount of Ru catalyst are taken as 100 mL and 1 g, respectively.

Table A.5.1: Rate Constants and Activation Energies for Forward & Reverse Reaction of Ammonia Synthesis Reaction Mechanism [50]

Steps	Preexponential factor	$E_{A forward}$, kJ/mol	Reactions	Preexponential factor	$E_{A forward}$, kJ/mol
1	5.6×10^{1}	33.0	$N_2 + 2* \rightleftharpoons 2N*$	2.0×10^{10}	137.0
2	6.0×10^{13}	111.0	**2 /** $N* + H* \rightleftharpoons NH* + *$	1.5×10^{14}	74.1
3	4.7×10^{13}	60.4	**2 /** $NH* + H* \rightleftharpoons NH_2* + *$	1.8×10^{13}	8.6
4	3.3×10^{13}	17.2	**2 /** $NH_2* + H* \rightleftharpoons NH_3* + *$	9.3×10^{12}	64.6
5	2.4×10^{13}	83.7	**2 /** $NH_3* \rightleftharpoons NH_3 + *$	2.1×10^{6}	0.0
6	5.5×10^{5}	0.0	**3 /** $H_2 + 2* \rightleftharpoons 2H*$	2.5×10^{13}	82.0

The intermediate steps of the ammonia synthesis reaction are given below:

Step 1. $N_2 + 2* \rightleftharpoons 2N*$

Step 2. $2N* + 2H* \rightleftharpoons 2NH* + 2*$

Step 3. $2NH* + 2H* \rightleftharpoons 2NH_2* + 2*$

Step 4. $2NH_2* + 2H* \rightleftharpoons 2NH_3* + 2*$

Step 5. $2NH_3* \rightleftharpoons 2NH_3 + 2*$

Step 6. $3H_2 + 6* \rightleftharpoons 6H*$

Forward and reverse rate constants of each intermediate steps are reported by O. Hinrichsen et al. and given below:

Step 1. $k_{+1} = 56 \exp\left(-\frac{3969}{T}\right)$ $\quad k_{-1} = 2.0 \times 10^{10} \exp(-\frac{16478}{T})$

Step 2. $k_{+2} = 6.0 \times 10^{13} \exp\left(-\frac{13351}{T}\right)$ $\quad k_{-2} = 1.5 \times 10^{14} \exp(-\frac{8913}{T})$

Step 3. $k_{+3} = 4.7 \times 10^{13} \exp\left(-\frac{7265}{T}\right)$ $\quad k_{-3} = 1.8 \times 10^{13} \exp(-\frac{1034}{T})$

Step 4. $k_{+4} = 3.3 \times 10^{13} \exp\left(-\frac{2069}{T}\right)$ $\quad k_{-4} = 9.3 \times 10^{12} \exp(-\frac{7770}{T})$

Step 5. $k_{+5} = 2.4 \times 10^{13} \exp\left(-\frac{10067}{T}\right)$ $\quad k_{-5} = 2.1 \times 10^{6}$

Step 6. $k_{+6} = 5.5 \times 10^{5}$ $\quad k_{-6} = 2.5 \times 10^{13} \exp(-\frac{9863}{T})$

Step 1.	$r_{+1} = k_{+1} P_{N_2} {\theta_v}^2$	$r_{-1} = k_{-1} {\theta_N}^2$
Step 2.	$r_{+2} = k_{+2} \theta_N \theta_H$	$r_{-2} = k_{-2} \theta_{NH} \theta_v$
Step 3.	$r_{+3} = k_{+3} \theta_{NH} \theta_H$	$r_{-3} = k_{-3} \theta_{NH_2} \theta_v$
Step 4.	$r_{+4} = k_{+4} \theta_{NH_2} \theta_H$	$r_{-4} = k_{-4} \theta_{NH_3} \theta_v$
Step 5.	$r_{+5} = k_{+5} \theta_{NH_3}$	$r_{-5} = k_{-5} P_{NH_3} \theta_v$
Step 6.	$r_{+6} = k_{+6} P_{H_2} {\theta_v}^2$	$r_{-6} = k_{-6} {\theta_H}^2$

Rate Equations for Each Step in differential form are given below:

Step 1.	$r_1 = k_{+1} P_{N_2} {\theta_v}^2 - k_{-1} {\theta_N}^2$
Step 2.	$r_2 = k_{+2} \theta_N \theta_H - k_{-2} \theta_{NH} \theta_v$
Step 3.	$r_3 = k_{+3} \theta_{NH} \theta_H - k_{-3} \theta_{NH_2} \theta_v$
Step 4.	$r_4 = k_{+4} \theta_{NH_2} \theta_H - k_{-4} \theta_{NH_3} \theta_v$
Step 5.	$r_5 = k_{+5} \theta_{NH_3} - k_{-5} P_{NH_3} \theta_v$
Step 6.	$r_6 = k_{+6} P_{H_2} {\theta_v}^2 - k_{-6} {\theta_H}^2$

Differential equations regarding to each surface intermediate and reactants were given below;

$$\frac{dP_{N_{2o}}}{dt} = \frac{P_{N_{2i}} * V_o}{V} - \frac{P_{N_{2o}} * V_o}{V} - (r_1 - r_{-1}) * \frac{W * R * T}{V_o}$$

$$\frac{dP_{H_{2o}}}{dt} = \frac{P_{H_{2i}} * V_o}{V} - \frac{P_{H_{2o}} * V_o}{V} - 3(r_6 - r_{-6}) * \frac{W * R * T}{V_o}$$

$$\frac{dP_{NH_{3o}}}{dt} = \frac{P_{NH_{3i}} * V_o}{V} - \frac{P_{NH_{3o}} * V_o}{V} + 2(r_5 - r_{-5}) * \frac{W * R * T}{V_o}$$

$$\frac{d\theta_N}{dt} = r_1 - r_{-1} - 2r_2 + 2r_{-2}$$

$$\frac{d\theta_{NH}}{dt} = 2r_2 - 2r_{-2} - 2r_3 + 2r_{-3}$$

$$\frac{d\theta_{NH2}}{dt} = 2r_3 - 2r_{-3} - 2r_4 + 2r_{-4}$$

$$\frac{d\theta_{NH3}}{dt} = 2r_4 - 2r_{-4} - 2r_5 + 2r_{-5}$$

$$\frac{d\theta_H}{dt} = -2r_2 + 2r_{-2} - 2r_3 + 2r_{-3} - 2r_4 + 2r_{-4} - 3r_6 + 3r_{-6}$$

$$\theta_V = 1 - (\theta_N + \theta_H + \theta_{NH} + \theta_{NH_2} + \theta_{NH_3})$$

All of the differential equations regarding microkinetic analysis of ammonia synthesis over Ru catalyst were solved via Finite Difference Method. In order to solve the equations with a tight increment of $1x10^{-13}$ second, a Fortran Code was written. The details of the code are given in Appendix part of the thesis. Outcomes of microkinetic modeling analysis were given in Results and Discussion part of this thesis.

A.5.4 Microkinetic Modeling of Ammonia Synthesis Reaction over Ru Catalyst

Ammonia synthesis reaction mechanism and rate constants regarding to this mechanism are published by O. Hinrichsen et al. [47]. The mechanism steps are

given in Materials and Methods section. The reaction mechanism and equilibrium constant calculation method are given in Table A.5.2.

Table A.5.2 Calculation method of thermodynamic parameters of ammonia synthesis

Steps	Reactions	Equilibrium Constant
1	$N_2 + 2* \rightleftharpoons 2N*$	$K_1 = {k_{1f}}/{k_{1r}}$
2	$2/N* + H* \rightleftharpoons NH* + *$	$K_2 = {k_{2f}}/{k_{2r}}$
3	$2/NH* + H* \rightleftharpoons NH_2* + *$	$K_3 = {k_{3f}}/{k_{3r}}$
4	$2/NH_2* + H* \rightleftharpoons NH_3* + *$	$K_4 = {k_{4f}}/{k_{4r}}$
5	$2/NH_3* \rightleftharpoons NH_3 + *$	$K_5 = {k_{5f}}/{k_{5r}}$
6	$3/H_2 + 2* \rightleftharpoons 2H*$	$K_6 = {k_{6f}}/{k_{6r}}$
T	$N_2 + 3H_2 \rightleftharpoons 2NH_3$	$K_{eq} = K_1 \times (K_2 \times K_3 \times K_4 \times K_5)^2 \times (K_6)^3$

Thermodynamic check of the reaction mechanism and the reaction rate constant are done and the heat of reaction obtained from the ammonia synthesis reaction mechanism data and natural heat of reaction for the ammonia synthesis data are found as in agreement each other. The details of the thermodynamic check were given in Table A.5.3.

Table A.5.3. Thermodynamic Check of Ammonia Synthesis Reaction Mechanism Published by O. Hinrichsen et. al. @ 298 K

Steps	Reactions	ΔS (J/mol-K)	ΔH (kJ/mol)	ΔG (kJ/mol)
1	$N_2 + 2* \rightleftharpoons 2N*$	-163.73	-104	-55.21
2	$2N* + 2H* \rightleftharpoons 2NH* + 2*$	-7.62	37	39.27
3	$2NH* + 2H* \rightleftharpoons 2NH_2* + 2*$	7.98	51.8	49.42
4	$2NH_2* + 2H* \rightleftharpoons 2NH_3* + 2*$	10.53	-47.4	-50.54
5	$2NH_3* \rightleftharpoons 2NH_3 + 2*$	135.12	83.7	43.44
6	$3H_2 + 6* \rightleftharpoons 6H*$	-146.59	-82	-38.31
T	$N_2 + 3H_2 \rightleftharpoons 2NH_3$		-99.80	-6.97

Table A.5.4. Thermodynamic properties of ammonia synthesis reaction at different temperatures

$N_2 + 3H_2 \rightleftharpoons 2NH_3$	298 K	600 K
ΔS, (J/mol-K)	0.20	0.23
ΔH, (kJ/mol)	-92.70	-104.10
ΔG, (kJ/mol)	-32.91	31.50

The changing of rate of N_2 dissociation step over Ru catalyst for ammonia synthesis reaction with respect to different feed ratios was given in Figure A.5.1. When Figure A.5.1. is examined, reaction rate decreases exponentially with increasing H_2:N_2 feed ratio. In other words, reaction rate of ammonia synthesis reaction increases with increasing of N_2 ratio in reactant feed. In literature, it is directly said that decreasing of reactant feed ratio from stoichiometric ratio of 3 to lower values increases the reaction rate of ammonia synthesis [16]. This finding is in agreement with the literature. On the other hand, according to literature, ammonia synthesis reaction over Ru catalyst is inhibited by H_2. So, decreasing the amount of H_2 should increase the reaction rate. These two different perspectives can be proven by the results based on the reaction rate with respect to reactant feed ratio.

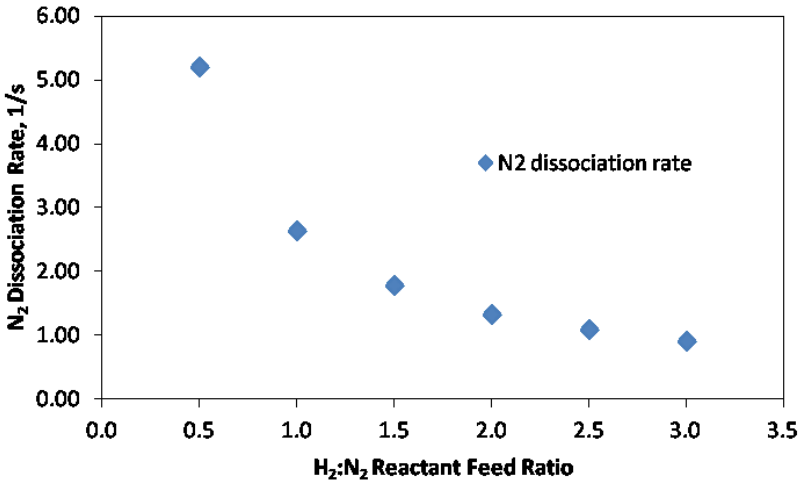

Figure A.5.1. Changing of Rate of Rate Limiting Step with respect to H_2:N_2 Feed Ratio Based on Microkinetic Analysis

The thermodynamic results of O. Hinrichsen et al.'s data and thermodynamic properties of ammonia synthesis reaction are in agreement with each other. After that checking step, the microkinetic model is started to be build up. Ammonia synthesis microkinetic model was set up as every variable such as concentrations and surface coverages are assumed as unsteady state. Microkinetic model was solved in a batch reactor at 673 K and 100 bar. The changes of all parameters with respect to time are calculated via Finite Difference (Euler) method. The results of microkinetic model are given through the Figure A.5.2. – A.5.5: Figure A.5.2. represents the surface coverage of nitrogen with respect to time. At the beginning of the process, surface coverage of nitrogen is about $1x10^{-8}$. After $1x10^{-7}$ second, a sharp increase is observed and the coverage of nitrogen comes nearly to 1. Figure A.5.3. shows the surface coverage change of hydrogen with respect to time. When Figure A.5.3. is examined carefully, it is observed that there is a gradual increase at the beginning of the process then after $1x10^{-7}$ second there is sharp decrease in coverage values. Finally, the change of coverage values of vacant sites and NH_x species with respect time (Figure A.5.4 and A.5.5) shows the gradual increase and decrease, respectively.

If the time periods between $1x10^{-13}$ and $1x10^{-7}$ are commented, the results of the surface coverages are in agreement with the literature data. In literature, dissociation of nitrogen over Ru surfaces is defined as the rate limiting step for ammonia synthesis [47,48]. So, being very small of nitrogen surface coverage is about $1x10^{-8}$ is an expected value. Besides this, the surface coverage of hydrogen is found as 0.94 at same time period. The surface coverages of the NH_x species are determined lower values in comparison to surface coverage of nitrogen. It is known from the literature that, there is a competitive adsorption process between H_2 and N_2 over Ru surface for ammonia synthesis reaction. Besides, literature reported that hydrogen inhibits the ammonia synthesis reaction due to excess amount of hydrogen adsorption over active surface. When all these arguments are placed side by side, the results of microkinetic analysis of ammonia synthesis showed that ammonia synthesis reaction is inhibited by adsorbed hydrogen species.

In Table A.5.5, the results of microkinetic analysis at different temperatures at 100 bar are summarized.

Table A.5.5. Surface coverages of ammonia synthesis reaction intermediates at different temperature at 100 bar ($1x10^{-13}$ - $1x10^{-7}$ sec.)

	298 K	**398 K**	**523 K**	**573 K**	**623 K**	**673 K**
θ_N	$1.86x10^{-11}$	$5.25x10^{-10}$	$6.03x10^{-9}$	$1.37x10^{-8}$	$3.68x10^{-8}$	$0.80x10^{-7}$
θ_H	0.998	0.998	0.992	0.983	0.968	0.946
θ_{NH}	$7.59x10^{-24}$	$1.66x10^{-17}$	$1.95x10^{-13}$	$1.82x10^{-11}$	$1.55x10^{-9}$	$0.24x10^{-7}$
θ_{NH2}	$2.75x10^{-31}$	$5.01x10^{-23}$	$4.17x10^{-17}$	$2.88x10^{-15}$	$5.01x10^{-13}$	$0.30x10^{-6}$
θ_{NH3}	$8.32x10^{-28}$	$8.91x10^{-19}$	$2.45x10^{-12}$	$1.95x10^{-10}$	$2.29x10^{-8}$	$0.30x10^{-6}$
θ_V	$2.29x10^{-3}$	$1.74x10^{-3}$	$7.76x10^{-3}$	0.02	0.03	0.05

The change of surface coverages of ammonia synthesis reaction intermediates with respect to time at 100 bar and 673 K are given in Figure A.5.2 –A.5.5.

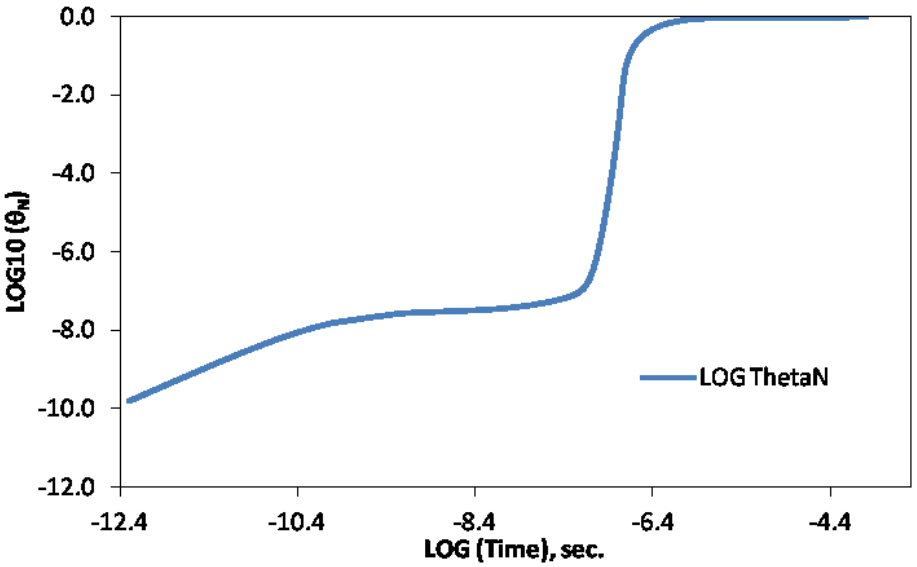

Figure A.5.2. Surface coverage of nitrogen @ 673 K

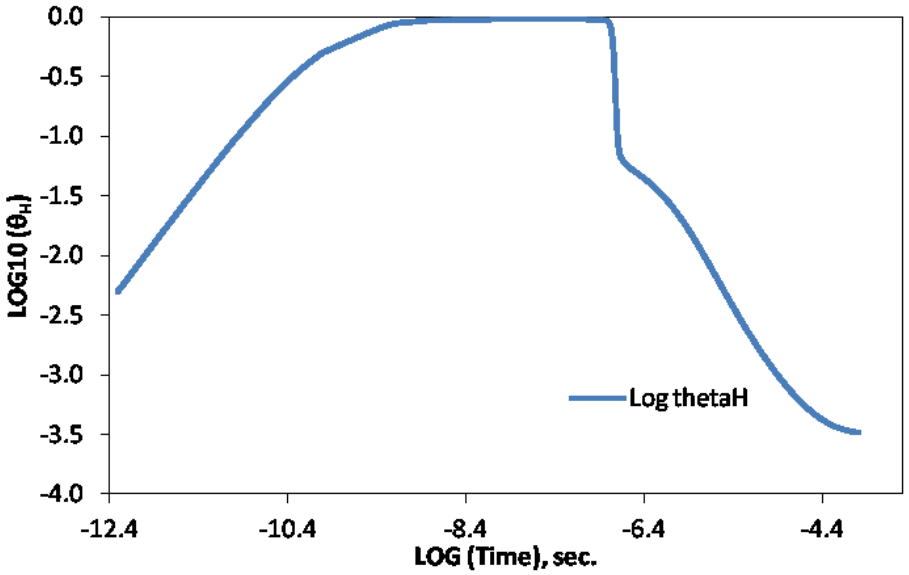

Figure A.5.3. Surface coverage of hydrogen @ 673 K

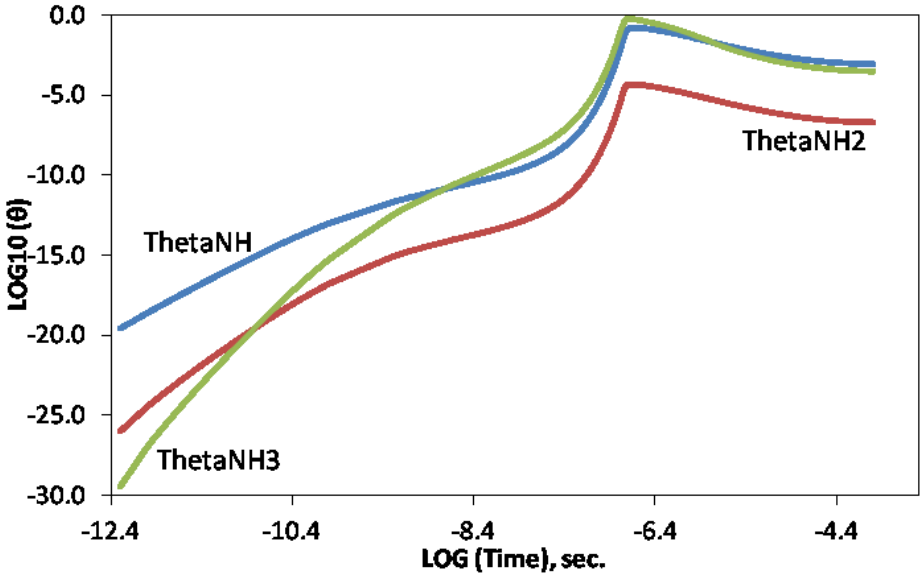

Figure A.5.4. Surface coverage of NH, NH_2 and NH_3 @ 673 K

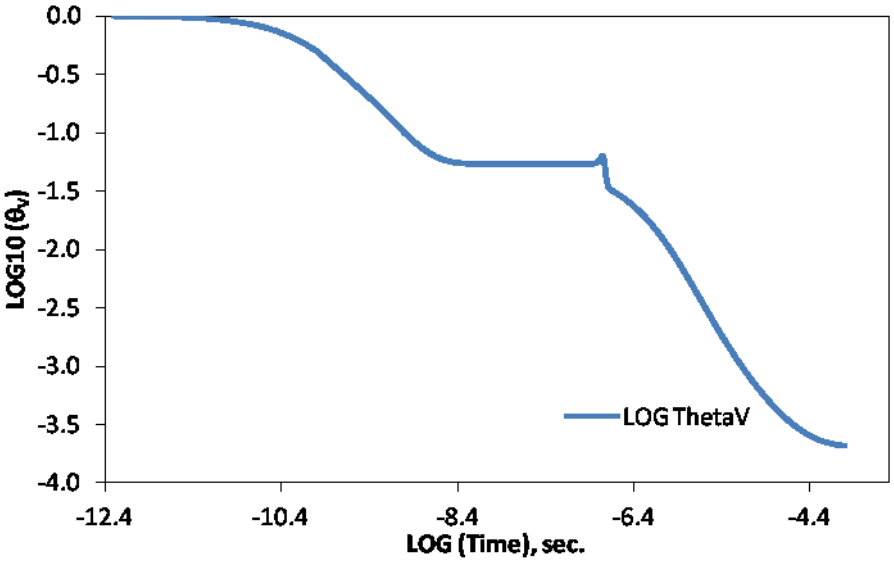

Figure A.5.5. Surface coverage of vacant sites @ 673 K